Alma Mater Studiorum – Università di Bologna

DOTTORATO DI RICERCA IN

CHIMICA

Ciclo XXIX

Settore Concorsuale di afferenza: 03/A1

Settore Scientifico disciplinare: CHIM/01- CHIMICA ANALITICA

Development and application of chemically modified electrodes for sensing and electrocatalysis

Presentata da: Vivek Vishal Sharma

Coordinatore Dottorato **Relatore**

Chiar.mo Prof. Aldo Roda **Prof.ssa. Domenica Tonelli**

Esame finale anno 2017

Index

CHAPTER 1

INTRODUCTION 1

1.1 CHEMICALLY MODIFIED ELECTRODES 2

1.2 MODIFICATION OF ELECTRODES 4

1.3 PROCESSES AT MODIFIED ELECTRODES 6

1.3.1 ACCUMULATION 7

1.3.2 ELCTROCATALYSIS 7

1.3.3 PERMEABILITY 10

1.3.4 IONIC EQUILIBRIA 11

1.4 HEXACYANOFERRATES 11

1.5 LAYERED DOUBLE HYDROXIDES 15

1.6 BIBLIOGRAPHY 18

CHAPTER 2

AIM OF THE THESIS 22

CHAPTER 3

EXPERIMENTAL SECTION 25

3.1 INSTRUMENTAL TECHNIQUES EMPLOYED 25

3.1.1 CYCLIC VOLTAMMETRY AND LINEAR SWEEP VOLTAMMETRY 25

3.1.2 CHRONOAMPEROMETRY 28

3.1.3 DIFFERENTIAL PULSE VOLTAMMETRY 30

3.1.4 SCANNING ELECTRON MICROSCOPY 31

3.1.5 FT-IR SPECTROSCOPY 34

3.2 INSTRUMENTATION 36

3.3 CHEMICALS, SAMPLES AND PROCEDURES 38

CHAPTER 4

RESULTS AND DISCUSSIONS 43

4.1 CMEs BASED ON COPPER COBALT HEXACYANOFERRATE FOR DETERMINATION OF THIOLS 43

4.1.1 ELECTROSYNTHESIS AND CHARACTERIZATION OF Cu-CoHCF MODIFIED GCE 43

4.1.2 CV STUDY OF pH EFFECT ON THE ANALYTICAL DETERMINATION OF THIOLS 51

4.1.3 CHRONOAMPEROMETRIC RESPONSE OF THIOLS 54

4.1.4. BIBLIOGRAPHY 61

4.2. CMEs BASED ON COPPER COBALT HEXACYANOFERRATE FOR DETERMINATION OF MERCURY 63

4.2.1. DETECTION OF MERCURY 63

4.2.2. INTERFERENCE STUDIES 67

4.2.2.1. Removal of Interference due to Cu^{2+} by chemical methods 70

4.2.2.2. Removal of Interference due to Cu^{2+} by electro-chemical methods 72

4.2.2.3. Removal of Interference due to Cu^{2+} by reaction kinetics 74

4.2.3. EXPERIMENTAL STUDIES ON PACKAGED MINERAL WATER SPIKED WITH Hg^{2+} 75

4.2.4. BIBLIOGRAPHY 77

4.3 CME BASED ON GRAPHENE OXIDE AND CARBON NANOTUBES 78

4.3.1 ELECTROCHEMICAL CHARACTERIZATION OF GO AND MWCNTs MODIFIED GCE 78

4.3.2 MEASUREMENT OF ELECTROCHEMICALLY ACTIVE AREA 79

4.3.3 MORPHOLOGICAL CHARACTERIZATIONS 82

4.3.4 FT-IR AND UV-Vis CHARACTERIZATIONS 85

4.3.5 ELECTROCHEMICAL BEHAVIOURS OF CATECHOL AND DOPAMINE 86
4.3.6 EVALUATION OF MODIFIED ELECTRODES FOULING 90
4.3.7. BIBLIOGRAPHY 91
4.4 LAYERED DOUBLE HYDROXIDES 92
4.4.1 LDHs BASED ON Ni, Mg AND Al 92

CHAPTER 5
CONCLUSIONS 95

ACKNOWLEDGMENTS 97

Chapter 1
INTRODUCTION

The interest to the development of analytical procedures for specific detection, quantification and determination of chemical species, even in the presence of interfering substances, has led to the necessity of developing new sensor systems. In general, a sensor is thought to respond to a particular chemical species in a selective way, and can be used for qualitative or quantitative determinations [1]. All sensors are composed of two main parts: a first one, the so-called detection element, where a more or less selective interaction with the "environment" occurs, and a second one, which is called the transducer, where the interaction is translated into a signal. Generally, "physical" sensors are considered as those that are devoted to measure a physical quantity, like temperature or pressure, and "chemical sensors" as those measuring quantities of chemical interest, like concentration. The actual proper distinction between "physical" and "chemical" sensors depends on the nature of the process occurring at the detection element. For instance, optical and gravimetric sensors are considered as physical sensors, while amperometric sensors are, among the few, properly defined as chemical sensors, since the measurement process imply a chemical reaction between the detection element and the analyte which in turn gives rise to an electrical current.

The transducer converts into a measurable signal the physical or chemical changes activated at the detection element. They usually produce an electrical signal, whose magnitude is linked, by a known physical law, to the concentration of the chemical species interacting with the detection element. The signal is often electronically amplified, converted into digital form, acquired by a computer, and finally stored on a mass memory. It is then possible to display it, as well as to treat it properly with various digital filtering procedures.

As regards the class of the electrochemical sensors, the most commonly used transducers are based on the measurement of current intensity (or of the amount of charge spent), of electromotive force or conductivity. They are identified as

amperometric, potentiometric, and conductometric sensors, respectively. In this Thesis, the amperometric transducers are primarily considered.

The development of electrochemical sensors continues to be a rapidly growing area of electrochemistry. Improvements in the stability, selectivity, and scope of such sensors are highly desirable to meet new challenges posed by clinical and environmental samples. The utility of solid electrode-based sensors is often hampered by a gradual fouling of the surface due to adsorption of large organic surfactants or of reaction products. Amperometric sensors lack the ability to discriminate between solutes possessing similar redox characteristics. Finally, the sensing of many important solutes is often hindered by their slow electron transfer kinetics at the commonly used electrodes materials. One field that offers great potential for alleviating the problems above, hence for enhancing the power and scope of electrochemical sensors, is that comprising chemically modified electrodes (CMEs). The field of CMEs, which has experienced a period of rapid growth over the past decade, has now reached a level of maturity that allows the use of these electrodes for routine sensing applications.

1.1. CHEMICALLY MODIFIED ELECTRODES

Chemically modified electrodes comprise a relatively modern approach to electrode systems that finds utility in 1) a wide spectrum of basic electrochemical investigations, including the relationship of heterogeneous electron transfer and chemical reactivity to electrode surface chemistry, electrostatic phenomena at electrode surfaces, and electron and ionic transport phenomena in polymers, and 2) the design of electrochemical devices and systems for applications in chemical sensing, energy conversion and storage, molecular electronics, electrochromic displays, corrosion protection, and electro-organic syntheses [2-4].

Compared with other electrode concepts in electrochemistry, the distinguishing feature of a CME is that a generally quite thin film (from a molecular monolayer to perhaps a few micrometers-thick multilayer) of a selected chemical is bonded to or coated on the electrode surface to endow the electrode with the chemical,

electrochemical, optical, electrical, transport, and other desirable properties of the film in a rational, chemically designed manner.

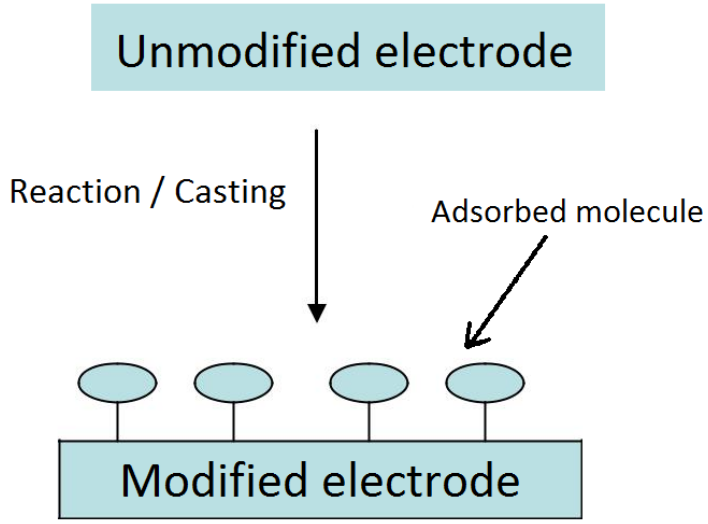

Figure 1.1 Preparation of a CME

Many compounds that are important biologically and environmentally show no response within a potential window at solid electrodes or necessitate an overpotential. Direct electrochemical detection (EC) usually requires high potential for such compounds. This can produce large background current, resulting in inferior detection limits. Also, passivation and/or deactivation of the electrode surface, due to the adsorption of macromolecules (e.g. proteins and surfactants) or of reaction products, greatly affect the stability of electrode response. More, coexisting components, which may be present in concentrations much larger than the analytes, may severely interfere with the determination of trace analytes. Complicated sample pretreatments are often employed to eliminate or separate interfering components [5]. The phenomena mentioned above often can be controlled by manipulating the chemical nature of the electrode surface and a promising route to overcome these problems is based on tailoring the electrode surface – the application of chemically modified electrodes – for improving qualitative and quantitative measurements. CMEs have attracted considerable interest over the past decades as researchers attempted to exert more direct control over the chemical nature of an electrode surface. By deliberately attaching

chemical reagents to it, one hoped that the electrode surface would take on the chemical properties of the attached reagents. If the proper reagents were chosen, desirable properties such as reagent-based control of the rates and selectivities of electrochemical reactions (e.g., electrocatalysis), freedom from adsorptive and coating effects, and special optic or excited state features might be obtained [5,6].

1.2. MODIFICATION OF ELECTRODES

Electrodes are usually chemically modified by one of four approaches:

(1) **Chemisorption** - adsorption in which the forces involved are the valence forces of the same kind as those operating in the formation of chemical compounds [7]. The chemical film is strongly and, ideally, irreversibly adsorbed (chemisorbed) onto the electrode surface. This approach usually yields monolayer (or less) coverage. Included in this type of modification are the substrate-coupled self-assembled monolayers (SAMs) in which uncorrelated molecules spontaneously chemisorb at specific sites on the surface of the electrode to form a superlattice [8].

2) **Covalent bonding** - linking agents, such as, e.g., organosilanes or cyanuric chloride, are used to covalently attach from one to several monomolecular layers of the chemical modifier to the electrode surface.

(3) **Polymer film coating** - electron-conductive and nonconductive polymer films are held on the electrode surface by some combination of chemisorption and low solubility in the contacting solution or by physical anchoring in a porous electrode. The polymer film can be organic, organometallic or inorganic; it can already contain the desired chemical modifier or that chemical can be added to the polymer in a second, functionalizing step; and can contain the equivalent of a few up to many thousands of monomolecular layers of the chemical modifier. Included in this form of modification are the substrate-decoupled SAMs in which adsorbate molecules are arranged on the electrode surface independently of any substrate structure [8].

(4) **Composite** - the chemical modifier is simply mixed with an electrode matrix material, as in the case of an electron-transfer mediator (electrocatalyst) combined with the carbon particles (plus binder) of a carbon paste electrode. Alternatively, intercalation matrices such as certain Langmuir-Blodgett films, zeolites, clays and molecular sieves can be used to contain the modifier.

CMEs can also contain multiple chemical modifiers, and sometimes these modifiers and/or the electrode substrate may have a particularly designed spatial configuration. That is, a CME may contain one electrocatalyst that reacts with a substrate or acts as a photodonor or acceptor, and a second one to transport charge between the first catalyst and the electrode. Or, the CME may consist of a substrate coated with two different chemical polymers, the second polymer overlaid on the first to form a bilayer of polymer films. These more complex CMEs may be called **microstructured electrodes** or **integrated chemical system electrodes**.

Polymer film-coated electrodes may be further subdivided by the process used to apply the film:

(1) **Dip-coating** - this procedure consists of immersing the electrode material in a solution of the polymer for a period sufficient for spontaneous film formation to occur by adsorption. The film quantity in this procedure may be augmented by withdrawing the electrode from the solution and allowing the film of polymer solution to dry on the electrode.

(2) **Solvent evaporation** - a droplet of a solution of the polymer is applied to the electrode surface and the solvent is allowed to evaporate. A major advantage of this approach is that the amount of polymer coverage is immediately known from the original polymer solution concentration and droplet volume. (Alternate term: **droplet evaporation**).

(3) **Spin coating (or spin casting)** - a droplet of a dilute solution of the polymer is applied to the surface of a rotating electrode. Excess solution is spun off the surface and the remaining thin polymer film is allowed to dry. Multiple layers are applied in the same way until the desired thickness is obtained. This procedure typically produces pinhole-free thin films.

(4) **Electrochemical deposition** (also called **redox deposition) -** this procedure relies on the variation of polymer solubility with oxidation (and ionic) state, so that film formation will occur, often irreversibly, when a polymer is oxidized or reduced to its less soluble state.

(5) **Electrochemical polymerization** - a solution of monomer is oxidized or reduced to an activated form that polymerizes to form a polymer film directly on the electrode surface. This procedure results in few pinholes since polymerization would be accentuated at exposed (pinhole) sites at the electrode surface. Unless the polymer film itself is redox active, electrode passivation occurs and further film growth is prevented.

(6) **Cross-linking** - a chemical step designed to couple chemical components of a film on an electrode to impart some desired properties to the film such as increased stability, decreased permeability, or altered electron transport characteristics. Cross-linked films are often formed by copolymerization of bifunctional and polyfunctional monomers. Cross-linking may be activated chemically, electrochemically, photolytically, radiolytically, or thermally [6,7,8].

In all the above cases, the redox moiety (electron-transfer mediator or electrocatalyst) may be bound to the monomer or polymer before application of the film to the electrode, or the polymer film may be derivatized (functionalized) subsequent to film application.

1.3. PROCESSES AT MODIFIED ELECTRODES

To prepare a CME, a thin film of a selected chemical is either bound or coated onto the electrode surface to endow the desirable properties of the film to the electrode in a chemically designed manner. This can be done in order to facilitate an electrode process that can otherwise only be carried out at a high over-potential η (such as the enzyme-catalysed oxidation of methanol), or to inhibit a reaction (such as metallic corrosion), or to produce selectivity towards a particular process (such as enzyme-catalysed oxidative determination of glucose in blood). These ends are achieved by developing within the structure of the CME a favorable interplay of the dynamics by

which electrons are conveyed between the electrode and the species whose oxidation or reduction is ultimately required to achieve that goal [9]. This section classifies some electrochemical processes, desirable for electroanalysis, that can occur at suitably modified electrodes.

1.3.1 ACCUMULATION

From dilute solutions, accumulation (or pre-concentration) of analyte from bulk solution can be performed at an electrode modified with a suitable layer. This analyte accumulation at the CME is followed by detection, and its main purpose is to improve detectability. If this accumulation is preferential, because of selective interactions between the analyte and immobilised reagent, then it can serve additionally as a separation step and, hence, improve the selectivity. Yantasee et al. [10] developed a highly selective voltammetric method for detection of Cd^{2+}, Cu^{2+} and Pb^{2+}, based on a carbamoylphosphonic acid self-assembled monolayer on mesoporous silica (SAMMS). Preconcentration allowed detection limits of 0.5 ppb to be reached.

1.3.2 ELECTROCATALYSIS

An important motivation for modifying electrode surface is electrocatalysis of the electrode reaction of an analytically desired substrate, being one of the most important topics of research on CMEs. Electrocatalysis at a modified electrode is usually an electron transfer reaction between the electrode and some analyte substrate which, when mediated by an immobilized redox couple (i.e., the mediator), proceeds at a lower overpotential than would otherwise occur at the bare electrode. CMEs employing immobilized redox mediators can facilitate the electron transfer of such analytes [11].

Almost all catalytic CMEs have relied on the immobilization of redox centers on the electrode surface. The immobilized redox center acts as a fast electron transfer mediator for substrate species, which is oxidized or reduced slowly (or not at all) at the

naked electrode. The basic principle involved in CMEs electrocatalysis by a surface confined electron-transfer mediator is illustrated in Figure 2, for a generalized oxidation process. In this sequence, the analyte diffuses from the bulk solution to the electrode surface, where it is oxidized in a purely chemical reaction with the oxidized form of the mediator (M_{Ox}). The potential of the electrode is maintained at a value sufficiently positive for M_{Ox} to be the stable state of the mediator and its reduced form (M_{Red}) to be rapidly re-oxidized to the catalytically active form. Thus, the heterogeneous electron transfer takes place between electrode and mediator and not directly between the electrode and analyte. In essence, then, the mediator can be considered to function simply as an electron shuttle between the electrode and the analyte.

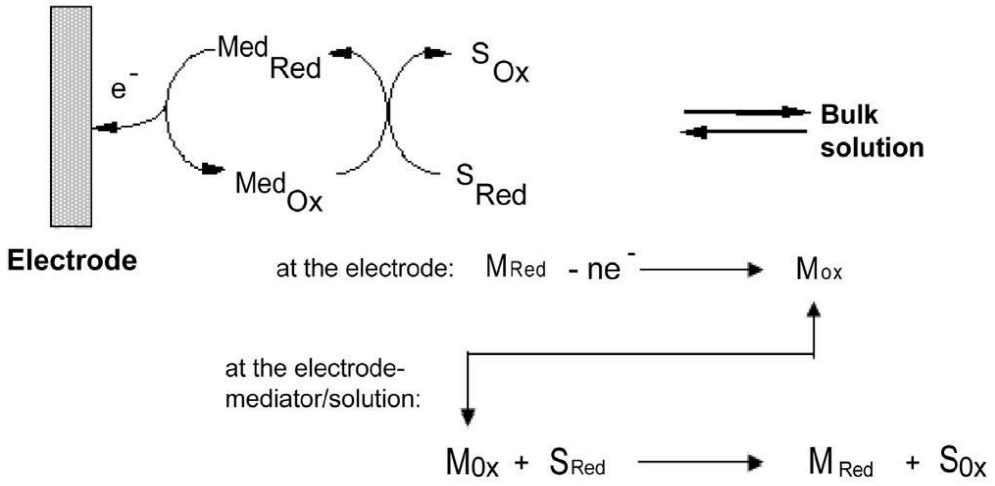

Figure 1.2 The model of electrocatalytic reaction on CME, where S_{Ox}/S_{Red} and M_{Ox}/M_{Red} are the oxidized and reduced forms of analyte to be detected and of mediator, respectively.

There are three important characteristics of mediated electrocatalysis. With an electrocatalytic CME, the oxidation (or reduction) of the analyte is made to take place at the redox potential of the mediator catalyst couple unless a catalyst-substrate adduct is formed, in which case reaction occurs at the potential for the adduct. Second, the mediator catalyst and substrate formal potentials should be similar. Finally, a successfully catalyzed reaction of S occurs at less negative or positive potential for

reduction or oxidation, respectively, than the naked electrode reaction of S would require.

While considering CMEs, it is important to keep in mind the concept of film homogeneity. The presence of variations in film properties at the interfaces between the electrode and solution can dramatically affect many of the other properties discussed below. While film homogeneity is not a necessity, without this property, the others are difficult to estimate and a complete description of the behaviour of a CME is hard, if not impossible, to achieve.

The theory of mediated charge transfer has been widely studied by many authors. The electrocatalytic signal depending on the analyte and/or mediator concentration is governed by four conceivable rate determining steps (or their combination) [12]:

1- Convective diffusion of analyte from bulk solution to the film-solution interface.
2- Diffusion of analyte through the film.
3- Diffusion-like propagation of charge within the film by self-exchange redox reaction.
4- Mediator/analyte cross-exchange redox reaction in the film.

Several different CMEs have been fabricated for electrocatalysis including mediators attached to monolayer films such as a ferrocene-tethered β-cyclodextrin self-assembled monolayer [13], conducting polymers such as polyaniline [14], and metal or semi-conducting nanoparticles dispersed in a host matrix such as carbon nanoparticles in polyaniline [15].

Electrocatalysis is commonly used in biosensing applications where electrochemically active biomolecules (e.g., redox enzymes) are used as the mediators. Usually electrocatalytic biosensors operate amperometrically. However, potentiometric detection has also been used [16]. The charge exchange between the electrode and the immobilised biomolecule, involved in a catalytic sequence with the biological analyte in solution, is either direct [16] or it is aided by an additional surface-bound mediator [14]. The improvements in sensitivity and selectivity that accrue from electrocatalytic CMEs have been illustrated for numerous analytical problems including the sensing of nicotinamide-adenine dinucleotide (NADH) using a Meldola's Blue modified electrode

[17], detection of sulphur dioxide on a silver-dispersed self-assembly [18], and DNA hybridisation detection using methylene blue and zirconia thin films [19].

1.3.3. PERMEABILITY

Permeability provides discriminative transport through a membrane coating that controls access of analyte and interfering substances to the electrode surface [12]. Mechanisms of the permeability transport are based on differences in properties, such as charge, size, polarity, shape, or chirality of the analyte from interfering substances. For instance, a cation exchange polymer film on an electrode is a membrane barrier to anions in solution while cations freely partition into it (Figure 1.3). Polyanionic perfluorosulphonated ionomers, e.g., Nation and poly(estersulphonic acid) of the Kodak AQ series are examples of widely used cation-exchange permselective membranes. The permeability of membranes can be combined with other properties such as electrocatalysis. For example, a conducting polymer, polycarbazole, modified with tyrosinase was used for electrocatalytic detection of D- and L-norepinephrine, where the polymer could exhibit a chiral differentation, due to a better permeation of the D-form [20].

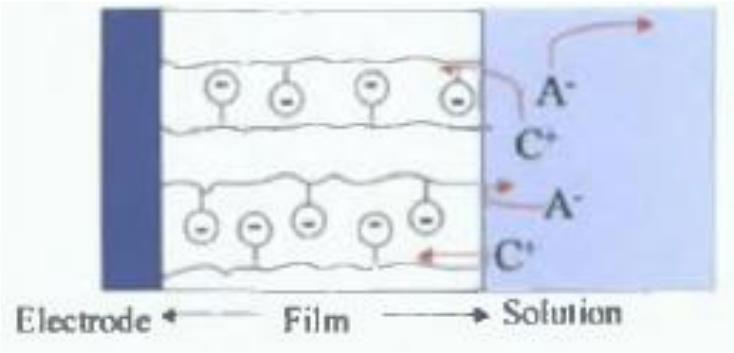

Figure 1.3 Schematic of a CME using a negatively charged polymer film to exclude anionic interferences.

1.3.4. IONIC EQUILIBRIA

CMEs with selective ion-exchange (ionophore) films are used as asymmetric ion-selective electrodes. That is, an electrolyte solution containing analyte ion is on one side of the membrane and a solid electrode on the other. These CMEs are predominantly used as potentiometric sensors.

1.4. HEXACYANOFERRATES

Transition metal hexacyanoferrates of the general formula $A_hM_k[Fe(CN)_6]_l.mH_2O$ (*h*, *k*, *l*, *m* = stoichiometric numbers, A = alkali metal cation, M = transition metal ion) (Table 1.1) represent an important class of mixed-valence compounds, of which Prussian blue or iron(III) hexacyanoferrate(II) (with A = K and M = Fe in the above generic formula) is the classical prototype. Aside from their interesting solid-state chemistry and structural attributes, these compounds have garnered intense recent interest because of their electrocatalytic, electrochromic, ion-exchange, ion-sensing, and photomagnetic properties.

metal	formula	M:Fe ratio	M, Fe formal oxidation state[a]
copper	$K_2Cu_3[Fe(CN)_6]_2$	3:2	II, II
	$Cu_3[Fe(CN)_6]_2$	3:2	II, III
palladium	$K_2Pd_3[Fe(CN)_6]_2$	3:2	II, II
	$Pd_3[Fe(CN)_6]_2$	3:2	II, III
	$K_2Pd[Fe(CN)_6]$	1:1	II, II
	$KPd[Fe(CN)_6]$	1:1	II, III
indium	$In_4[Fe(CN)_6]_3$	4:3	III, II
	$KIn_4[Fe(CN)_6]_3(SO_4)_2$	4:3	III, III
	$KIn[Fe(CN)_6]$	1:1	III, II
	$In[Fe(CN)_6]$	1:1	III, III
vanadium	$K_2(VO)_3[Fe(CN)_6]_2$	3:2	II, II
	$(VO)_3[Fe(CN)_6]_2$	3:2	II, III
	$K_3(VO_2)_3[Fe(CN)_6]_2$	3:2	I, III
	$K_{1.4}(VO)_{1.3}[Fe(CN)_6]$	4:3	II, II
	$K_{0.4}(VO)_{1.3}[Fe(CN)_6]$	4:3	II, III
cobalt	$K_2Co_3[Fe(CN)_6]_2$	3:2	II, II
	$Co_3[Fe(CN)_6]_2$	3:2	II, III
	$K_{1.4}Co_{1.3}[Fe(CN)_6]$	4:3	II, II
	$K_{0.4}Co_{1.3}[Fe(CN)_6]$	4:3	II, III
	$K_2Co[Fe(CN)_6]$	1:1	II, II
	$KCo[Fe(CN)_6]$	1:1	II, III
	$Co[Fe(CN)_6]$	1:1	III, III
nickel	$K_2Ni_3[Fe(CN)_6]_2$	3:2	II, II
	$Ni_3[Fe(CN)_6]_2$	3:2	II, III
	$K_2Ni[Fe(CN)_6]$	1:1	II, II
	$KNi[Fe(CN)_6]$	1:1	II, III

Table 1.1 Compound Stoichiometries and Metal Oxidation States in Prussian Blue (MHCF) Analogues

Metal hexacyanoferrates have a face-centered cubic lattice (unit cell length: ~ 10.2 Å) with octahedral co-ordination of the M and Fe ions by -N≡C and -C≡N ligands, respectively [21,22]. The alkali metal cations, A (which provide charge compensation), are located in the tetrahedral sites in these structures, which may also contain coordinated water molecules and anions in some cases. Representative structures and the corresponding compound stoichiometries are contained in Figure 1.4 for M and Fe in the +2 and +3 oxidation states, respectively.

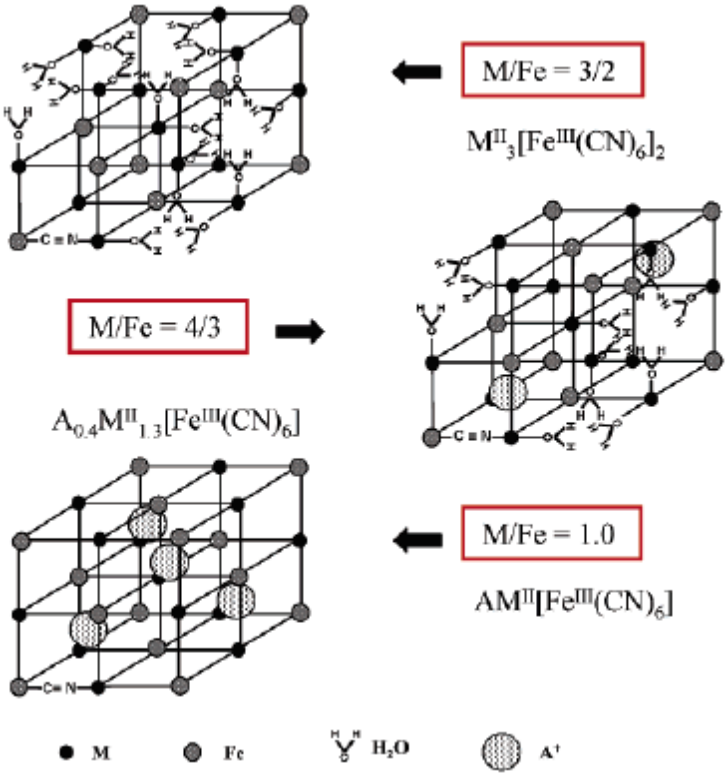

Figure 1.4 Schematic Unit cell representation of $M_3[Fe(CN)_6]_2$, $A_{0.4}M_{1.3}$-$[Fe(CN)_6]$, and $AM[Fe(CN)_6]$. The A+ cations are located in the cell interstitial sites, and the cyanide groups are between M and Fe but have been largely omitted in this representation for the sake of clarity.

Table 1.1 provides a listing of the electrochemically relevant compounds along with the corresponding M:Fe stoichiometries and formal oxidation states of the M and Fe sites for the six metals considered in this review. A change on the M oxidation state from +2 to +3 brings about a contraction of the M octahedral coordination manifold. This in turn manifests as a decrease in the unit cell dimensions a trend particularly well exemplified by the CoHCF compound system. In contrast, the octahedral coordination geometry is not significantly perturbed in size by the Fe oxidation state, as borne out by the similarity between the unit cell parameters of $K_4[Fe(CN)_6]$ and $K_3[Fe(CN)_6]$, respectively [23]. In the case of the vanadium analogue, X-ray photoelectron spectroscopy (XPS) and IR evidence [24,25] support the presence of VO^{2+} (vanadyl) ions in the compound structure. This would imply an octahedral coordination environment for the vanadium metal sites in which one of the six bridging CN ligands

is occupied by a terminal oxygen. On the other hand, the measured V:Fe ratio of 1.5 ± 0.03 [25] suggests a trend in the vanadium system that is common with the Cu, Pd, In, Co, and Ni analogues (Figure 1.4 and Table 1.1). Contrasting with an earlier study [24], evidence has been presented [25] for redox transitions in this compound to involve only the Fe sites, leaving the VO^{2+} sites intact.

Mixed metal hexacyanoferrates have been prepared both as thin films and bulk precipitates (powders) [26]. Mixed valence hexacyanometallates (most often as hexacyanoferrates, MeHCFs) have been employed for electroanalytical applications as they are excellent electron transfer mediators. In this respect, CoHCF, CuHCF, CrHCF, RuO/RuHCF, ZnO/ZnHCF-RuOHCF, and several others have been investigated [27-30]. Our group studied the electrochemical response to hydrogen peroxide by copper-based hexacyanoferrates [31]. One advantage of hexacyanoferrates is that they can be electrodeposited onto various electrode surfaces to provide insoluble films through repetitive redox cycling of a solution containing ferro or ferricyanide and a soluble M salt. Sometimes, as for CuHCF, it is possible to employ an electrosynthesis involving a double step which consists of a potentiostatic deposition of copper followed by a potential cycling within a more anodic window in the presence of $K_3[Fe(CN)_6]$ [32].

Unfortunately, one of the major drawbacks of MHCFs lies in their limited stability both during operation in neutral and alkaline pHs and during potential cycling [33]. In order to improve the operational stability of MHCFs, different strategies have been proposed so far, including the use of surfactants/stabilizers or the fabrication of composites [33, and references therein]. An alternative, simple route was applied to a Prussian Blue (PB) coating by de Mattos et al., which involved a thermal treatment step following the electrochemical deposition in order to improve the stability and sensitivity of the CME towards hydrogen peroxide detection [34].

Another way is the introduction of one more metal center in addition to M in MHCFs (hybrid hexacyanoferrates) [26,35,36], and this approach has been successfully employed for the determination of L-cysteine and glucose. In this thesis, we carried out a research aimed to use a hybrid copper-cobalt hexacyanoferrate (Cu-CoHCF) to develop a CME for the amperometric determination of three thiols, namely L-cysteine and L-glutathione (as "model" amino thiols), and 1,4-butanedithiol (as an example of

alkane dithiol). Since fouling is a major drawback in the case of thiols determination, we investigated the effect of thermal treatment on the stability of the HCF film and on the analytical performance of the sensor. To our knowledge, this is the first time that such a comparative investigation is performed on a hybrid HCF used as a redox mediator for the electrocatalytic oxidation of thiols. Furthermore, this kind of analytical method has been applied for the first time towards the determination of 1,4-butanedithiol.

1.5. LAYERED DOUBLE HYDROXIDES

In this thesis, a brief study of layered double hydroxides (LDHs) has been carried out, employing them as catalytic precursors, after electrodeposition on FeCrAl foams. LDHs belong to a family of compounds called clays that could be mainly divided in two large groups: anionic and cationic clays. Both types are made up of several hydroxide layers. In cationic clays these layers present a negative charge and they are mostly composed by Si and Al hydroxides. The negative charge is balanced by cations situated in the interlayer region. On the contrary, anionic clays are characterized by positive charge layers and interlayer anions to obtain the electroneutrality.

LDHs or hydrotalcite-like (HT-like) compounds are anionic clays materials. A few kinds of anionic clays have been found in nature but most of them could be artificially synthesized in the laboratory [37]. These layered materials have rich intercalation properties. The structure of most of them corresponds to that of the mineral hydrotalcite which is a natural magnesium-aluminum hydroxycarbonate ($Mg_6Al_2(OH)_{16}CO_3 \cdot 4H_2O$). These compounds consist of positively charged brucite-type octahedral sheets alternating with interlayers containing carbonate anions, in the natural mineral, or other exchangeable anions in the synthetic HT-like compounds, together with water molecules [38]. Brucite is the common magnesium hydroxide $Mg(OH)_2$.

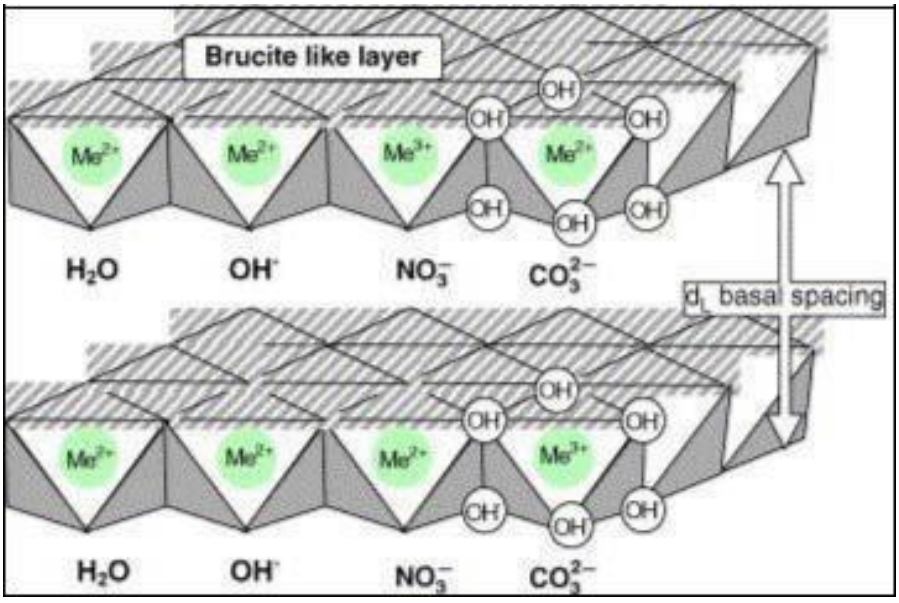

Figure 1.5 Schematic representation of LDH compounds structures

LDHs can be represented by the general formula $[M_{1-x}^{2+}M_x^{3+}(OH)_2]^{x+}(A^{n-})_{x/n}\cdot mH_2O$, where M^{2+} and M^{3+} are divalent and trivalent cations, respectively. The value of x is equal to the molar ratio of $M^{3+}/(M^{2+}+M^{3+})$, whereas A is the interlayer anion of valence n. The identity of M^{2+}, M^{3+}, x and A^{n-}, and the x value may vary over a wide range, thus giving rise to a large class of isostructural materials with different physicochemical properties [39].

The divalent and trivalent metal listed in Table 1 are all found to form LDHs through replacing, fully or partially, Mg^{2+} or Al^{3+}, in the brucite-like layer [37]. In general ions that have ionic radius similar to that of Mg^{2+} can be accommodated in the holes of the close-packed OH groups in the brucite-like sheets to form LDHs [37,39].

M^{2+}	Radius (nm)	M^{3+}	Radius (nm)
Fe	0.061	Al	0.054
Co	0.065	Co	0.055
Ni	0.069	Fe	0.055
Mg	0.072	Mn	0.058
Cu	0.073	Ga	0.062
Zn	0.074	Rh	0.067
Mn	0.083	Ru	0.068
Pd	0.086	Cr	0.069
Ti	0.086	V	0.074
Cd	0.095	In	0.080
Ca	0.100	Y	0.090
		La	0.103
V^{4+}	0.058		
Ti^{4+}	0.061	Li^{+}	0.076
Sn^{4+}	0.069	Na^{+}	0.102
Zr^{4+}	0.072		

Table 1.2 Divalent and trivalent metals found in LDH compounds

LDHs have been used as catalyst precursors for the steam reforming (SR) [40,41] of natural gas. Steam reforming is a method for producing hydrogen, carbon monoxide, or other useful products from hydrocarbon fuels such as natural gas.

STEAM REFORMING OF METHANE

The steam reforming of methane is the main commercial route for hydrogen and syngas production [42] and about 50% of hydrogen demand is satisfied by means of methane SR [43]. It consists of an endothermic reaction between the hydrocarbon and vaporized water that can be written as:

$CH_4 + H_2O \rightarrow CO + 3H_2$ $\quad H° = 206$ KJ/mol

LDH materials can be directly synthesized using precipitation at a varying or constant pH. The pH is one of the most important parameters in the precipitation of this kind of materials and a defined interval of pH corresponds to the precipitation of a hydroxide or a LDH. In this thesis, LDHs based on nickel, magnesium and aluminium was synthesized to see if it was possible to increase the amount of the bivalent cations in the LDHs.

1.4 Bibliography

[1] R.W. Cattrall, Chemical Sensors (1997) Pp 1-2, Oxford: Oxford University Press.

[2] R.W. Murray, "Chemically Modified Electrodes," Electroanalytical Chemistry, Vol. 13, A.J. Bard, ed., Marcel Dekker Inc., NY, 1984.

[3] R.W. Murray, A.G. Ewing, R.A. Durst, Anal. Chem. 59, 379A (1987)

[4] "Molecular Design of Electrode Surfaces," R.W. Murray, ed., Techniques of Chemistry, John Wiley and Sons, NY, 1992.

[5] R.P. Baldwin, K.N. Thomsen, Talanta 38 (1991) 1-16.

[6] K. Kalcher, Electroanalysis 2 (1990) 419-433.

[7] V. Gold, K.L. Loening, A.D. McNaught, and P. Sehmi, Compendium of Chemical Terminology, IUPAC Recommendations, Blackwell Scientific Publications, Oxford, 1987.

[8] D.L. Allara, Biosens. Bioelectronics 10 (1995) 771.

[9] A. Bard, L. Faulker, Electrochemical Methods (2001) Second Edition, Wiley & Sons Inc., New York.

[10] W. Yantasee, Y. Lin, G. Fryxell, B. Busche, Anal. Chim. Acta 502 (2004) 207-212.

[11] A. Ciucu, R.P. Baldwin, In: Biosensors for Environmental Monitoring. Chemically modified electrodes based on enzymes. Biosensors for Environmental Monitoring (2000) Bucharest, Romania.
[12] W. Kutner, J. Wang, M. L'Her, R. Buck, Pure App. Chem. 70 (1998) 1301 -1318.
[13] G. Favero, L. Campanella, A. D'Anmbale, T. Ferri, Microchem. J. 76 (2004) 77-84.
[14] K. Grennan, G. Strachan, A. Porter, A. Killard, M.R. Smyth, Anal. Chim. Acta. 500 (2003) 287-298.

[15] A. Zimer, R. Bertholdo, M. Grassi, A. Zarbin, L. Mascaro, Electrochem. Comm. 5 (2003) 983-988.

[16] L. Rotariu, C. Bala, V. Magearu, Anal. Chim. Acta 513 (2004) 119-123.
[17] B. Prieto-Simon, E. Fabregas, Biosens. Bioelectron. 19 (2004) 1131-1138.
[18] D. Shankaran, N. Uehera, T. Kato, Sens. Actuat. B 87 (2002) 442-447.
[19] N. Zhu, A. Zhang, Q. Wang, P. He, Y. Fang, Anal. Chim. Acta, 510 (2004) 163-168.
[20] S. Cosnier, A. LePellec, R. Marks, K. Pene, J. Lellouche, Electrochem. Comm. 5 (2003) 973-977.
[21] A. Ludi, H.U. Gudel, In Structure and Bonding, Dunitz, J. D., Ed., Springer-Verlag: Berlin, 1973, Vol. 14, pp 1-21.
[22] F. Herren, P. Fischer, A. Ludi, W. Halg, Inorg. Chem. 19 (1980) 956.
[23] A.G. Sharpe, The Chemistry of Cyano Complexes of the Transition Metals; Academic Press: New York, 1976.
[24] D. Shaojun, L.J. Fengbin, J. Electroanal. Chem. 210 (1986) 31-44.
[25] M.K. Carpenter, R.S. Conell, S.J. Simko, Inorg. Chem. 29 (1990) 845-850.
[26] P.J. Kulesza, M.A. Malik, R. Schmidt, A. Smolinska, K. Miecznikowski, S. Zamponi, A. Czerwinski, M. Berrettoni, R. Marassi, J. Electroanal. Chem. 487 (2000) 57-65.

[27] N. Sattarahmady, H. Heli, An electrocatalytic transducer for L-cysteine detection based on cobalt hexacyanoferrate nanoparticles with a core-shell structure, Anal. Biochem. 409 (2011) 74-80.

[28] M.R. Majidi, K. Asadpour-Zaynali, B. Hafezi, Sensing L-cysteine in urine using a pencil graphite electrode modified with a copper hexacyanoferrate nanostructure, Microchim. Acta 169 (2010) 283-288.

[29] R. Shen, X. Li, G. Lium, Y. Ji, G. Wang, B. Fang, Synthesis and Characterization of Chromium Hexacyanoferrate/Multiwalled Carbon Nanotube Composite and Its Biosensing for L-Cysteine, Electroanalysis 22 (2010) 2383-2388.

[30] H.-W. Chu, R. Thangamuthu, S.-M. Chen, Preparation, characterization and electrocatalyticbehavior of zinc oxide/zinc hexacyanoferrate and ruthenium oxide/hexacyanoferrate hybrid film-modified electrodes, Electrochim. Acta 53 (2008) 2862-2869.

[31] L. Guadagnini, D. Tonelli, M. Giorgetti, Improved copper hexacyanoferrate electrode for hydrogen peroxide detection, Electrochimica Acta 55 (2010) 5036-5039.

[32] O. Makowski, J. Stroka, P. J. Kulesza, M. A. Malik, Z. Galus, Electrochemical identity of copper hexacyanoferrate in the solid-state: evidence for the presence and redox activity of both iron and copper ionic sites, J. Electroanal. Chem. 532 (2002) 157-164.

[33] L. Guadagnini, E. Salatelli, A. Kharina, D. Tonelli, Electrochemically deposited thiophene-based polymers as protective agents for prussian blue thin films, J. Solid State Electrochem. 18 (2014) 2731–2742.

[34] I.L. de Mattos, L. Gorton, T. Ruzgas, A.A. Karyakin, Sensor for Hydrogen Peroxide Based on Prussian Blue Modified Electrode: Improvement of the Operational Stability, *Anal. Sci.* 16 (2000) 795-798.

[35] L. Guadagnini, M. Giorgetti, D. Tonelli, Pure copper vs. mixed copper and palladium hexacyanoferrates for glucose biosensing applications, J. Solid State Electrochem. 17 (2013) 2805–2814.

[36] P.J. Kulesza, M.A. Malik, J. Skorek, K. Miecznikowski, S. Zamponi, M. Berrettoni, M. Giorgetti, R. Marassi, Hybrid Metal Cyanometallates - Electrochemical

Charging and Spectrochemical Identity of Heteronuclear Nickel/Cobalt Hexacyanoferrate, J. Electrochem. Soc. 146 (1999) 3757-3761.

[37] Z. P. Xu, J. Zhang, M. O. Adebajo, H. Zhang, C. Zhou, Applied Clay Science 53 (2011) 139–150.

[38] A. N. Ay, B. Zümreoglu-Karan, A. Temel, L. Mafra, Applied Clay Science 51 (2011) 308– 316.

[39] K. H. Goha, T.T. Lima, Z. Dong, Water Research 42 (2008) 1343–1368.

[40] A. Fonseca Lucredito, E. M. Assaf, Journal of Power Sources 159 (2006) 667.

[41] A. Fonseca, E.M. Assaf, Journal of Power Sources 142 (2005)154.

[42] Z. Chen, Y. Yan, S. S. E. H. Elnashaie, Chemical Engineering Science 58 (2003) 4335.

[43] M. E. E. Abashar, 29 (2004) 799.

Chapter 2

AIM OF THE THESIS

The primary objective of this thesis can be summed up as the study and development of novel electrochemical sensors based on chemically modified electrodes (CME) that could complement or even substitute for traditional sensors in the determination of various oxidizable analytes. The work on electrochemical sensors was broadly divided in two parts: 1) CMEs based of hybrid hexacyanoferrates of copper and cobalt and 2) CMEs based on carbon nanomaterials like graphene oxide (GO) and multi-walled carbon nanotubes (MWCNTs).

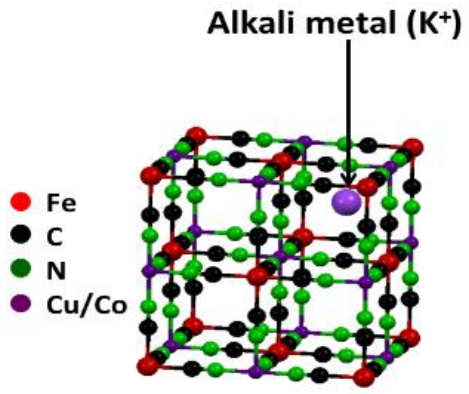

Figure 2.1 3 dimensional crystal structure of Copper Cobalt hexacyanoferrate (Cu-CoHCF)

Mixed valence hexacyanometallates (most often as hexacyanoferrates, MeHCFs) have often been used for sensing since they are excellent electron transfer mediators. One advantage of the hexacyanoferrates is that they can be electrodeposited onto various electrode surfaces to provide insoluble films through repetitive redox cycling of a solution containing ferro or ferricyanide and a soluble Me salt. However, one major drawback of MeHCFs lies in their limited stability both during operation in neutral and alkaline pHs and during potential cycling. To overcome this drawback and to improve the stability of the HCF, in this study additional steps like thermal treatment following the electrochemical deposition of the HCF was carried out. Besides, introduction of one more metal center in addition to Me in MeHCFs had been known

to further increase the stability of the HCF films [ref], this fact was also employed and hence a mixed hexacyanoferrate of copper and cobalt was prepared.

L-cysteine (CySH) and L-glutathione (GSH) are low molecular-mass biological endogenous amino thiols, widely occurring in animal tissues and fluids with significant biological significance. Having in mind the importance of thiols and the properties of metal hexacyanoferrates, in this work we carried out research aimed to employ hybrid copper-cobalt hexacyanoferrate (Cu-CoHCF) to develop a CME for the amperometric determination of three thiols, including 1,4-butanedithiol.

Further, we also aimed to develop an electrochemical sensor for the indirect electrochemical determination of Mercury (Hg^{2+}) exploiting the fact that, in the presence of a thiol and Hg^{2+}, an electro-inactive complex is formed. Generally, the determination of Hg^{2+} in any sample requires the use of large and expensive instruments like inductively coupled plasma atomic emission spectroscopy (ICP-AES) or atomic absorption spectroscopy (AAS). Since it was theoretically possible to develop a sensor for the determination of Hg^{2+} if the Cu-CoHCF modified glassy carbon electrode (GCE) was able to give promising results for the determination of thiols, we decided to pursue with the development of such a sensor.

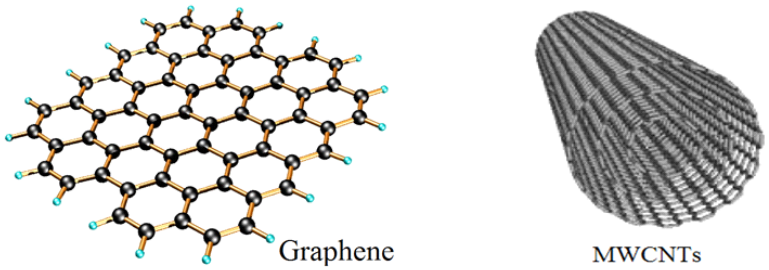

Figure 2.2 – Structural representation of grapheme and multiwalled carbon nanotubes

In the field of chemically modified electrodes, multiwalled carbon nanotubes (MWCNTs) have been widely used due to their unique structural, electronic and physical properties with one of the most important characteristics being their reported ability to promote electron-transfer processes. Very recently graphene (GR), a 2D

carbon material comprised of a single sheet of hexagonally packed carbon atoms, has attracted tremendous attention because of its unique nanostructure and extraordinary electro-catalytic properties, such as high surface area, excellent conductivity, and high mechanical strength. Based on these characteristics, GR is considered as an ideal electrode material for electrochemical and biosensing. However, synthesis of graphene is expensive; hence we used graphene oxide (GO) which can be easily reduced electrochemically to obtain a material almost equivalent to graphene for use as a modifier.

There are multiple ways of preparing CMEs based on carbon nanomaterials like drop casting, spin coating and electrochemical deposition. The aim here was to carry out an extensive investigation of various configurations of the CMEs comprising of GO and MWCNTs *vis-à-vis* only GO, only CNTs, bilayers with CNTs on top and vice-versa and a composite configuration composing of a mixture of GO and MWCNTs in solution. Furthermore, the CMEs were used for determination of various oxidizable analytes like catechol and dopamine which are representative of polyphenols.

Additional work was also conducted on development of layered double hydroxides (LDH) containing Ni, Mg and Al for catalytic applications within the time constraints of the PhD. Preliminary investigation on the electrochemical synthesis of catalytic precursors for the steam reforming and the catalytic methane partial oxidation reactions shall be conducted.

Chapter 3

EXPERIMENTAL SECTION

3.1. INSTRUMENTAL EMPLOYED TECHNIQUES

3.1.1. CYCLIC VOLTAMMETRY AND LINEAR SWEEP VOLTAMMETRY

Cyclic voltammetry (CV) is the most widely used controlled potential technique suitable to acquire qualitative and often, quantitative information about the electrochemical reactivity of species in solution. In particular, CV allows rapid estimation of the redox potentials of the electroactive species under study. It is performed in a solution where a suitable concentration of supporting electrolyte is present, so that the mass transfer to the electrode surface occurs essentially by diffusion.

A CV test consists of scanning linearly the potential of a stationary electrode, according to a triangular potential waveform, as reported in Figure 3.1-A, Single or multiple subsequent cycles can be performed. During the potential sweep, the current is continuously measured; the plot of the current *vs.* the potential is called a *cyclic voltammogram.*

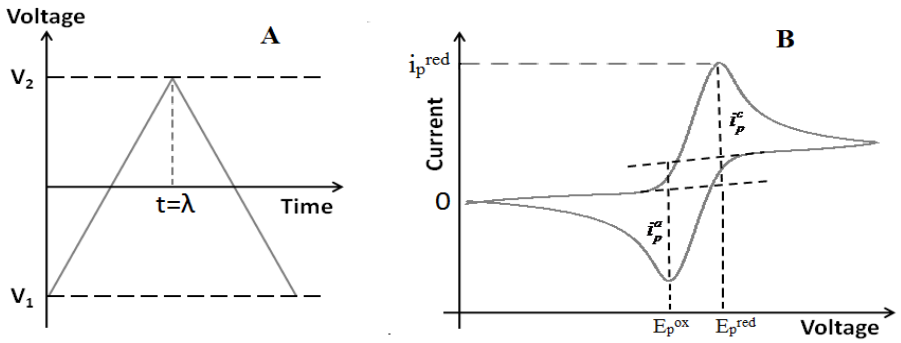

Figure 3.1 – CV experiment: a) Potential/time excitation signal, λ=time of sweep reversal; b) typical cyclic voltammogram for a reversible Ox + ne^- ↔ Red redox process.

In Figure 3.1-B the typical response of a reversible redox couple Ox/Red is shown, both species being soluble and stable in the solution phase. Assuming that only the oxidised form Ox is present initially in the solution, as the applied potential approaches the standard potential value of the redox couple, a cathodic current starts arising and increases until reaching a maximum. After traversing the current maximum relative to reduction, the direction of potential sweep is reversed. Then, the Red species generated in the proximity of the electrode during the forward scan is re-oxidised back to Ox, and an anodic peak is recorded. The characteristic peak shapes of the cyclic voltammograms are accounted for by the evolution of the concentration profile of the electroactive species within the diffusion layer, near the electrode surface, and reflect the changes of the concentration gradient at the electrode with potential and at time passing. The peak potentials and the peak currents of the direct and reverse responses reflect the reversibility degree of the Red/Ox couple. For an uncomplicated reversible system the heights of the forward and reverse current peaks are equal to each other when the backward peak current value is measured properly (see Figure 3.1-B). For a non-reversible reduction, an appreciable "overpotential" is required for the electrode reactions to take place: the potentials of the forward and reverse peaks shift to more negative and more positive values, respectively, and are sweep-rate dependent, in contrast with the reversible case. The height of the backward peak with respect to the forward one, as well as the peak potential separation, depend on the degree of irreversibility of the charge transfer and on the potential sweep rate.

By considering an electrode modified by a monolayer of electroactive species, diffusion does not constitute the rate-limiting step of the process anymore, since the electroactive species is on the electrode surface. The cathodic-anodic response looks like that in Figure 3.2. Both the forward and backward peaks are symmetric in shape and located at the same potentials: for both peaks, the current falls to zero after consuming the amount of charge required to full transformation into the alternative oxidation state. The peaks assume similar shape and height.

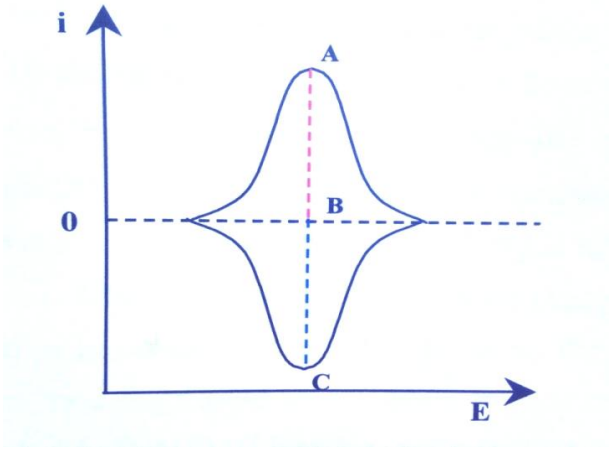

Figure 3.2 – Typical voltammetric plot obtained with an electrode surface modified by a monolayer. A – B = i_p^{red} ; B – C = i_p^{ox}.

At variance with the case of a surface monolayer reversibly reduced/oxidised, the i *vs.* E curve typically recorded for CP electrode coatings is asymmetric in shape and exhibits more or less large forward to backward peak separation. Furthermore, referring to the p-doping process, the current still assumes high values after traversing a maximum, rather than falling to zero, as it is the case for a monolayer deposit. The response is actually conditioned by many concomitant processes of charge percolation through the CP, ion migration and diffusion, the relevant weight depending on the thickness of the deposit, on its porosity and conductivity, as well, of course, by the characteristics of the solution.

CV responses are very sensitive to the conditions under which the deposit is prepared and to the medium in which the voltammetry is performed; in particular, preparation and cycling conditions have strong influence on structure and morphology of the film. Of chief importance is the mobility of counterions, which is strongly influenced by the porosity and by the degree of solvation of the film, as well as by the nature of the counterions(s).

In any case, when only forward potential scan is applied to the electrode, the terms *Linear Sweep Voltammetry (LSV)* is generally used.

3.1.2. CHRONOAMPEROMETRY

Chronoamperometry is an electrochemical technique in which the current is measured versus time as a response to a (sequence of) potential pulse. The recorded current can be analysed and its nature can be identified from the variations with time. For example: at short times the capacitive current is dominant ($\propto e^{-t/RC}$; with R = solution resistance and C = capacitance) while at longer time scales, the diffusion limited faradaic current prevails ($\propto t^{-1/2}$).

Principle of chronoamperometry

At the beginning of the transient experiment the potential of the working electrode is held at E_i (Fig. 3.3-a). At *t=0*, the potential is instantaneously changed to a new value E_1, and corresponding current time response is recorded as shown in Fig. 3.3-b.

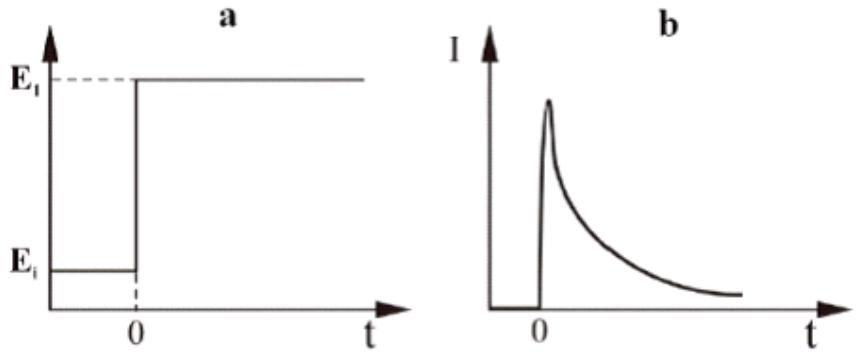

Figure 3.3 - The chronoamperometric experiment. a) The potential-time profile applied during experiment, E_i is initial value where no reduction of O occurs and E_1 is a potential at which the reduction occurs . b) The corresponding response of the current due to changes of the potential.

In order to determine the exact form of current-time dependence for a planar electrode, Cottrell equation is used:

$$|I| = \frac{nF\sqrt{D_o}\, c_o^{\infty}}{\sqrt{\pi t}}$$

For a *diffusion controlled process*, it can be noticed that the current falls as $t^{-1/2}$. This feature is frequently used as a test for this type of process and from the slope of I *vs.* $t^{-1/2}$ the diffusion coefficient D_O can be calculated.

It is important that such an analysis has to be applied over a broad time interval in order to ensure the reliability of results. At short times the current consists of a large non faradaic component due to charging of the double-layer capacitance. The non-faradaic current decays exponentially with time constant R_uC_d, where R_u is an uncompensated resistance and C_d is the double layer capacitance:

$$|\mathrm{I}| = \frac{E}{R_u} e^{-t/R_u C_d}$$

Thus, the time constant R_uC_d will determine the shortest time required to conduct the chronoamperometric experiment. Therefore, measurements should be performed for times which are much greater than R_uC_d. After passing the time equal to R_uC_d, the double layer capacitance is charged by 63 % and after $3R_uC_d$ by 95 %, see Eq. 3.3. Thus, knowing the time constant one can easily estimate the time needed for double layer charging.

At long time, however, the natural convection (may be caused by temperature and concentration gradients) comes into effect, and diffusion, in that case, is not the only mode of the mass transport. Hence, the typical time range of chronoamperometric measurements lies normally in the range from 0.001 to 10 s. However, there are a number of additional instrumental and experimental limitations. For example, current and voltage characteristics of a potentiostat can limit the current maximum and time resolution.

Even though chronoamperometry is relatively a simple technique, there are a number of difficulties, which are related to the interpretation of the current-transient curve. Hence, it is very important to find the possibility of comparative analysis of the chronoamperometric results with the results of cyclic voltammetry and other

techniques. This type of comparison will also help to understand the studied system more completely and with better precision.

3.1.3. DIFFERENTIAL PULSE VOLTAMMETRY

Differential Pulse Voltammetry (DPV) technique is one of the most widely used electrochemical technique for analytical applications. This is due to the possibility to strongly reduce the signal to the noise ratio with respect to LSV. In this case, the potential is progressively increased by applying a series of potential pulses of fixed small amplitude, variable typically from 10 to 100 mV, superimposed to a slowly changing base potential. The duration of the pulse, τ, is usually 1 to 100 msec and the interval between subsequent pulses is typically 0.1 to 5 sec. The current measurement is made at two points for each period, the first one located just before the application of the pulse and the second one at the end of the pulse. A typical potential waveform is shown in Figure 3.4. All the reported electrochemical parameters are selected to allow for the decay of the non-faradaic (charging) current down to a negligible value, while faradaic current, which is directly correlated to the electrochemical process, is still significant.

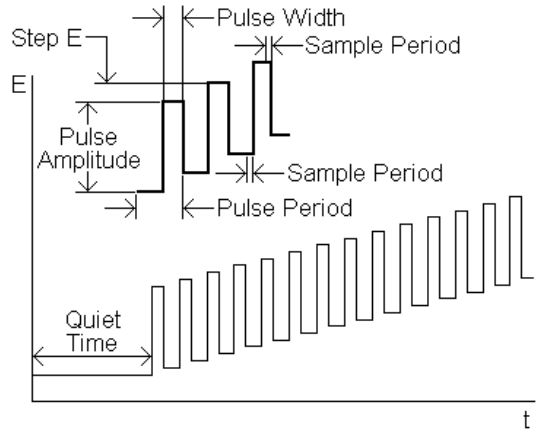

Figure 3.4 – Potential waveform for Differential Pulse Voltammetry

The resulting voltammogram displays on the abscissa axis the potential to which the pulse is stepped and on the ordinate the difference between the two current measures corresponding to each pulse.

3.1.4. SCANNING ELECTRON MICROSCOPY

Scanning Electron Microscopy (SEM) constitutes a fundamental technique for the characterisation of different surfaces. This technique is based on the interaction between an electron beam and the surface of a sample. The electron beam is firstly produced, by different kinds of sources, and is then accelerated from 1 to 40 keV energy. The emitted electrons are then focussed by a suitable system of magnetic lenses, in order to form a very small spot on the surface sample. The spot is moved to different points of the sample by a suitable system of scanning coils. A general scheme of the SEM instrument is reported in Figure 3.5-a.

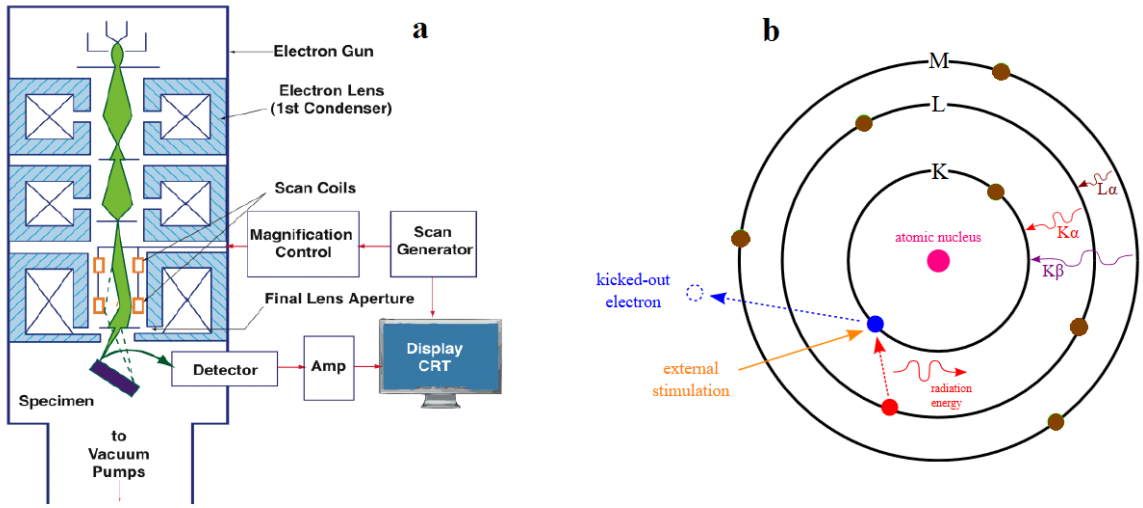

Figure 3.5 – a) Block diagram of a typical SEM; b) processes at the base of EDX

The interaction between the electron beam and the surface generates different signals, each one bearing different information about the morphology and the composition of the sample. Two important types of interactions occur between the incident electrons and the sample's atoms, resulting in the three primary signals (Fig. 3.6). First, some of the incident electrons interact with the electrons associated with the atoms of the sample, "knocking them out" of the conduction band and other orbitals, and generating secondary electrons (SE). The atoms from which electrons have been removed are now in "excited states" and "relax" as electrons from higher energy levels fill the vacated sites. Second, each of these relaxation events is accompanied by the release of energy equal to the difference in energies between the two atomic energy levels involved.

Transitions involving inner shell electrons often result in the generation of x-ray photons. This is identical to the atomic process described in case of x-ray fluorescence spectroscopy. As in x-ray fluorescence spectroscopy, the energies of these x-rays can be compared to the known characteristic energies of each element, enabling the atoms in the sample to be chemically identified. And third, other incident electrons interact with the much heavier nuclei of the atoms in the sample. These electrons typically "bounce back," as would a ping pong ball striking a bowling ball. For obvious reasons, these are termed backscattered electrons.

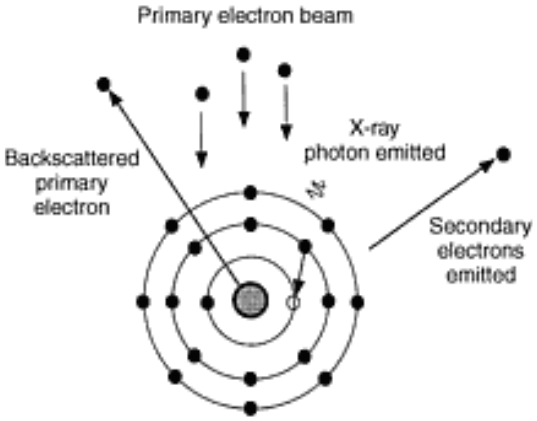

Figure 3.6 Interaction of the primary electron beam with atoms in the sample resulting in backscattered primary electrons, secondary electrons, and characteristic x-rays

The electron beam penetrating through the sample produces a large amount of secondary electrons, due to inelastic scattering processes, possessing a low energy (typically below 50 eV). For this reason, they are detected when emitted from the regions close to the surface of the sample, typically from the depth smaller than a few tens of nm, depending on the nature of the material. The secondary electrons are detected by a suitable detector.

Backscattered electrons (BSE) consist of high-energy electrons originating in the electron beam, that are reflected or back-scattered out of the specimen interaction volume by elastic scattering interactions with specimen atoms. Since heavy elements

(high atomic number) backscatter electrons more strongly than light elements (low atomic number), and thus appear brighter in the image, BSE are used to detect contrast between areas with different chemical compositions.

The number of secondary electrons reaching the detector also depends on the geometrical factors, in particular, on the angle between the incident electron beam and the sample surface, as well on the position of the detector with respect to the sample. These geometrical factors are the basis for the formation of images bearing information about the morphology of the sample: when the spot is moved by the scanning coils in a position corresponding to a bump of the sample surface, the number of secondary electrons reaching the detector is relatively high, and the region appears bright in the images; on the contrary, in correspondence to a depression, the number of electrons is rather small and the region appears dark in the images.

Finally, it is worth noticing that SEM experiments are generally performed in high vacuum conditions (typically below 10^{-5} torr) in order to avoid collisions between the electrons of the beam and the gas molecules present in the instrument chamber, which lead to the reduction of the number of electrons reaching the surface and to the increase of the spot size, negatively affecting the resolution of the images. It is important to control that the alterations of the sample surface induced by the electron beam are limited.

The incident electron beam also induces the formation of a core hole in the atoms of the sample (Figure 3.5-b). This hole is filled by an outer electron; this process implies a release of energy in form of X-rays, especially when the sample contains heavy atoms. The energy of the emitted X-rays is related to the nature of the atoms present in the sample, while the number of photons is dependent on their concentration. *Energy Dispersive X-Ray Spectroscopy* (EDX), often coupled to SEM, is based on the measurement of the number of photons possessing a specific energy and constitutes a widely employed technique for fast qualitative and semi-quantitative analysis of the composition of the thin films. A suitable solid state detector is normally located close to the sample surface, laterally with respect to the ensemble of the lenses.

3.1.5. FT-IR SPECTROSCOPY

Mid-Infrared (IR) spectroscopy is an extremely reliable and well recognized fingerprinting method. Many substances can be characterised, identified and also quantified. One of the strengths of IR spectroscopy is its ability as an analytical technique to obtain spectra from a very wide range of solids, liquids and gases. However, in many cases some forms of sample preparation are required in order to obtain a good quality spectrum. Traditionally IR spectrometers have been used to analyse solids, liquids and gases by means of transmitting the infrared radiation directly through the sample. Where the sample is in a liquid or solid form the intensity of the spectral features is determined by the thickness of the sample and typically this sample thickness cannot be more than a few tens of microns.

Attenuated Total Reflectance (ATR) accessories remove the need for transmission cells and KBr pellets when performing measurements on liquid, semi-solid and solid materials. The ATR spectroscopy works especially well for opaque samples or samples that are too thick for transmission measurements. The technique gives information about the surface properties and condition of materials and can be useful for both qualitative and quantitative measurements.

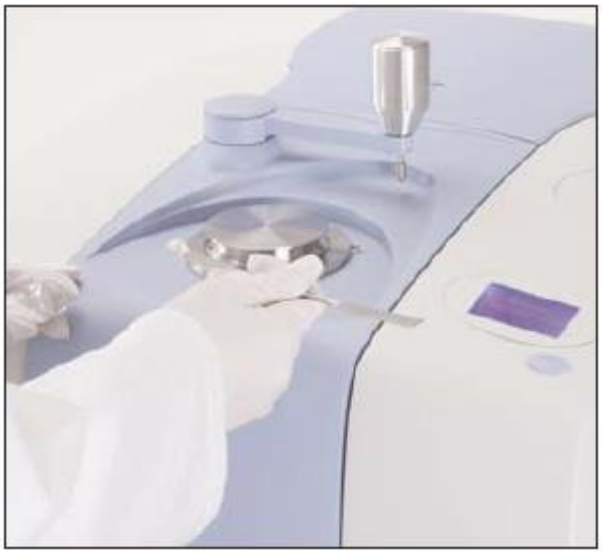

Figure 3.7 Placing a powder sample onto the Universal diamond ATR top-plate for analysis

Principles of ATR

An attenuated total reflection accessory operates by measuring the changes that occur in a totally internally reflected infrared beam when the beam comes into contact with a sample (Figure 3.8).

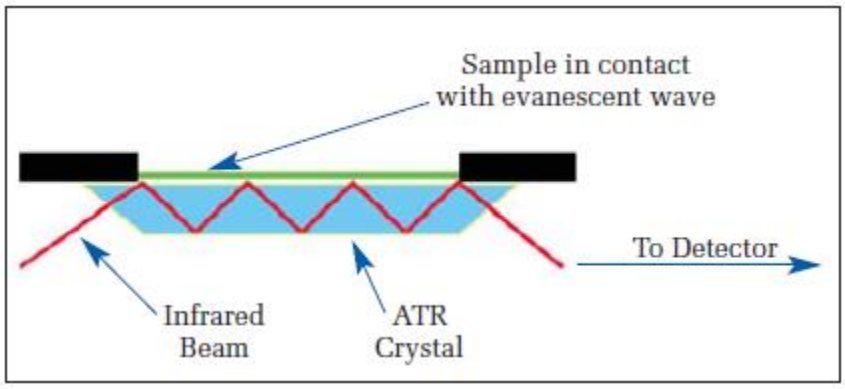

Figure 3.8 A multiple reflection ATR system.

An infrared beam is directed onto an optically dense crystal, with a high refractive index, at a certain angle. This internal reflectance creates an evanescent wave that extends beyond the surface of the crystal into the sample held in contact with the crystal. It can be easier to think of this evanescent wave as a bubble of infrared that sits on the surface of the crystal. This evanescent wave protrudes only a few microns (0.5 μm - 5 μm) beyond the crystal surface and into the sample.

Consequently, there must be good contact between the sample and the crystal surface. In regions of the infrared spectrum where the sample absorbs energy, the evanescent wave will be attenuated or altered. The attenuated energy from each evanescent wave is passed back to the IR beam, which then exits the opposite end of the crystal and is passed to the detector in the IR spectrometer. The system then generates an infrared spectrum. For the technique to be successful, the following two requirements must be met:

• The sample must be in direct contact with the ATR crystal as the evanescent wave protrudes only a few microns. Generally in case of most analyses, the diamond crystal is used for ATR-IR analysis in case of solids.

• The refractive index of the crystal must be significantly greater than that of the sample or else internal reflectance will not occur – the light will be transmitted rather than

internally reflected in the crystal. Typically, ATR crystals have refractive index values between 2.38 and 4.01 at 2000 cm^{-1}. It is safe to assume that the majority of solids and liquids have much lower refractive indices.

In summary, ATR is an IR sampling technique that provides good quality data in conjunction with the best possible reproducibility of any IR sampling technique. Since, we were working with carbon nanomaterials to prepare the modified electrodes, it was better to take the IR spectra with the ATR-IR setup than a conventional IR instrument.

3.2. INSTRUMENTATION

The electrochemical experiments were performed on a potentiostat/galvanostat electrochemical workstation CHI 660C (CH Instruments Inc, Austin, TX, USA) interfaced with a personal computer. A three-electrode conventional electrochemical cell was employed, with a 3 mm diameter glassy carbon electrode (GCE) as the working, a saturated calomel electrode (SCE) as the reference and a Pt wire as the counter electrode, respectively. A thin film of the required modifier (Cu-CoHCF or the carbon nanomaterials) was coated onto the GCE. The electrochemical experiments were performed in an environment of nitrogen as and when the case required.

Figure 3.9 CHI 660C Potentiostat interfaced with a personal computer

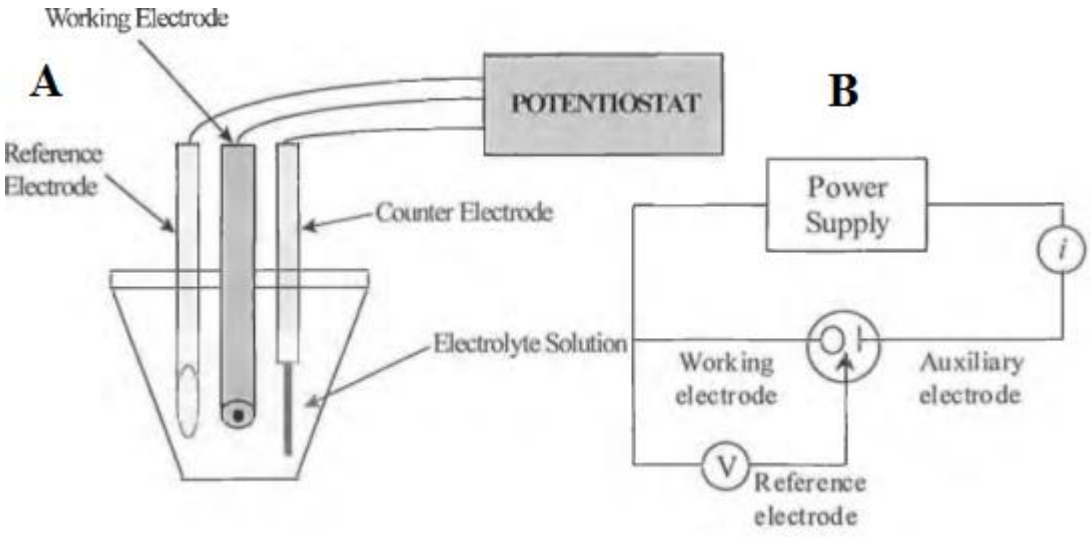

Figure 3.10 (A) Simple schematic of a typical 3-electrode voltammetric cell and (B) diagram showing how potentiostat (power supply) controls cell potential.

An EVO 50 Series (LEO ZEISS) Scanning Electron Microscope (SEM) using an OXFORD INCA 350 EDS was employed to investigate the morphology of HCF films and study their local elemental composition. The instrument acquired magnified topographic images of the sample at an accelerating voltage of 20 kV with the beam current as 100 pA.

Atomic force microscopy (AFM) images were taken by using a Scanning probe microscope Vista 100 (Burleigh Instruments) operating in contact mode with standard silicon nitride tip at a force of 29 nN for the as-such Cu-CoHCF modified GCE and 30 nN for the thermally treated electrode.

X-ray diffraction patterns were obtained with Cu-K radiation in reflection mode directly on the graphite electrodes by means of an X'Pert PANalytical diffractometer equipped with a fast X' Celerator detector, 0.065° step, 20s/step. The slow scans were recorded with 600s/step integration time.

Infrared spectra (IR) of the Cu-CoHCF deposited on graphite paper were taken on a Perkin Elmer Spectrum Two™ Attenuated Total Reflectance (ATR) FTIR spectrometer. Flame atomic absorption spectrometry (FAAS) (ICE 3000 Series,

ThermoScientific, Rockford, IL, USA) was used to analyze copper to cobalt molar ratio in the thermally treated Cu-CoHCF electrode. The spectrometer was equipped with a copper/cobalt hollow cathode lamp, and a deuterium lamp for background correction. An air-acetylene flame was used for atomization using a solution acidified with HNO_3 after dissolving the HCF in 0.5 M aqueous LiOH. The instrument was operated under the conditions recommended by the manufacturer and calibrated using standard solution of Co^{2+} and Cu^{2+} in HNO_3 (Carlo Erba Reagents, Val-de-Reuil, France). UV/Vis spectra of sample coatings on ITO electrodes (Delta Tech, R_s = 4–8 Ω cm^{-1}) were recorded in reflectance using an OceanView spectrophotometer at room temperature.

3.3. CHEMICALS, SAMPLES AND PROCEDURES

All chemicals were of analytical reagent grade and were used as received, without further purification. All aqueous solutions were prepared with doubly distilled (DD) water.

3.3.1. CMEs BASED ON COPPER COBALT HEXACYANOFERRATE

L-cysteine, L-glutathione, 1,4-butanedithiol, $Co(NO_3)_2 \cdot 6H_2O$ and KNO_3 were provided by Sigma-Aldrich (St. Louis, Missouri). The solutions of L-cysteine, L-glutathione and 1,4-butanedithiol were prepared daily fresh, deoxygenated before use, and were stored at 4º C when not in use. $CuCl_2 \cdot 2H_2O$ was purchased from Merck (Germany), $HgCl_2$ and H_3PO_4 from Farmitalia Carlo Erba SpA (Milan, Italy) and $K_3[Fe(CN)_6]$ from Riedel-de Haën (Germany). Phosphate buffer solution (PBS) was prepared from a 0.1 M solution of H_3PO_4 with the pH being set to the chosen value by subsequent addition of KOH.

3.3.1.1. Preparation of the chemically modified electrode

Prior to surface modification, the glassy carbon surface was gently polished on a fine (4000 grit) wet SiC sandpaper until a mirror finish was obtained. Then it was thoroughly rinsed with DD water and cycled many times in 0.25 M KNO_3 at 0.050 V s^{-1} between 0 and +1.2 V, until superimposable voltammograms were recorded (blank signal).

The working electrode, soaked in a de-aerated solution of 0.25 M KNO_3, was modified with the film of Cu-CoHCF by a classic potentiodynamic method. To this aim, the solutions of the required salts were added, under magnetic stirring, in the following order so as to obtain the concentrations: 0.125 mM $CuCl_2$, 0.125 mM $Co(NO_3)_2$ and 0.125 mM $K_3Fe(CN)_6$. 40 cycles between 0 and +1.0 V, at 0.050 V s^{-1}, were applied to induce the precipitation of the Cu-CoHCF film on the GCE. After rinsing with water, some electrodes were dried at room temperature (25° C) until dryness and some were dried at 100°C for 1 h (thermal treatment). This treatment was aimed to increase the stability of the Cu-CoHCF film as previously demonstrated for Prussian Blue (PB). In fact, the presence of water molecules inside the PB polycrystal affects the conducting properties and, as a consequence, the stability of the corresponding PB modified electrodes. When GC electrodes modified with a PB film were kept at 100°C for 1 hour, an increase in the amount of electroactive PB was demonstrated [de Mattos et al. Anal. Sci. 16 (2000) 795-798]. A similar procedure as that for glassy carbon was deployed for graphite paper in the deposition of Cu-CoHCF which was used to record directly the XRD pattern and to find out the molar ratio of Cu to Co by flame atomic absorption spectroscopy.

3.3.1.2. Chronoamperometric determination of mercury

The Cu-CoHCF modified GCE was immersed in a conventional three electrodes electrochemical cell in the presence of 0.1 M KNO_3 and 0.1 M PBS, pH 4. It was poised at +0.65 V and the current was recorded until a stable background was reached. Then the thiol (CySH or BdSH) was added to the solution so that an appropriate concentration

was obtained. When the oxidation current was stable, subsequent additions of $HgCl_2$ were carried out, and, consequently, rapid decreases of current were recorded. This was possible as Hg^{2+} has a strong affinity for the sulphur present in the thiol group and in the presence of thiol forms an electro-inactive complex which could be measured by the rapid drecerease in the oxidation current due to the thiol.

$$R\% = \frac{(i_0 - i_R)}{i_0} \cdot 100 \qquad \text{(Eq. 3.1)}$$

where i_0 and i_R are the oxidation currents in the absence and in the presence of Hg^{2+}, respectively, and R% is proportional to Hg^{2+} concentration.

3.3.2. CME BASED ON GRAPHENE OXIDE AND CARBON NANOTUBES

Aqueous GO solution (4 mg ml^{-1}), MWCNTs (O.D. × wall thickness × L = 20-30 nm × 1-2 nm × 0.5-2 μm), anhydrous sodium acetate (99% pure), dopamine hydrochloride (98% pure), H_3BO_3 and $Ru[(NH_3)_6]Cl_3$ (98% pure) were obtained from Sigma-Aldrich. H_3PO_4 was obtained from Farmitalia Carlo Erba S.p.A., $K_3[Fe(CN)_6]$ (> 99% pure) from Riedel-de Haën and catechol (>99% pure) from ACROS Organics. The solutions of catechol and dopamine hydrochloride were prepared and deoxygenated before use, and were stored at 4º C when not in use. Phosphate buffer solution was prepared from a 0.1 M solution of H_3PO_4 with the pH being set to the chosen value by subsequent addition of KOH. Acetate buffer solution was prepared from a 0.1 M solution of CH_3COONa with the pH being set to the chosen value by subsequent addition of pure acetic acid. All aqueous solutions were prepared with doubly distilled water with the exception of the multiwalled carbon nanotubes which were suspended in N,N-dimethyl formamide (DMF, 2 mg ml^{-1}). The suspension was submitted to ultrasonic treatment for 20 min at 40% maximum power using a Bandelin Sonorex Super Sonicator (RK 103 H). The DMF solution was kept in ice bath during sonication to prevent loss of the solvent by evaporation.

3.3.2.1. Preparation of the chemically modified electrode

Prior to the electrochemical measurements, the glassy carbon surface was gently polished on a wet (4000 grit) SiC sand paper until a mirror finish was obtained. Then it was thoroughly rinsed with DD water and left for drying at room temperature.

The chemically modified electrode was prepared by drop casting the carbon nanomaterials (GO or MWCNTs) directly on the glassy carbon surface. Different amounts of GO and MWCNTs in DMF were tried to prepare the chemically modified electrodes. Three different configurations were tested as shown below, indicating the carbon nanomaterial(s) used, and the deposition order in the case of the bilayers.

1-Bilayer MWCNTs/GO (Bil-1)

2-Bilayer GO/MWCNTs (Bil-2)

3-Composite GO-MWCNTs (Composite)

In addition, two other CMEs were fabricated employing only GO or MWCNTs (named as GO and MWCNTs) in order to compare the electrochemical performances of the mixed systems and to understand if a synergism between the two nanomaterials occurs. Each kind of CME was prepared using the same total mass of carbon nanomaterials (0.4 g, corresponding to 0.2 g + 0.2 g of GO and MWCNTs). In any case, after casting a material the electrodes were dried at 60° C in an oven for 15 min.

Figure 3.11 Drop casting of carbon nanomaterials on bare GCE

Electrochemical reduction of GO is typically achieved by applying a negative potential, around -1.0 or -1.2 V, to GO films casted on conductive substrates, or repeated voltammetric cycles with the lowest potential of about -1.2 V.

Chapter 4

RESULTS AND DISCUSSIONS

4.1. CMEs BASED ON COPPER COBALT HEXACYANOFERRATE FOR DETERMINATION OF THIOLS

4.1.1. ELECTROSYNTHESIS AND CHARACTERISATION OF Cu-CoHCF MODIFIED GCE

Fig. 4.1 shows the cyclic voltammogram recorded during the electrodeposition process of the Cu-CoHCF film. The steadily increasing currents both for the anodic and cathodic peaks with increasing number of scans shows that the HCF films are deposited continuously on the GC surface.

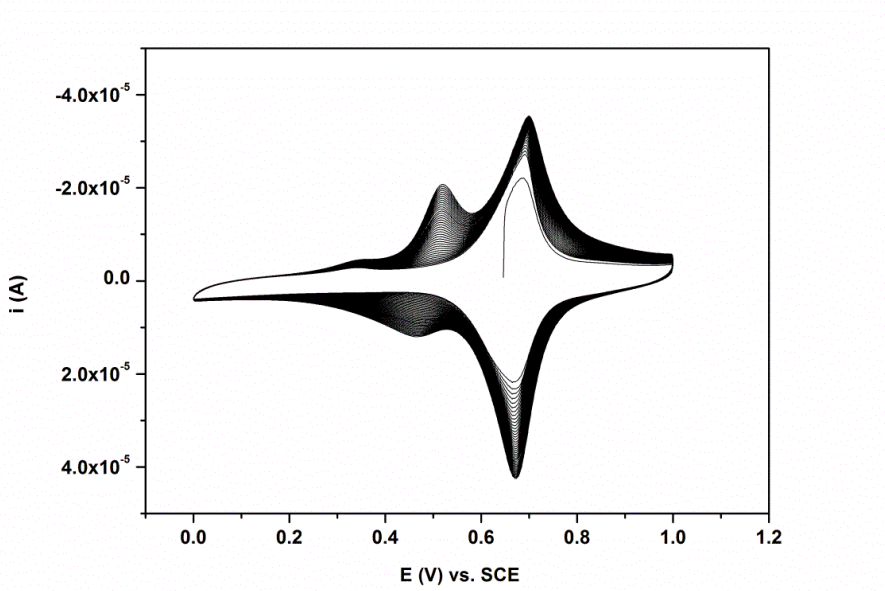

Figure 4.1 CV for electrodeposition process of a hybrid Cu-CoHCF film on bare GC electrode, 40 cycles between 0 and +1.0 V (vs. SCE). Scan rate: 0.050 Vs^{-1}

To better characterise the nature of the HCF modifier in terms of crystallinity of the phase present on the electrode surface, an X-ray diffraction pattern was obtained. As shown in Fig. 4.2, the scans recorded at 20s/step revealed only the crystal phase (graphite) of the electrodes, but some noise in the background suggested carrying out a

deeper investigation. The need for strong conditions is due to the low amount of deposited material and to the presence of nanosized Cu-CoHCF aggregates, as shown by SEM images (Fig. 4.7 B and C).

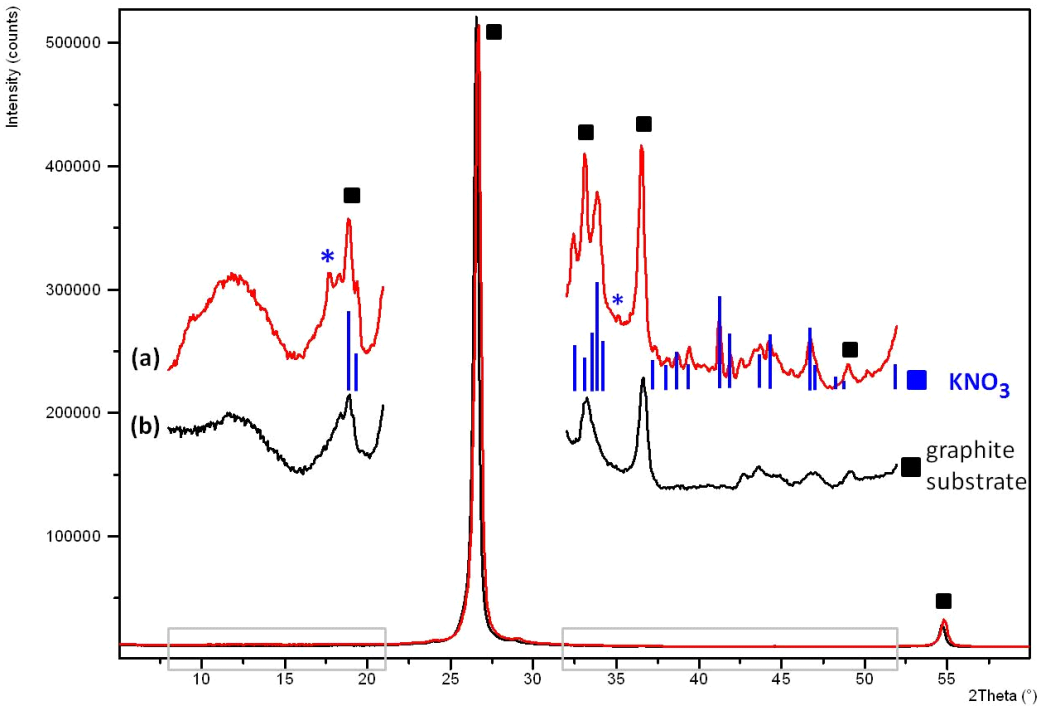

Figure 4.2 XRD patterns of Cu-CoHCF deposited on graphite electrode (in black) and of only graphite electrode (in red).

In the inset of Fig. 4.2 is reported the collection at very slow speed of the 2Θ intervals highlighted by grey rectangles. The histogram is the graphic plot of KNO_3 diffraction peaks (file 5-0377 International Centre of Diffraction Data). The asterisks show the peaks not assigned to KNO_3 or graphite electrode which can be attributed to the (200) and (400) planes of CoHCF, as suggested by Kaplun et al. (Russian Journal of Electrochemistry, Vol. 37, No. 9 (2001) 914-923). By using very long data collection times, it was possible to distinguish the contribution of the graphitic substrate from the one due to the Cu-CoHCF, but only for the deposited material which had been thermally treated. Among the peaks, the principal ones are attributable to KNO_3 crystals (see below for explanation), but the small reflections at 17.7° and 35.3° (d=0.4995 and 0.2553 nm) are consistent with the most intense peaks (200) and (400) of CoHCF, as reported by Kaplun

et al. (as above). The presence of copper which can substitute for cobalt can be a further reason that makes it difficult to obtain good quality crystals.

Cu-CoHCF was deposited on a graphite paper under the same electrochemical conditions as those of glassy carbon. For ATR-IR studies, the graphite paper was chosen as the substrate because the sample holder of the equipment requires a very good contact between the sample and the diamond crystal for accurate measurement, which did not occur in the case of GCE. We recorded the ATR-IR spectra of both the as prepared and thermally treated Cu-CoHCF deposited on graphite support. As shown, both spectra display the typical C-N stretching band which is clearly visible at around 2100 cm^{-1} (Fig. 4.3). The main difference between the spectra is related to the presence of the broad absorption centred at 3400 cm^{-1} and the medium intensity band centred at 1762 cm^{-1} in the as prepared HCF which can be attributed to the water O-H stretching, and H-O-H bending vibrations, respectively.

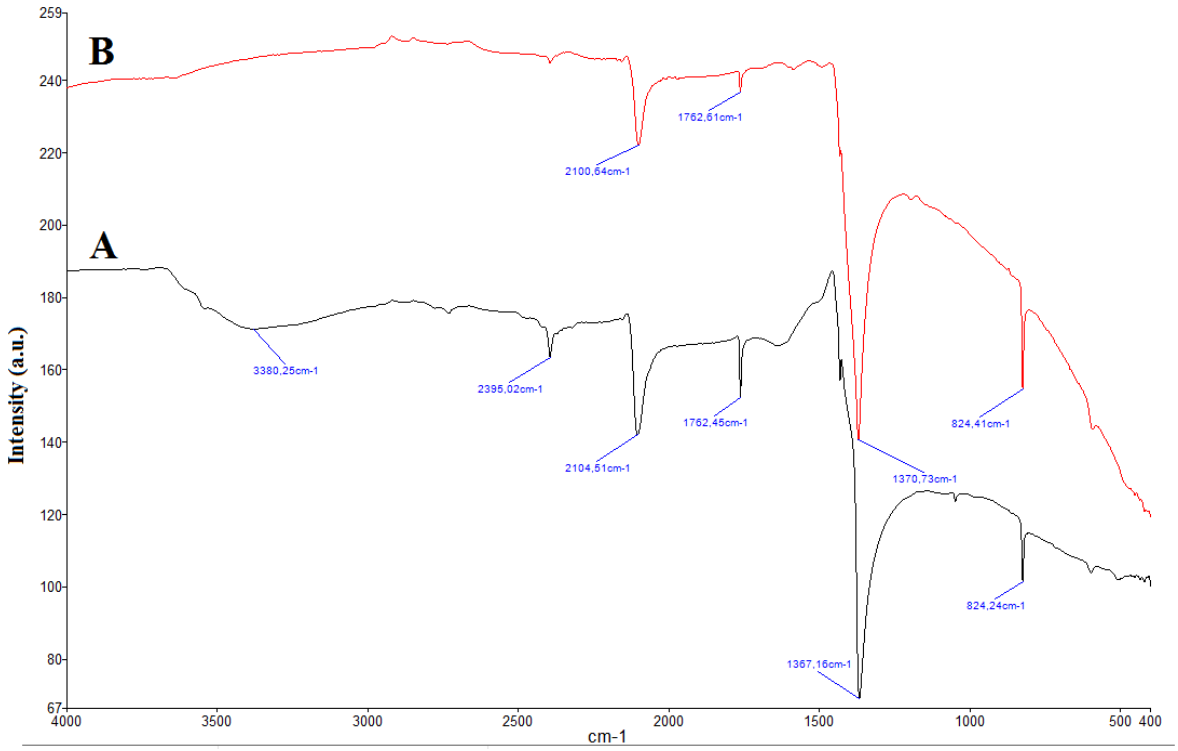

Figure 4.3 ATR-IR spectra of Cu-CoHCF deposited on graphite electrode as-prepared (A) and after thermal treatment (B).

After submitting the material to the thermal treatment the former band completely disappears and the latter becomes less intense, so confirming the loss of water molecules from the HCF, as suggested by De Mattos et al. for Prussian Blue [1]. In both spectra a very strong band at 1370 cm^{-1} and two other bands of medium intensity centred at 2394 and 824 cm^{-1}, respectively, are also present, which could be attributed to the presence of potassium nitrate after performing the following experiment. A piece of graphite paper was dipped in an aqueous solution containing only KNO_3 for 15 min, then it was removed from the solution and dried at room temperature. The ATR-IR spectrum of this graphite support was also recorded (Fig. 4.4).

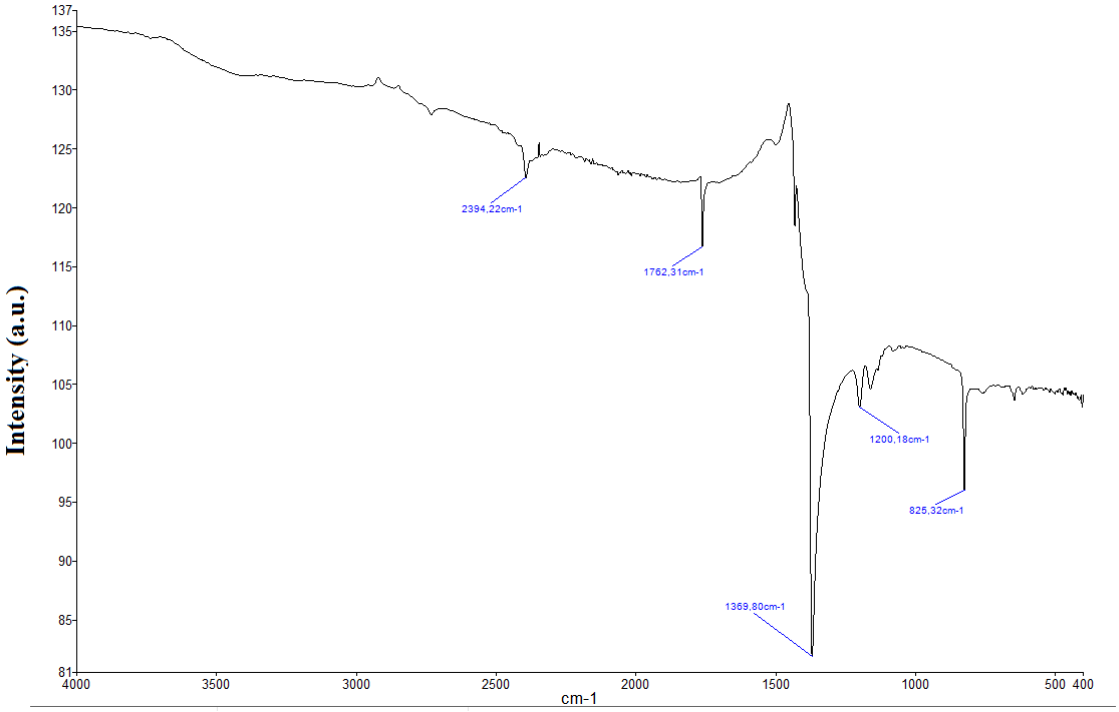

Figure 4.4 ATR-IR spectra of graphite electrode dipped in only KNO_3 solution.

The copper to cobalt molar ratio was evaluated for the thermally treated HCF by FAAS and resulted about 1:4, a value which is in agreement with the result reported by Cui et al. which performed a study to correlate the ratio displayed by the

electrosynthesised HCF with respect to the concentration ratio of Cu^{2+} and Co^{2+} in the electrolytic solution [2].

Typical voltammetric responses of Cu-CoHCF/GCEs in 0.1 M PBS solution, pH 3, containing 0.1 M KNO_3 are shown in Fig. 4.5 A. Here, we can observe two couples of unsymmetrical peaks (I_a,I_c and II_a,II_c) whose formal potentials ($E^{\circ\prime}=(E_{pa} + E_{pc})/2$) are 0.488 and 0.677 V vs. SCE, respectively, which are very close to the values reported in the literature at 0.490 and 0.690 V for the same Cu-CoHCF [3]. These two peak systems have been ascribed to the transformations between Fe(II) and Fe(III) in hexacyanoferrates differing for the number of potassium ions paired to the iron centres [3,4]. Furthermore, the peak potential separation is close to zero and this trend is diagnostic of the surface-confined location of the MeHCF redox process, which was confirmed also by performing CVs at different scan rates (from 0.005 to 0.2 V s^{-1}). In fact, a linear relation between I_{pa} and I_{pc} for the more anodic peak of the two iron redox systems and scan rate was found out as shown in Fig. 4.6.

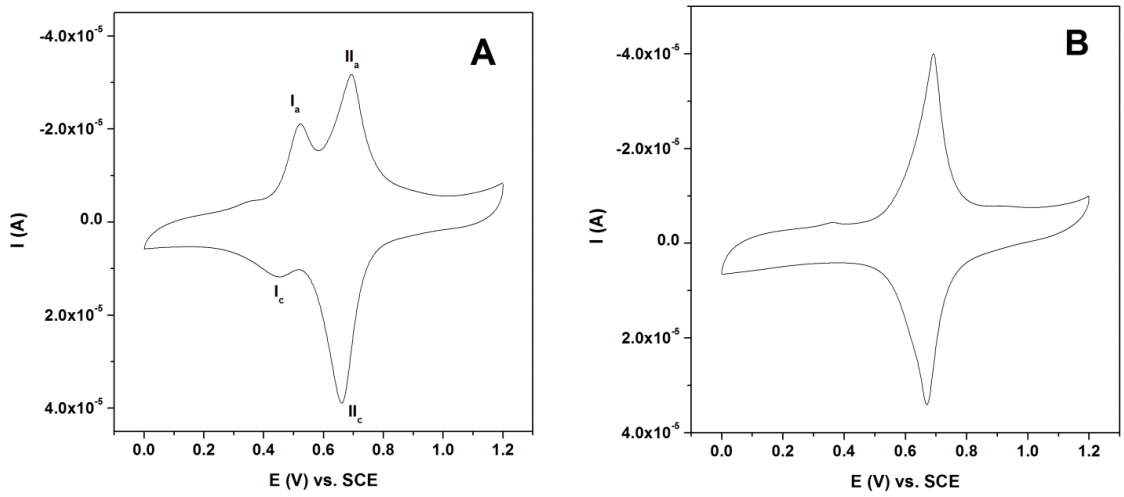

Figure 4.5 CVs recorded between 0 and +1.2 V for the Cu-CoHCF/GCE characterization in 0.1 M PBS (pH = 3) containing 0.1 M KNO_3. Scan rate: 0.050 V s^{-1}

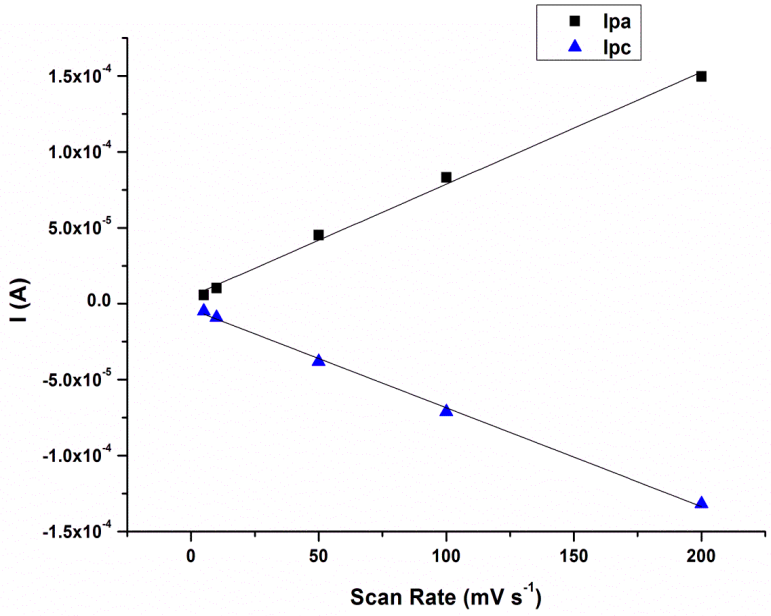

Figure 4.6 Plot of peak current vs. scan rate for the more anodic peak (0.65 V vs. SCE) of Cu-CoHCF modified GCE in 0.1 PBS (pH 4).

All the electrochemical characterisations of HCF films were carried out in the presence of potassium ion as cation, since from the very early studies on MeHCFs it is well known that the sensitivity of the voltammetric profiles is strongly dependent on the alkali cation present in the electrolytic solution, whose flux into and out of the layer is critical to maintain the local charge neutrality during film redox activity [5].

We observed that the CV recorded after the electrodeposition of HCF film on GCE often did not display both the redox couples but only the more intense one, located at more anodic potential (see Fig. 4.5 B). A similar profile of the voltammogram has been already obtained by Mo et al. when they described an all solid state potentiometric microsensor for hydrazine based on a carbon fiber modified by Cu-CoHCF [6]. We believe that the presence or absence of the less anodic feature can be attributed to the surface conditions of glassy carbon. This hypothesis is supported from the data provided by atomic force microscopy (see fig. 4.8) and cyclic voltammetry that the morphology and electrochemical characterization of CoHCF systems are dependent on the growth history of the film. In particular, it was found out that both the time elapsed from the preparation of the electrolytic solution to the application of the potential cycles and the

extent of passivation of the gold substrate are critical factors [1]. Moreover, another hypothesis might be related to the formation of HCF thin films with different morphology, i.e., nanoparticles *vs.* bulk deposit as already observed for CoHCF which exhibited such an electrochemically driven conversion. The cyclic voltammograms of the nanocompounds presented only one reversible redox process, whereas the corresponding bulk compound displayed a more complex redox behavior involving two redox reversible features [2].

After the electrodeposition of the HCF, some CMEs were dried at room temperature (25° C) and some were dried at 100° C for 1 h (thermal treatment). This treatment was aimed to increase the stability of the Cu-CoHCF film as previously demonstrated for Prussian Blue [1]. In that work it was found out that the presence of water molecules inside the PB polycrystal affects the conducting properties and, as a consequence, the stability of the corresponding PB modified electrodes. In fact, when GC electrodes modified with a PB film were exposed at 100°C for 1 hour, an increase of PB electroactivity was demonstrated [1].

As to the Cu-CoHCF, we did not find out such an increase in the electroactivity of the iron centers since the characterization CVs of the CMEs submitted to thermal treatment did not show any significant change in comparison with the ones recorded for the CMEs just prepared. To better investigate the effect of thermal treatment a morphological study of the HCF films was carried out by SEM and AFM analysis.

SEM micrographs of the as-prepared (Fig. 4.7 B) and thermally treated CME (Fig. 4.7 C) show an even and compact film of Cu-CoHCF on the GC surface at magnification of 10,000 ×. In case of the thermally treated CME, there was an increase in particle size of the electrosynthesized material due to aggregation. This observation is in agreement with the loss of water molecules from the HCF polycrystal, as already verified for Prussian Blue.

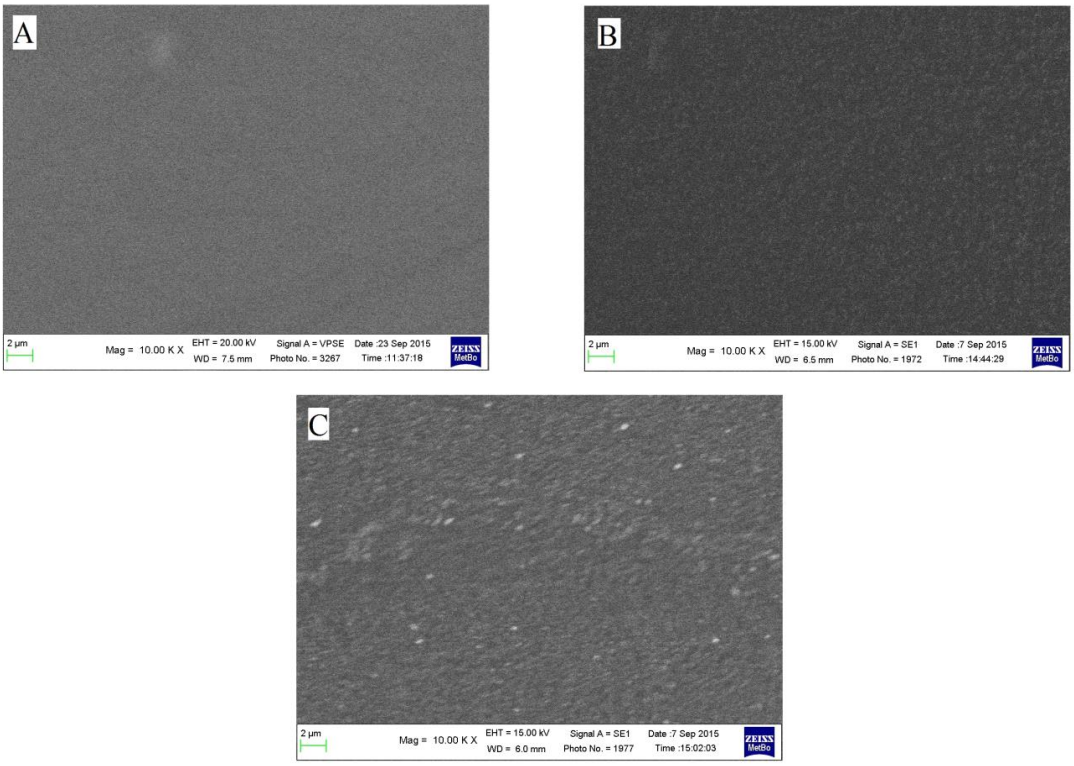

Figure 4.7 SEM images of (A) bare GC (B) the as-prepared CME and (C) thermally treated CME at a magnification of 10,000 ×.

AFM was employed to get information on the roughness and morphology of the HCF films. Fig. 4.8 shows the three dimensional AFM images for the as-such (A) and thermally treated (B) CMEs. The mean roughness of the as-such CME appears higher than the one displayed by the thermally treated CME. In fact the root mean square factor of the roughness was 55 for the former, while it was 28 for the latter. Besides, the mean peak to valley ratio for the as-such CME was 230 while that for the thermally treated CME was 140. These results can be attributed to the loss of H_2O molecules from the HCF after the thermal treatment.

Lastly, we evaluated the thickness of the two films recording an AFM image after mechanical removal of the modifier by performing a line engravement. The thickness was practically the same for both coatings resulting in an average value of 200 nm, which is in agreement with the finding that the peak current depends linearly on the scan rate, as expected for a thin layer electrochemical behavior (see Fig. 4.6).

This is probably the reason why the as-such and the thermally treated Cu-CoHCF display almost identical characterization CVs.

In conclusion, the results from the electrochemical characterization of the HCF modifiers and from SEM and AFM analyses demonstrate that the thermal treatment of the Cu-CoHCF has a major effect on the morphological properties of the film rather than the electrochemical activity of the iron centers.

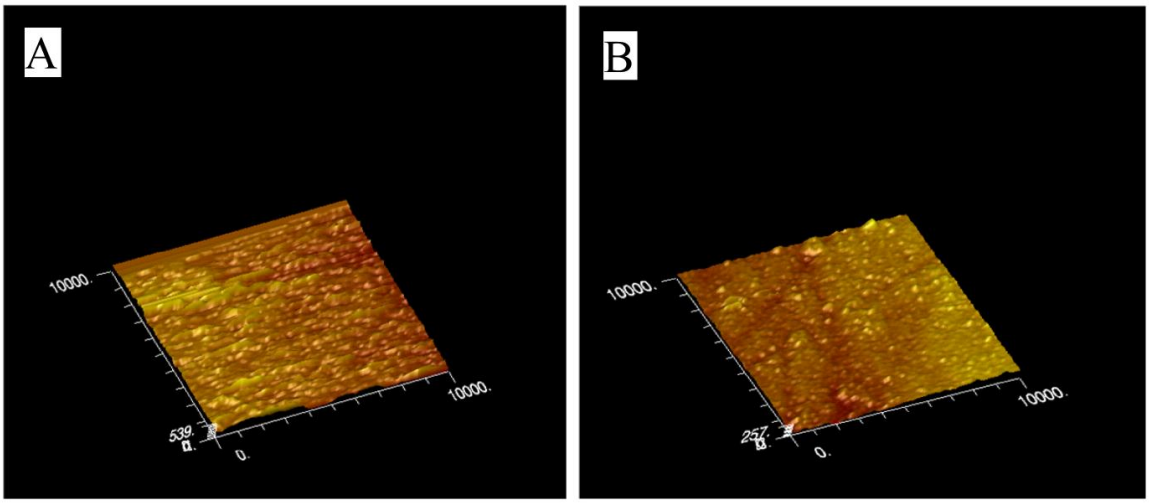

Figure 4.8 Three dimensional AFM images of the (A) the as-prepared CME and (B) thermally treated CME collected in contact mode at a force of 29 nN and 30 nN respectively.

4.1.2. CV STUDY OF pH EFFECT ON THE ANALYTICAL DETERMINATION OF THIOLS

Preliminary CV studies were performed to find out the best working pH for the analytical determination of the three thiols. The investigated range was 2-7 using phosphoric acid couple as the buffer system. The electrochemical response of L-cysteine, L-glutathione and 1,4-butanedithiol at the GCE modified with the as-prepared Cu-CoHCF was investigated in the potential range from 0 to +1.2 V, at a scan rate of 0.05 V s^{-1} in PBS containing 0.1 M KNO_3. The voltammetric response was also recorded at the CME submitted to thermal treatment after the addition of thiols to the

buffer solution. As an example, Fig. 4.9 shows the CV response of the as-prepared CME to the addition of 0.1 mM L-cysteine in PBS, pH 3. In the presence of the thiol an increase of the anodic current is evident starting from a potential value of 0.45 V. The electrochemical behavior of the three analytes was also investigated at the bare GC in order to confirm the catalytic activity of the Cu-CoHCF. The increase in current beyond 0.8 V in Fig. 4.9 can be attributed to the oxidation of the thiol at the bare GC. Obviously, an enhancement of the oxidation current was observed in case of detection of the thiols by the CMEs as compared to the bare GCE.

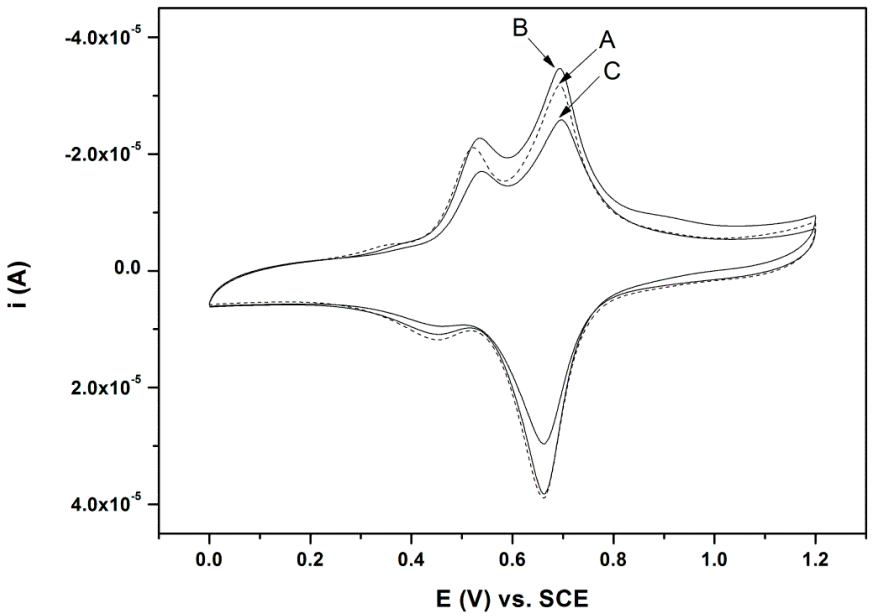

Figure 4.9 Cyclic voltammograms of the as-prepared CME in the absence (A) and presence of 0.1 mM L-Cysteine (B), in 0.1 M PBS, pH 3, containing 0.1 M KNO_3. CV of the same CME in blank buffer solution after performing the thiol electrocatalysis (C). Scan rate = 0.05 Vs^{-1}.

Fig. 4.9 also shows the CV (trace C) recorded at the CME in the buffer solution containing only the supporting electrolyte after having recorded the CV in the presence of cysteine. It is evident that some fouling has occurred since all the current values result slightly lower than the ones of the trace A. On the contrary, if the same experiment was

repeated at the CME submitted to the thermal treatment, the HCF stability was very good since the traces A and C were practically superimposable, so confirming that fouling did not occur. Therefore, in case of CySH detection the thermal treatment was beneficial since the Cu-CoHCF electrochemical behaviour was not altered after having been in contact with the thiol. The percentage current variation of the anodic peak centred at 0.65 V, after the addition of thiols for both the as-prepared and thermally treated CMEs, was evaluated and the results are reported in Table 4.1. As shown, the best pH range for the detection of the 3 thiols is 2-4 since the HCF is more stable in these conditions as compared to higher pHs. At these values there is also significant fouling of both the as prepared and thermally treated CMEs, as it is evident from the decreasing peak currents of the CVs recorded before and after the thiol addition. The fouling occurrence was also confirmed by recording the CV in the presence of only the supporting electrolyte after the contact with thiol compound as shown in Fig. 4.9.

Table 4.1 Percentage variation of the peak current (anodic peak centred at 0.65 V) recorded by CV at the as-prepared and thermally treated CMEs for an addition of the three thiols, corresponding to a concentration 0.1 mM, to 0.1 M PBS containing 0.1 M KNO_3. pH range: from pH 2 to 7; scan rate = 0.05 Vs^{-1}.

	L-cysteine		L-glutathione		1,4-butanedithiol	
pH	As-prepared	Thermally treated	As-prepared	Thermally treated	As-prepared	Thermally treated
2	13.3	11.2	0.1	6.5	14.1	11.5
3	8.7	9.2	1.8	1.1	8.4	0.3
4	-6.0	2.2	1.2	2.0	4.7	-0.5
5	-47.8	0	-2.2	-7.9	-9.2	-1.0
6	-34.5	-8.0	-8.8	-11.2	2.1	-9.5

7	-52.2	-24.5	-27.6	-32.4	-56.3	-80.4

4.1.3. CHRONOAMPEROMETRIC RESPONSE OF THIOLS

On the basis of the preliminary CV experiments, chronoamperometric measurements were carried out at a working potential of 0.65 V *vs.* SCE both for the as-prepared and thermally treated CME in 0.1 M PBS containing 0.1 M KNO_3, with the pH ranging from 2 to 4. The aim was to determine the effect of thermal treatment on the sensitivity and stability of the CME towards the detection of thiols. Table 4.2 shows that for CySH the best sensitivity was observed in the case of thermally treated CME, working at pH 3. For GSH too, the thermally treated CME showed a better sensitivity than the as-prepared one, however, in this case the best performance was observed at pH 4. Interestingly, in case of BdSH the best sensitivity was observed with the as-prepared CME with pH fixed at 4. Among the 3 thiols GSH displayed the worst sensitivity and CySH the best one.

Table 4.2 Sensitivity values (in A $mol^{-1}L$) for chronoamperometric measurements of the three thiols in PBS containing 0.1 M KNO_3 at different pHs and at a working potential of 0.65 V vs. SCE.

	L-cysteine		L-glutathione		1,4-butanedithiol	
	As prepared	Thermally treated	As prepared	Thermally treated	As prepared	Thermally treated
pH = 2	0.0247	0.0282	0.0011	0.0022	0.022	0.0157

pH = 3	0.0563	0.0575	0.0133	0.0083	0.0283	0.0234
pH = 4	0.0428	0.0455	0.0116	0.0218	0.0327	0.0242

Chronoamperometric measurements were also carried out at potentials lower than the value of the anodic peak related to the Fe^{2+}/Fe^{3+} couple to verify if the sensitivity decreased, as expected, with a lower working potential, and to establish the minimum value of the overpotential at which the electrocatalytic effect occurred to a significant extent. We found out the expected trend of sensitivity vs. potential and it was confirmed that the best sensitivity was observed for a working potential of 0.65 V, for all thiols. Furthermore, the lowest detection potential at which an appreciable sensitivity could be observed was 0.50 V.

Higher anodic potentials than 0.80 V were not tested as it had been already checked that at these overpotentials the thiol oxidation occurs at the bare GC.

During the amperometric measurements it was also observed that all the CMEs showed a wider concentration range of detection towards thiols at the lowest investigated pH (= 2) coupled with less noise which would be very helpful in case of dealing with real samples where the background signal is often less stable. It was also observed that increasing the number of additions of the thiol under investigation, the signal noise became higher and higher which can be attributed to the fouling of the electrode occurring to a greater extent.

For this reason, the CME was freshly prepared after every calibration. This fact is not a problem since the electrode modification is rapid and the reproducibility of the procedure is very good. Coulometric experiments were also performed for the three thiols in order to determine the number of electrons (n) involved in the electrocatalysis. To this aim a known amount of the thiol in 20 mL of PBS (pH = 2) containing 0.1 M KNO_3 was bulk oxidized, under stirring at 0.65 V, on a large Cu-CoHCF modified electrode until the current was reduced to 2% of the initial value. Then the electrode

surface was cleaned and a new Cu-CoHCF film was electrogenerated. The same experiment was then repeated in the presence of only the supporting electrolyte in order to find the charge to be subtracted from the value determined in the first experiment. The so calculated net charge was employed for the determination of n which resulted 2 for the three thiols.

On the basis of this result and the electrochemistry of Cu-CoHCF [3,7], the electrocatalytic oxidation of the three thiols can be described as follows:

$2\ \text{Cu-CoHCF}_{red} \rightarrow 2\text{Cu-CoHCF}_{ox} + 2\ e^-$

$2\text{Cu-CoHCF}_{ox} + 2\text{RSH} \rightarrow \text{RSSR} + 2H^+ + 2\text{Cu-CoHCF}_{red}$

net reaction: $2\text{RSH} \rightarrow \text{RSSR} + 2H^+ + 2\ e^-$

In Fig. 4.10 a typical chronoamperometric experiment obtained for BdSH under the optimized conditions is reported and in Table 4.3 the analytical parameters related to the quantitative determination of the three thiols by chronoamperometry are shown. The calibration graphs were constructed by plotting the limiting current as a function of thiol concentration: the sensitivity, expressed as the slope of the resulting line, the LOD and LOQ values were calculated as suggested by Miller and Miller [8] and are reported in Table 4.3.

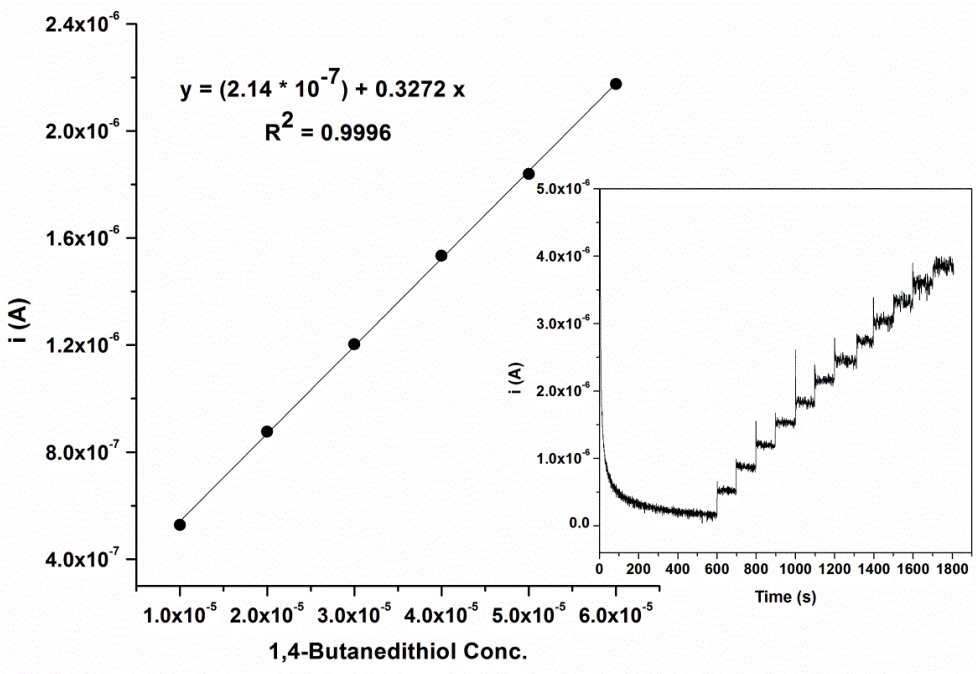

Figure 4.10 Chronoamperometric response of BdSH with the as-prepared CME in 0.1 M PBS containing 0.1 M KNO_3 (pH = 4), 10 µM additions of the thiol at the working potential of 0.65 V, biased vs. SCE.

Table 4.3 Analytical parameters of the calibration of CySH, GSH, and BdSH by chronoamperometry in PBS containing 0.1 M KNO_3 at 0.65 V vs. SCE (pH = 3 and thermally treated CME for CySH, pH = 4 and thermally treated CME for GSH, pH = 4 and as-prepared CME for BdSH)

	L-cysteine	L-glutathione	1,4-butanedithiol
Sensitivity, A $mol^{-1}L$	0.0575	0.0218	0.0327
Linear range (µM)	5 - 60	5 - 90	5 - 120
Correlation coefficient	0.99993	0.99389	0.99986
LOD (µM)	0.75	2.5	2.0
LOQ (µM)	2.5	8.3	6.6

Repeatability, RSD%	5	6	4

An average of four measurements was used for the construction of the calibration graphs using each time a new CME. The repeatability of the quantitative determination was estimated with five consecutive measurements at the same thiol concentration (0.5×10^{-4} M) and results were in good agreement since the average value of the percentage relative standard deviation was between 4 and 6, as shown in Table 4.3.

The calibration graphs were also obtained by biasing the CME at potentials lower than 0.65 V, in order to minimize possible interferences coming from oxidizable substances present in a real sample. As already stated above, at 0.50 V it was possible to record a catalytic current but the slopes of the calibration lines were too low to be exploitable for a quantitative determination. On the other hand, working at 0.55 V the following slopes were obtained under the optimized conditions: 0.0272 A $mol^{-1}L$ for CySH, 0.00233 A $mol^{-1}L$ for GSH**,** and 0.0271 A $mol^{-1}L$ for BdSH. If compared with the values displayed at 0.65 V (see Table 3), working at 100 mV lower overpotential causes a decrease of the sensitivity of 50% for CySH, 20% for BdSH, but of almost ten times for GSH.

A comparison of the performances of the CME here proposed with those of electrodes modified with the same or similar HCFs is shown in Table 4.4. The analyte which has generally been investigated is L-cysteine. As to this aminothiol, we would like to say that our CME compares favourably with the other sensors already described in the literature, in terms of sensitivity, as given by the limit of detection value, even if the width of the linearity range is smaller. As far as glutathione determination is concerned, we did not find any paper reporting an analytical determination with good performance based on electrode modified with only HCFs. This was achieved by using a composite based on a HCF (containing Ni) and Au NPs. GSH normally does not undergo detectable electrochemical sensing at NiHCF based CMEs, but the presence of AuNPs improves the electrochemical performance due to the strong interaction between Au and SH group. In case of a Pt UME modified with such a composite [9] a very low

limit of detection was obtained but the upper limit of linearity was only 1 µM. When a CPE was prepared by adding the composite NiHCF/AuNPs [10] both the limit of detection and width of the linearity range was better than that displayed by our sensor. On the contrary, an electrode made of edge plane pyrolytic graphite displayed worse performances both in terms of sensitivity and linearity range, as reported in the literature [11]. A comparison with the performances as to the quantitative determination of butandithiol is not possible since, as already remarked, this is the first work describing such a determination with a GC electrode modified with a mixed HCF.

Table 4.4 Comparison of the analytical performances of various electrodes with different modifiers for the determinations of thiols.

Electrode	Modifier	Analyte	Linear Range	LOD	Reference
CPE GCE	CuCoHCF CoHCF	CySH	6 - 1000 µM 1.5 - 200 µM	4 µM 1 µM	2 12
GCE	CuHCF		5.0 - 250 pmol	2.5 pmol	13
GCE	CuCoHCF	CySH GSH BdSH	5 – 60 µM 5 – 90 µM 5 – 120 µM	0.75 µM 2.5 µM 2.0 µM	15
SPE	CoHCF	Thiocholine	0.5 – 10 µM	0.5 µM	14
Edge Plane	-	CySH GSH	17 - 208 µM	2.6 µM	11

pyrolytic graphite			10 – 80 µM	2.7 µM	
Pt UME	NiHCF/CTAB*/AuNPs	GSH	0.2 - 1 µM	0.08 µM	9
CPE	NiHCF/AuNPs	GSH	1-1400 µM	0.5 µM	10

* Cetyltrimethylammonium bromide

The CME was applied to determine the amount of GSH present in a nutraceutical drug purchased from the local market. 5 tablets of the nutraceutical were crushed and ground to powder with a mortar and pestle. The powder was dissolved in 200 mL of doubly distilled water and kept under stirring for 5 minutes. The solution was then filtered through a funnel to remove the filler and other loading agents and collected in a volumetric flask. The volume was then made up to 250 mL by addition of doubly distilled water. Chronoamperometric measurements were carried out by drawing out 60 µL with the help of a micropipette from the above solution and dropping them into 20 mL of PBS (pH 4). From the calibration plot it was possible to determine the concentration of the GSH solution prepared from the nutraceutical. Four such measurements were conducted and the amount of GSH per tablet was determined as 0.49 ± 0.08 g which is in close agreement to the value declared on the label (i.e. 0.5 g).

4.1.4. BIBLIOGRAPHY

[1] I.L. de Mattos, L. Gorton, T. Ruzgas, A.A. Karyakin, Sensor for Hydrogen Peroxide Based on Prussian Blue Modified Electrode: Improvement of the Operational Stability, *Anal. Sci.* 16 (2000) 795-798.

[2] N. R. de Tacconi, K.Rajeshwar, R.O. Lezna, Metal Hexacyanoferrates: Electrosynthesis, in Situ Characterization, and Applications, Chem. Mater. 15 (2003) 3046-3062.

[3] X. Cui, X. Lin, Hybrid copper-cobalt hexacyanoferrate films modified glassy carbon electrode as an electrochemical sensor for hydrogen peroxide, Anal. Lett. 35 (2002) 663-675.

[4] A. Abbaspour, A. Ghaffarinejad, Electrocatalytic oxidation of L-cysteine with a stable copper-cobalt hexacyanoferrate electrochemically modified carbon paste electrode, Electrochim. Acta 53 (2008) 6643-6650.

[5] A. B. Bocarsly, S. Sinha, J. Electroanal. Chem. 140 (1982) 167-172.

[6] J-W Mo, B. Ogorevc, X. Zhang, B. Pihlar, Cobalt and Copper hexacyanoferrate modified electrode carbon fiber microelectrode as an all-solid potentiometric microsensor for hydrazine, Electroanalysis 12 (2000) 48-54.

[7] P.J. Kulesza, M.A. Malik, J. Skorek, K. Miecznikowski, S. Zamponi, M. Berrettoni, M. Giorgetti, R. Marassi, Hybrid Metal Cyanometallates - Electrochemical Charging and Spectrochemical Identity of Heteronuclear Nickel/Cobalt Hexacyanoferrate, J. Electrochem. Soc. 146 (1999) 3757-3761.

[8] J. C. Miller, J. N. Miller, Statistics for Analytical Chemistry, Wiley, New York, 1988.

[9] H. Hongxia, D. Jie, H. Yaqi, R. Jing, L. Xiaoquan, Talanta, 115 (2013) 381-385.

[10] P. C. Pandey, A. K. Pandey, Anayst, 137 (2012) 3306-3313.

[11] R.R. Moore, C.E. Banks, R.G. Compton, Electrocatalytic detection of thiols using an edge plane pyrolytic graphite electrode, Analyst 129 (2004) 755-758.

[12] G. Shi, J. Lu, F. Xu, W. Sun, L. Jin, K. Yamamoto, S. Tao, J. Jin, Anal. Chim. Acta., 391 (1999) 307-313.

[13] J. Zhou, E. Wang, Electroanalysis, 6 (1994) 29-35.

[14] F. Arduini, A. Cassisi, A. Amine, F. Ricci, D. Moscone, G. Palleschi, J. Electroanal. Chem., 626 (2009) 66-74.

[15] V. V. Sharma, L. Guadagnini, M. Giorgetti, D. Tonelli, Electrocatalytic determination of thiols using hybrid copper cobalt hexacyanoferrate modified glassy carbon electrode, Sens. Actuators B 228 (2016) 16-24.

4.2. CMEs BASED ON COPPER COBALT HEXACYANOFERRATE FOR DETERMINATION OF MERCURY

Cu-CoHCF modified glassy carbon electrode was also employed for the detection of mercury. All protocols for the preparation of the CMEs were the same as employed for the determination of thiols.

4.2.1. DETECTION OF MERCURY

The analytical determination of CySH and BdSH by chronoamperometry, using a Cu-CoHCF modified GCE, was previously established by our group in a previous work. Next, the two thiols were also quantitated by differential pulse voltammetry in order to evaluate which analytical technique would lead to a better sensitivity. In case of DPV, various values for the pulse period, pulse width and sample period were tried before arriving at the optimum parameters, so as to have the maximum current value. In case of CySH, the maximum current value was observed for pulse width = 5 s, pulse period = 10 s and sample width = 0.1 s. As an example, in Figs. 4.11 A and B the calibration plots obtained for CySH by chronoamperometry and DPV, respectively, are shown. In the case of DPV, the sensitivity was found out to be 0.118 A M^{-1} cm^{-2}, which is about seven times lower than the value obtained by chronoamperometry (0.814 A M^{-1} cm^{-2}). Hence, chronoamperometry was selected to find out the optimized conditions for the indirect electrochemical determination of Hg^{2+}.

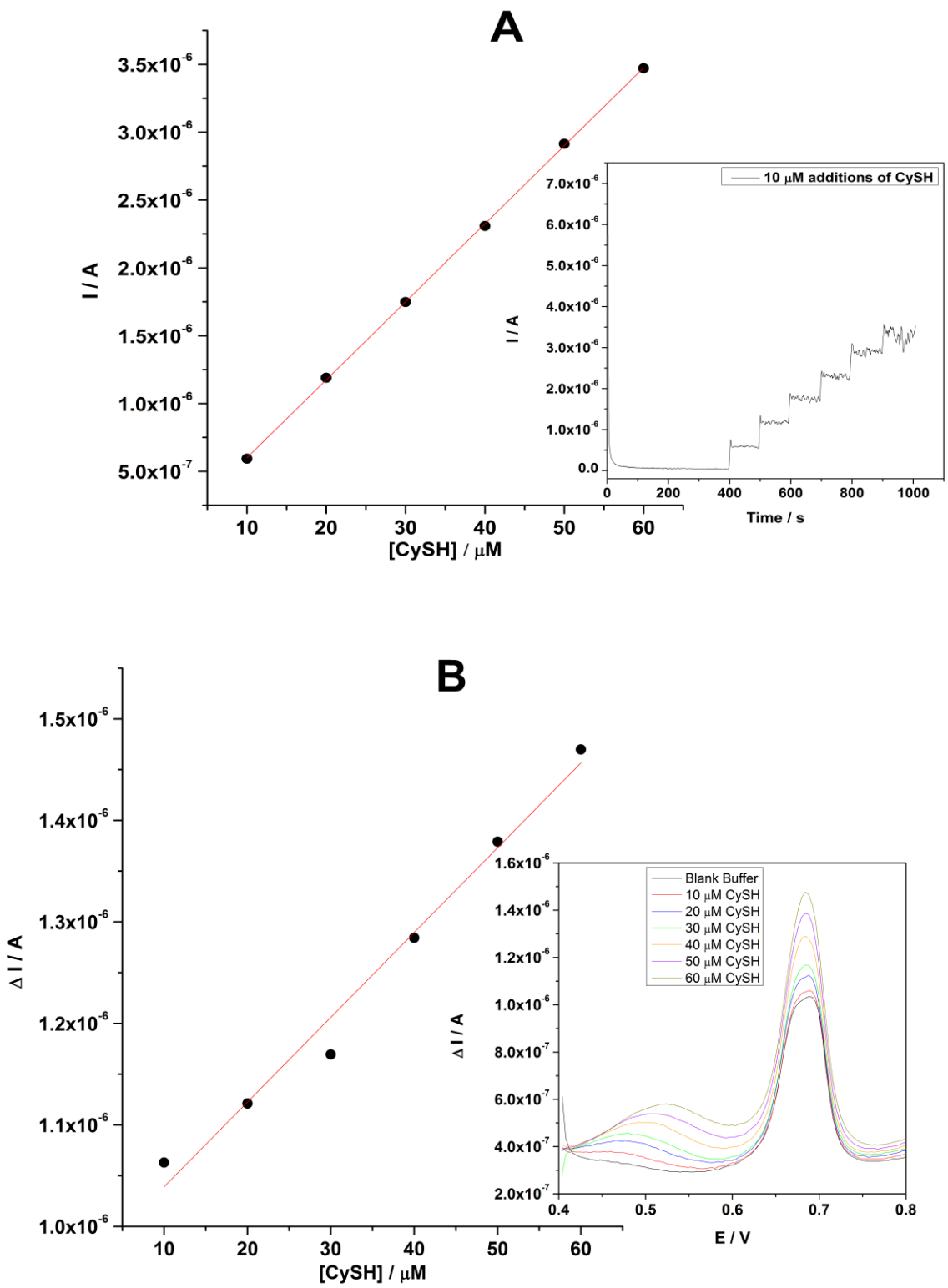

Figure 4.11 Calibration plot for CySH additions (10 µM each) to 0.1 M PBS using (A) chronoamperometry and (B) differential pulse voltammetry.

In the absence of mercury, thiols are oxidized at the electrode following the reaction $2RSH \rightarrow RSSR + 2e^- + 2H^+$, resulting in the formation of disulphides. However, in the presence of mercury, the sulphur present in the thiol reacts rapidly with the mercury to form an electro-inactive complex. Calibration curves for Hg^{2+} determination could be obtained from the % decrease of the thiol oxidation current (R%), after subsequent additions of a standard solution of Hg^{2+}, applying the following equation:

$$R\% = \frac{(i_0 - i_R)}{i_0} \cdot 100 \qquad (1)$$

where i_0 and i_R are the oxidation currents in the absence and in the presence of Hg^{2+}, respectively, and R% is proportional to Hg^{2+} concentration,.

In order to find the optimum match in terms of limit of detection and limit of linearity for Hg^{2+} quantitative determination different concentrations of thiols were investigated. As an example in Fig. 4.12 is shown the calibration line obtained for CySH at a 10 µM concentration. The same procedure was adopted in the case of BdSH obtaining similar results. The limit of detection (LOD) for Hg^{2+} was found to be 80 nM for CySH and 130 nM for BdSH, respectively, and was calculated as suggested by Miller and Miller [1]. Moreover, CySH showed a higher sensitivity (315.5 μM^{-1} cm^{-2}) as compared to BdSH (144.3 μM^{-1} cm^{-2}). This result can be attributed to the stoichiometry of the complex between CySH and Hg^{2+} which is 2:1, while in the case of BdSH is 1:1.

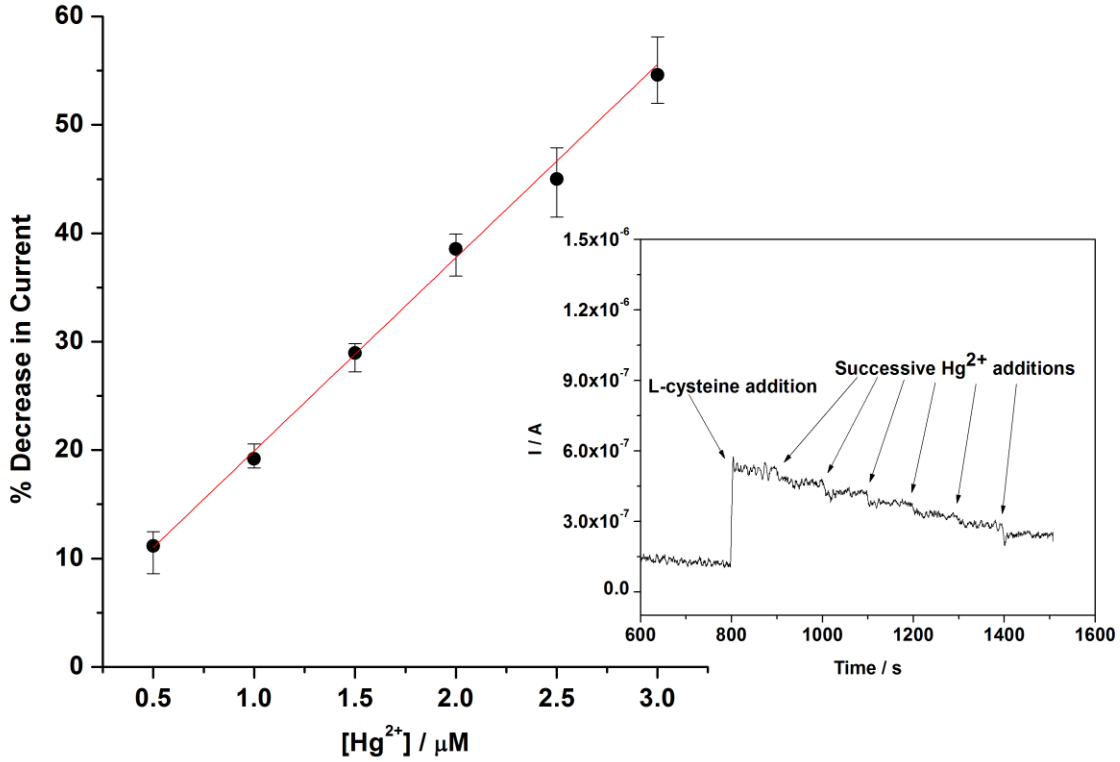

Figure 4.12 Calibration plot of percentage decrease in current versus Hg^{2+} concentration when CA was performed in the presence of 10 µM CySH. Inset: CA plot for addition of 10 µM CySH to pH 4 PBS and subsequently six Hg^{2+} additions (each one 500 nM). In the calibration plot, the error bar represents the standard deviation of three replicated measurements.

Due to the greater sensitivity displayed by CySH, it was further used for detection of Hg^{2+} in spiked mineral water samples and for interference studies. Clearly, the CySH concentration determines the detectable levels of mercury as the analytical method for determination of mercury is based on the determination of thiol. We investigated three levels of concentration, *i.e.* 1, 5 and 10 M, and the analytical parameters of the relevant calibration lines are shown in Table 4.5. The limit of quantification (LOQ) was also calculated as suggested by Miller and Miller [1]. Actually, it was not possible to accurately evaluate the current decrease after mercury addition for 1 M CySH solution due to the very small value of current and the high noise associated with the signal.

Table 4.5 Analytical parameters for the calibration plot of Hg^{2+} determination using two different concentrations of CySH.

L-cysteine Conc. (µM)	Sensitivity (μM^{-1} cm^{-2})	Linearity Range (µM)	LOD (µM)	LOQ (µM)
5	380	0.25 – 2.5	0.080	0.25
10	365	0.25 – 5.0	0.080	0.25

A reproducibility study was carried out with five CMEs. Working with a thiol concentration of 5.0 µM, the average slope value of the five calibration plots was found to be (375 ± 20) μM^{-1} cm^{-2}. Since the percentage coefficient of variation was about 5 %, we can conclude that the reproducibility of the proposed sensor is very good.

4.2.2. INTERFERENCE STUDIES

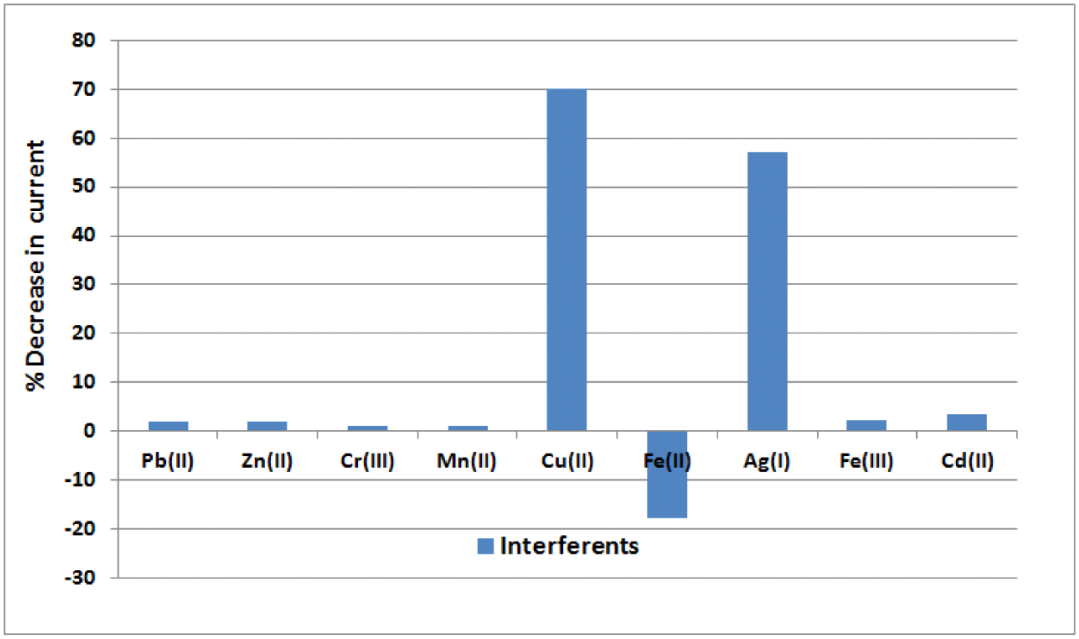

Figure 4.13 Percentage decrease in current of 10 µM CySH on 5 µM additions of the interferents. Tests carried out in 0.1 M PBS, pH 4, with the thermally treated Cu-CoHCF modified GCE biased at +0.65 V.

Various cations were tested for their possible interference with a given concentration (10 µM) of CySH. All the cations were added to the solution at the same concentration (5 µM) as Hg^{2+} which caused a full disappearance of the CySH current. Fig. 4.13 shows that Cu^{2+} and Ag^{+} are the major interferents, with only negligible interference from other metal ions. CA responses of the various cations towards CySH are shown in Fig. 4.14, 4.15 and 4.16.

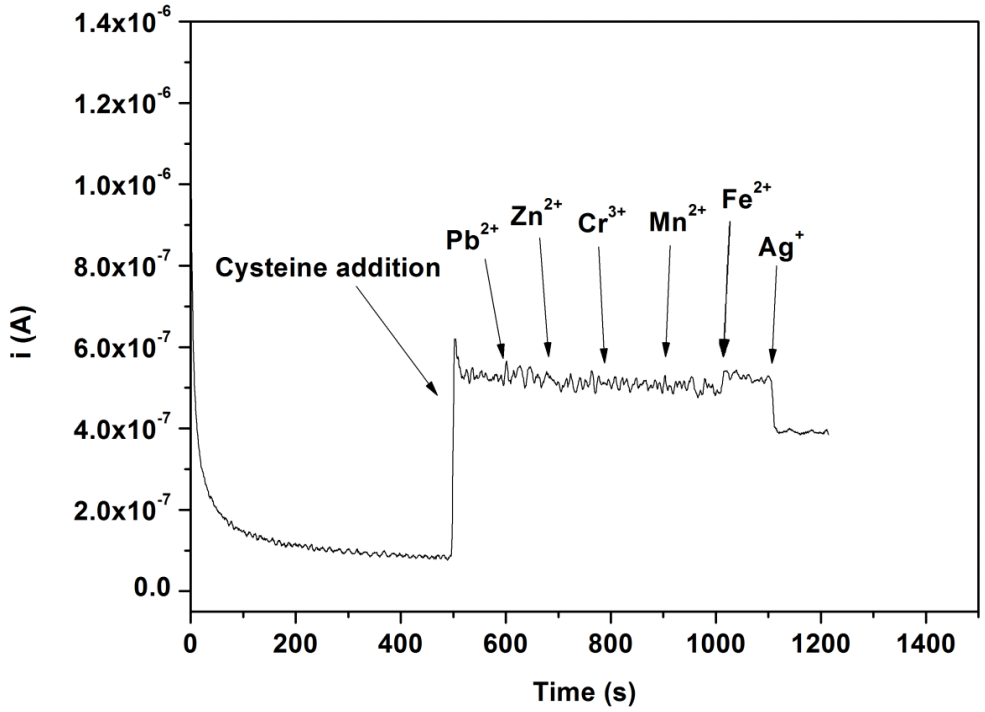

Figure 4.14 Chronoamperometric plot for successive additions of metal ions as inteferents (each addition corresponding to 5 µM concentration) to a solution containing 10 µM CySH. Tests carried out in 0.1 M PBS, pH 4, with the thermally treated Cu-CoHCF modified GCE biased at +0.65 V.

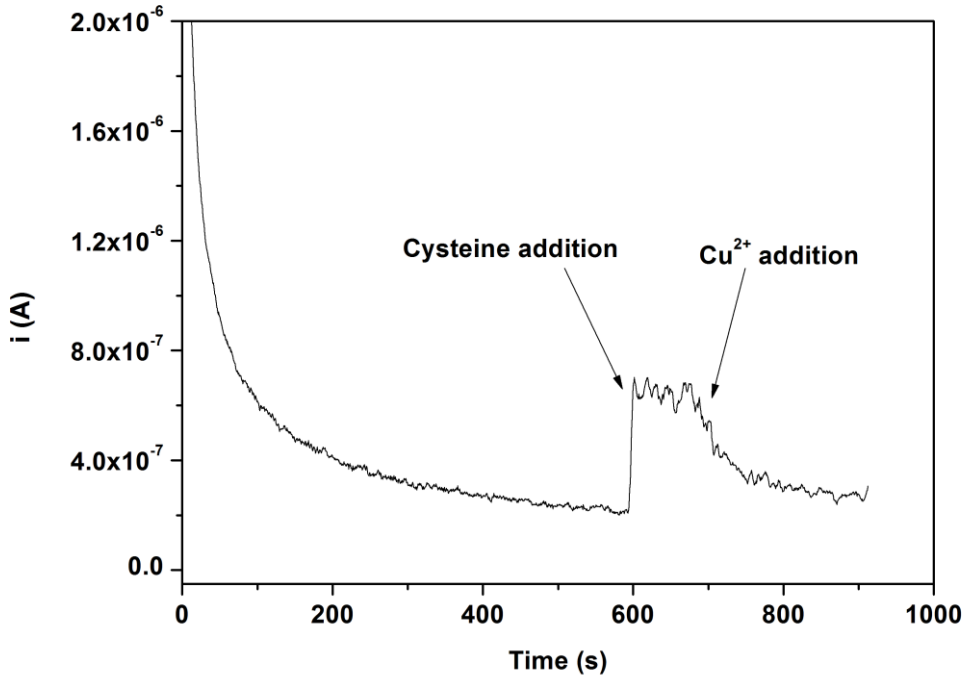

Figure 4.15 Chronoamperometric plot for successive additions of Cu^{2+} as inteferent (5 µM) to a solution containing 10 µM CySH. Tests carried out in 0.1 M PBS, pH 4, with the thermally treated Cu-CoHCF modified GCE biased at +0.65 V.

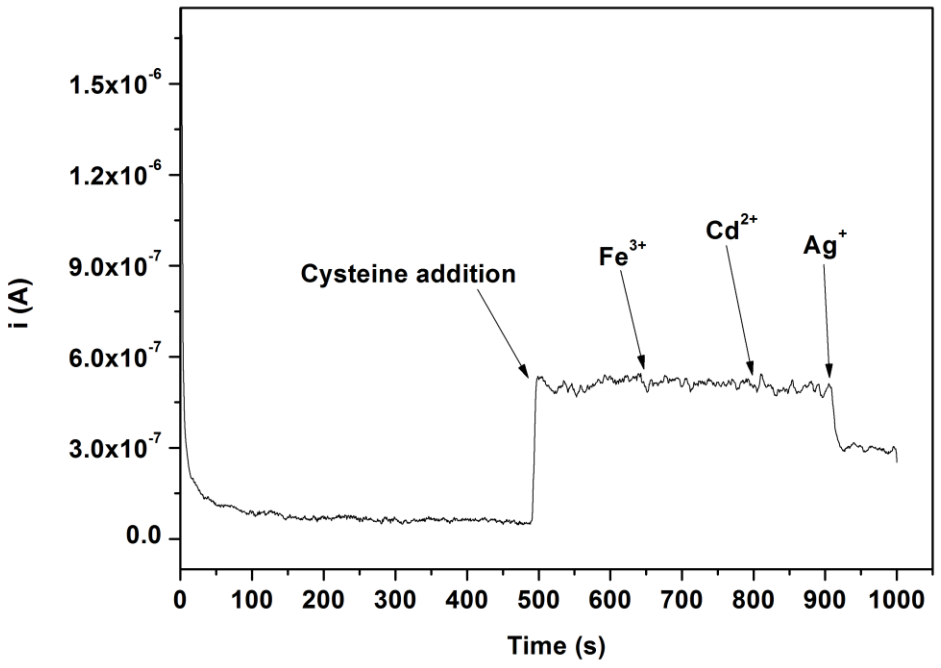

Figure 4.16 Chronoamperometric plot for successive additions of the indicated metal ions as inteferents (5 µM) to a solution containing 10 µM CySH. Tests carried out in 0.1 M PBS, pH 4, with the thermally treated Cu-CoHCF modified GCE biased at +0.65 V.

In the case of Fe(II) in Fig. 4.14, the increase in current is due to the fact that such an ion is oxidized at the operative potential; the probability that iron is present in a real sample in its reduced form is, however, very low. If this is the case, the interference from Fe(II) can be eliminated, e.g., by adding a selective masking agent, like 1,10-phenanthroline. Since, Ag^+ is present in environmental water samples at extremely low concentrations (of the order of 10^{-10} M), the interference from Ag^+ can be neglected for practical purposes. However, Cu^{2+} is a major interferent and various methods (both chemical and electrochemical) were deployed to remove its adverse effect on mercury determination.

4.2.2.1. Removal of Interference due to Cu^{2+} by chemical methods

First we tried to avoid the interference of Cu^{2+} by chemical methods, using masking agents, such as 8-hydroxyquinoline (oxine) [2], 2,2'-bipyridyl (bPy) [3], and allyl alcohol [4]. In the case of oxine, we observed that the ligand does not form a precipitate with Cu^{2+} if the concentration is at µM level. For bPy there was a complex formation with Cu^{2+}, however, the ligand had an adverse effect on the stability of the HCF film, which was evident from the reduced current value in the cyclic voltammogram of the blank buffer solution (Fig. 4.17).

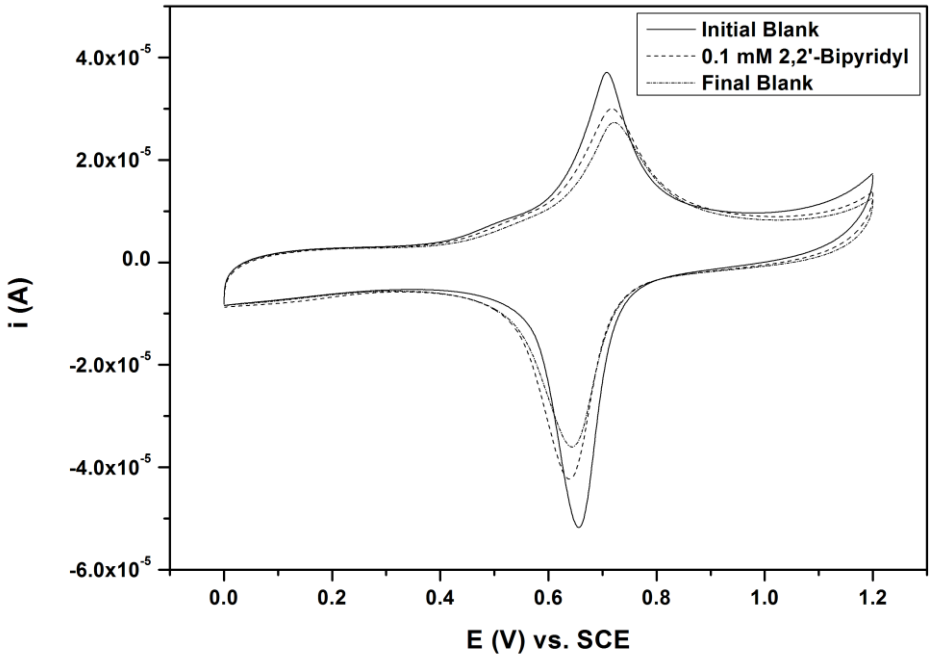

Figure 4.17 CVs recorded for the addition of 0.1 mM 2,2'-bipyridyl to 0.1 M PBS, pH 4, solution where the thermally treated CME was soaked, which shows its fouling.

In the case of allyl alcohol, the ligand forms a stable complex with Cu(I), therefore a reducing agent like L-ascorbic acid was first added to Cu^{2+} containing solution, followed by allyl alcohol. However, allyl alcohol was unable to mask the interference from Cu^{2+} since the produced Cu(I) could oxidize cysteine before forming the complex with the alcohol, as evident from the CA plot in Fig. 4.18. Therefore, the chemical approach was not successful.

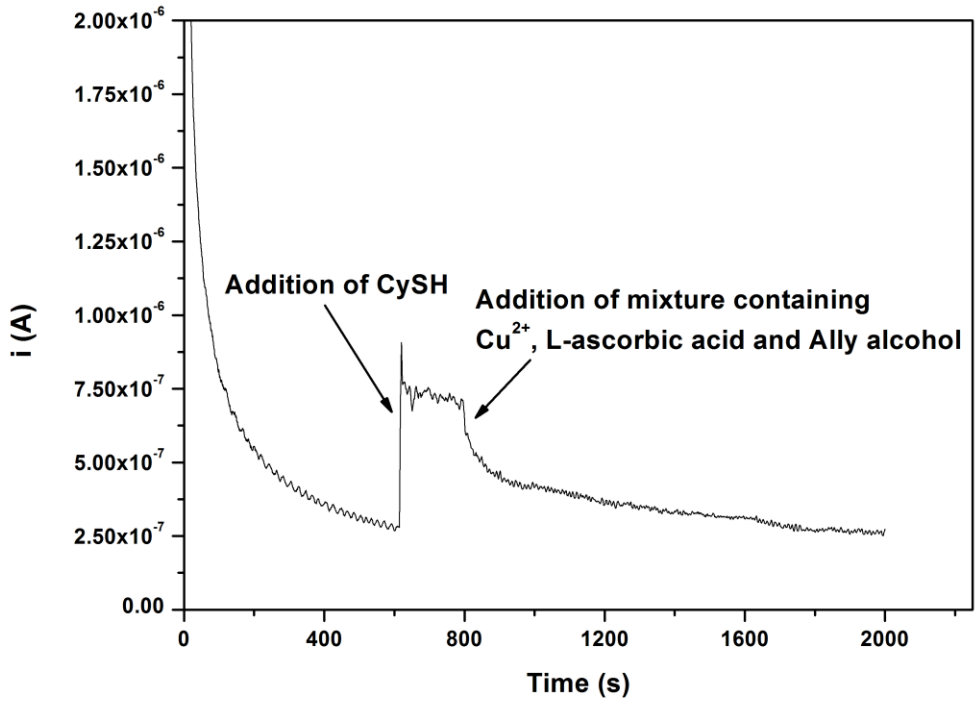

Figure 4.18 Chronoamperometric plot for the addition of a mixture containing Cu^{2+} (5 µM), L-Ascorbic acid (10 µM) and allyl alcohol (10 µM) to a 10 µM CySH solution. Tests were carried out in 0.1 M PBS, pH 4, with the thermally treated Cu-CoHCF modified GCE biased at +0.65 V.

4.2.2.2. Removal of Interference due to Cu^{2+} by electro-chemical methods

An electrochemical approach was also attempted to remove the interference from Cu^{2+} by reduction to $Cu^{(0)}$, without affecting Hg^{2+}, working both in acetate buffer and aqua regia (7 times diluted) solutions. The latter was used to simulate the oxidative treatment often applied to environmental water samples. The reduction of the solutions containing Cu^{2+} or Hg^{2+} was carried out by linear sweep voltammetry at both the bare GC and the HCF modified electrodes. In all cases we found that Hg^{2+} was reduced at less cathodic potentials than Cu^{2+}. As shown in Fig. 4.19 and Fig. 4.20, the first reduction peak for Cu^{2+} appears around 0.35 V while in case of Hg^{2+} it is at around 0 V. So, also the electrochemical approach was not feasible.

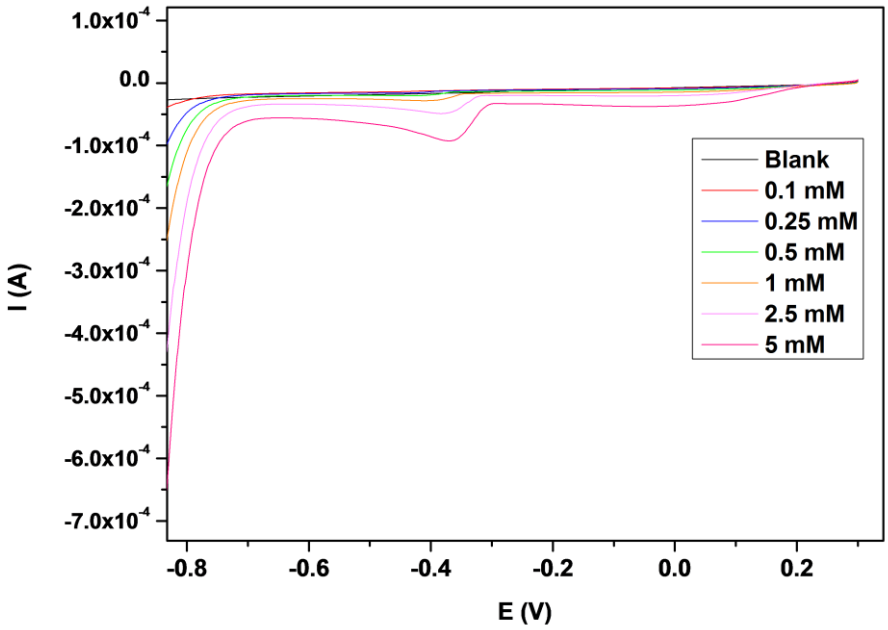

Figure 4.19 Linear sweep voltammetric plot for the reduction of Cu^{2+} for the addition of a mixture containing Cu^{2+} (5 µM), L-Ascorbic acid (10 µM) and allyl alcohol (10 µM) to a 10 µM CySH solution. Tests were carried out in 0.1 M Acetate Buffer, pH 4, with the thermally treated Cu-CoHCF modified GCE.

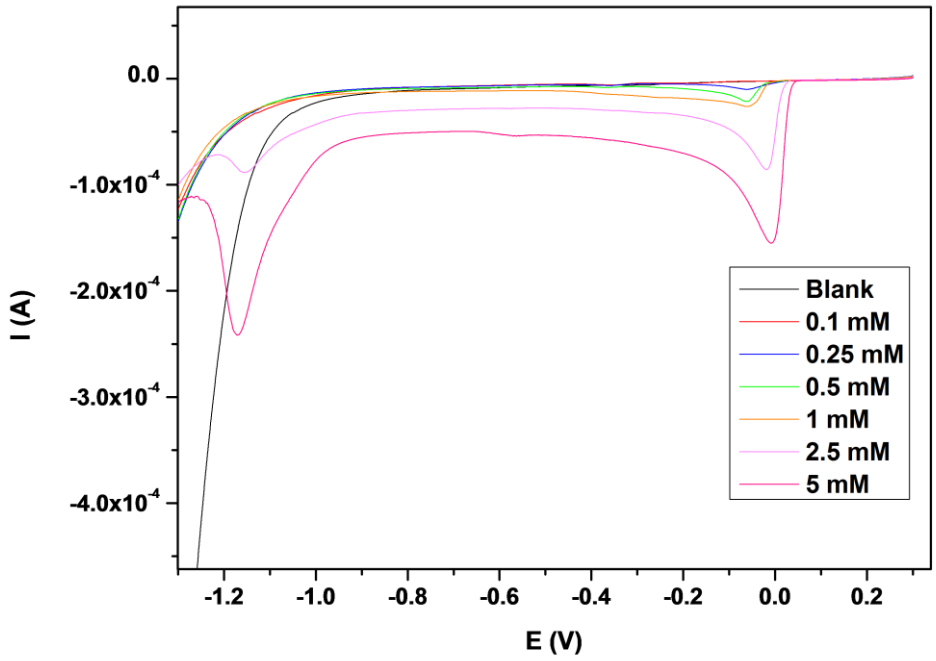

Figure 4.20 Linear sweep voltammetric plot for reduction of Hg^{2+} for the addition of a mixture containing Cu^{2+} (5 µM), L-Ascorbic acid (10 µM) and allyl alcohol (10 µM) to a 10 µM CySH solution. Tests were carried out in 0.1 M Acetate Buffer, pH 4, with the thermally treated Cu-CoHCF modified GCE.

4.2.2.3. Removal of Interference due to Cu^{2+} by reaction kinetics

Fig. 4.21 shows the two CA responses obtained by adding Hg^{2+} and Cu^{2+} (separately) at a concentration of 5 µM, to a 10 M CySH solution. It is well evident that the kinetics of the complex formation is much slower in the case of Cu^{2+} as compared to Hg^{2+}. Therefore, the Hg^{2+} determination could be carried out accurately also in the presence of Cu^{2+}, if the current measurement was performed soon after (within 10 s) the addition of the mixture. Additional measurements were conducted by adding solutions with a constant Hg^{2+} (2 µM) and varying Cu^{2+} (from 1 to 4 µM) concentrations to a PBS containing 10 µM CySH. The results showed that the response of the CME was as expected for the presence of only Hg^{2+}. In conclusion, it can be said that Hg^{2+}

determination is accurate also in the presence of Cu^{2+}, exploiting the different kinetics of complexes formation.

Some common anions were also studied to verify if their presence could interfere in mercury determination. No interference was observed for CH_3COO^-, Cl^-, NO_3^-, SO_4^-, HCO_3^- ions, for a concentration up to 1 mM.

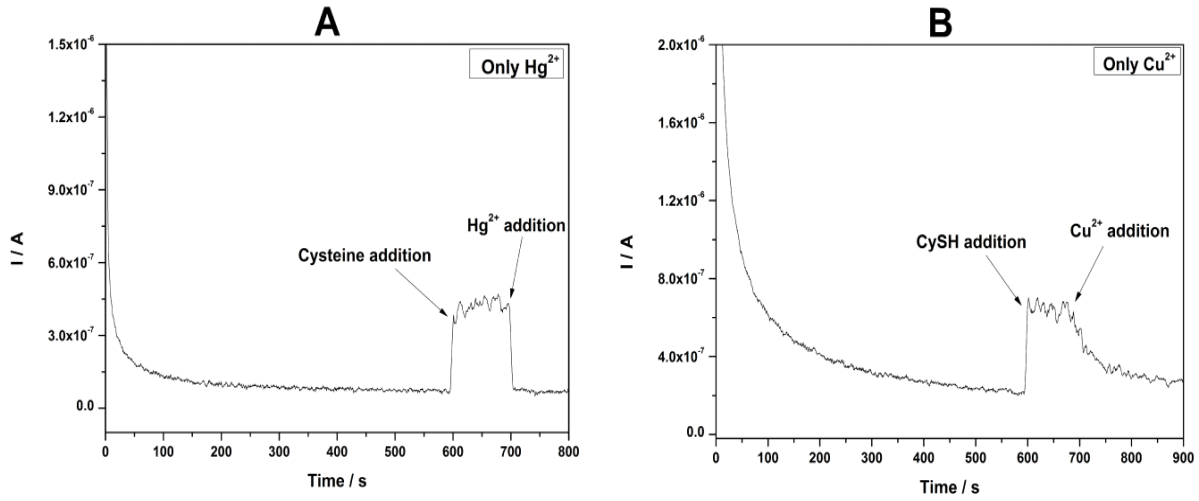

Figure 4.21 Chronoamperometric response for the addition of 5 µM Hg^{2+} (A) and 5 µM Cu^{2+} (B) to a 10 µM CySH solution (same conditions as in Fig. 4.18).

4.2.3. EXPERIMENTAL STUDIES ON PACKAGED MINERAL WATER SPIKED WITH Hg^{2+}

Packaged mineral water samples were spiked with Hg^{2+} (250 and 500 nM) and examined by the CME. The average concentration values (n = 5) were found to be 235 and 524 nM so that the percentage recovery ranged between 96 and 105, respectively, so confirming that the proposed sensor can be applied for the accurate determination of Hg^{2+} in polluted environmental water samples (Figure 4.22). Furthermore, the reproducibility of the analytical determination was good since the percentage coefficient of variation was about 6 %.

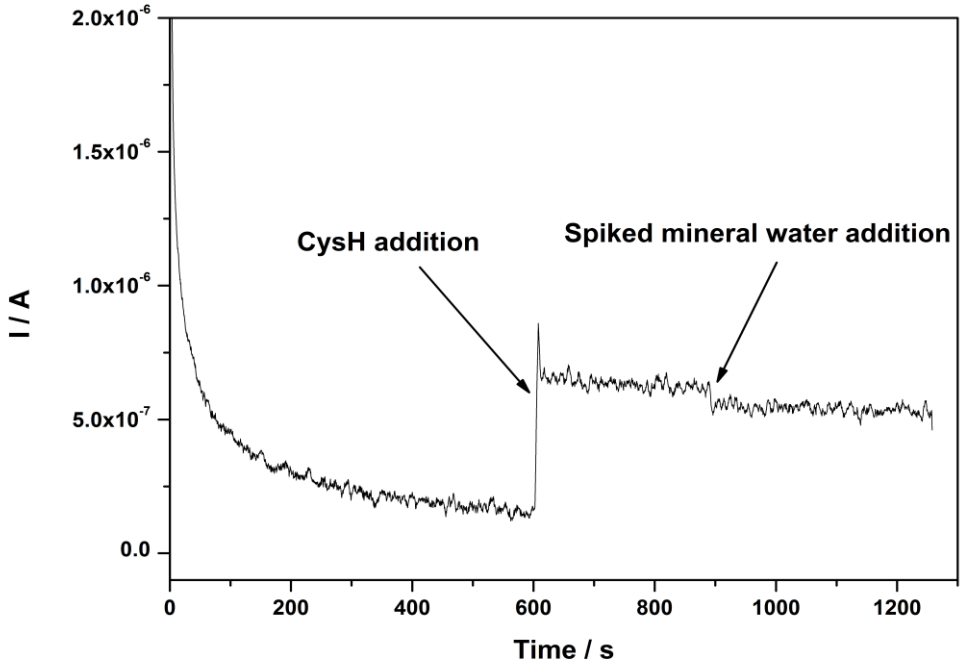

Figure 4.22 Chronoamperometric response for a spiked (500 nM Hg^{2+}) mineral water sample after the addition to a 10 µM CySH solution (same conditions as in Figure 4.18).

Additional tests were also carried out on spiked mineral water samples containing both Hg^{2+} and Cu^{2+} ($[Hg^{2+}] : [Cu^{2+}] = 1 : 2$) which gave accurate results for the concentration of Hg^{2+} (Fig. 4.23).

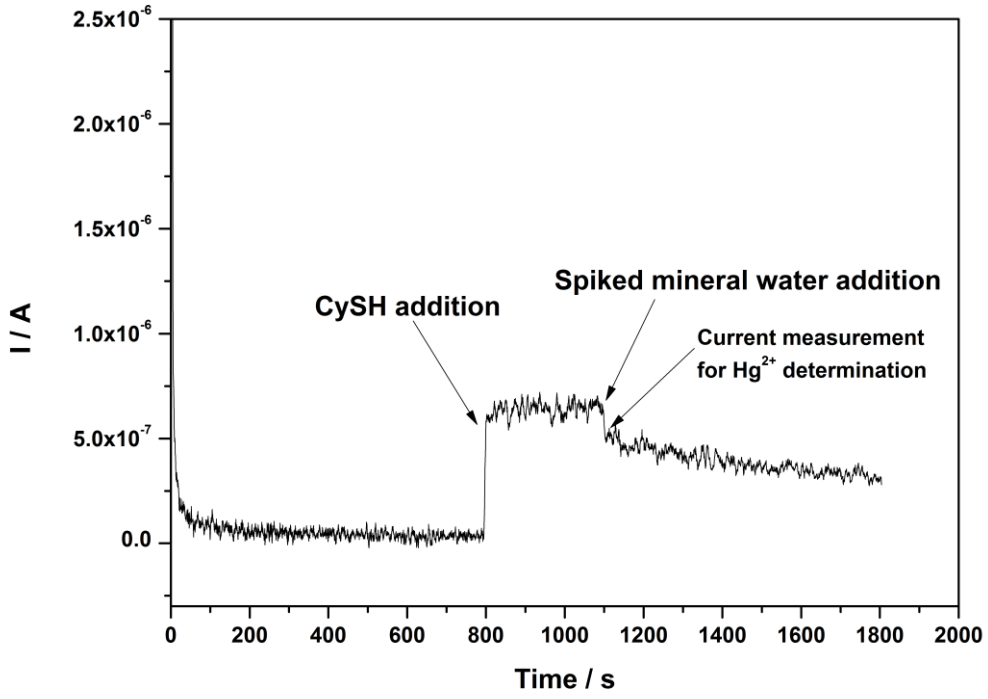

Figure 4.23 Chronoamperometric plot for the addition of a mixture containing 1 µM Hg^{2+} and 2 µM Cu^{2+} spiked mineral water sample to a 10 µM CySH solution (same conditions as in Fig. 4.13).

4.2.4. BIBLIOGRAPHY

[1] J.C. Miller, J.N. Miller, Statistics for Analytical Chemistry, Wiley, New York, 1988.

[2] I.M. Kolthoff, E.B. Sandell, E.J. Meehan, S. Bruckenstein, Analisi chimica quantitiva, Vol. 1, Piccin Editore, Padova, 295-297.

[3] B. Narayana, N.G. Bhat, K.S. Bhat, C.H.R. Nambiar, B. Ramachandra, A. Joseph, Selective complexometric determination of copper in ores and alloys using 2,2'-bipyridyl as masking agent, Microchem. J. 64 (2000) 221-225.

[4] G. D. Ulibarri, T. Ogura, J. H. Tzeng, N. Scott, Q. Fernando, Allyl alcohol as masking agent in determination of copper(I) and copper(II) in aqueous mixtures, Anal. Chem. 54, 13 (1982) 2307-2310.

4.3. CMEs BASED ON GRAPHENE OXIDE AND CARBON NANOTUBES

4.3.1. ELECTROCHEMICAL CHARACTERIZATION OF GO AND MWCNTs MODIFIED GCE

Graphene oxide functions as an electrical insulator, because of the disturbance of its sp^2 bonding networks. It is important, therefore, to reduce the graphene oxide so as to recover the honeycomb hexagonal lattice of graphene, in order to restore electrical conductivity. Since fabrication of graphene by conventional methods is quite expensive so far, electroreduction of graphene oxide which was the starting material in our case, was carried out so as to obtain a material almost equivalent to graphene. Electrochemical reduction of GO is typically achieved by applying a negative potential, around -1.0 or -1.2 V, to GO films casted on conductive substrates, or repeated voltammetric cycles with the lowest potential of about -1.2 V in solutions with pH from 1.5 to 12.5 [1]. This strategy has several advantages in comparison with chemical reduction [2,3,4]. First, it does not require any chemical reagents, and therefore it is environmentally friendly. Furthermore, highly negative potentials are beneficial for removing more oxygen functionalities in the production of high quality reduced GO (rGO). Lastly, the resulting rGO is in good contact with electrically conductive substrates, which simplifies the electrode fabrication process and makes it suitable for further electrochemical applications employing cathodic potentials.

Fig. 4.24 shows the cyclic voltammogram recorded during the electroreduction treatment of the GCE modified with the composite containing both GO and MWCNTs. The steadily decreasing cathodic currents with increasing the number of scans show that there is a continuous reduction of the oxygen containing functionalities of GO deposited on the GC surface. It is also evident that from 8^{th} scan onwards the recorded currents are practically indiscernible from each other, so confirming the full reduction of GO.

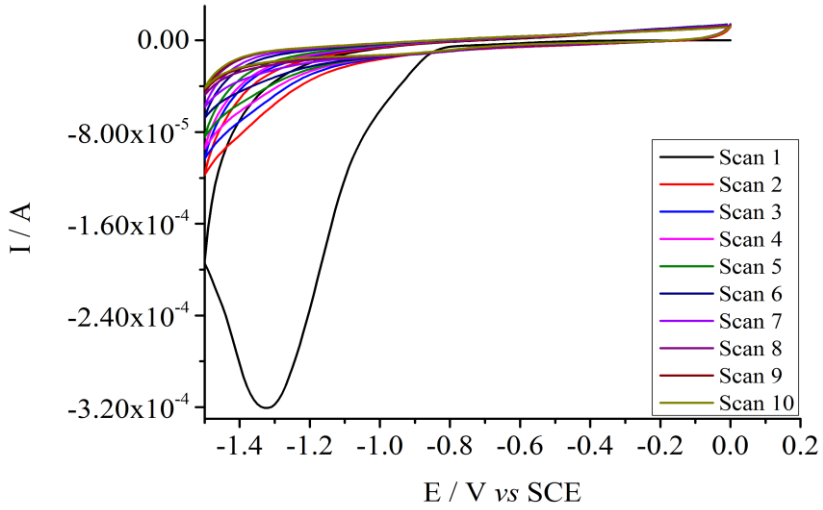

Figure 4.24 Cyclic voltammograms recorded for the electroreduction of composite (GO-MWCNTs) based CME in phosphate buffer.

Finally, GO films deposited were electrically characterized before and after the electrochemical reduction. The sheet resistance changed from 85000 kΩ/sq, measured for the oxidized film, to 2.8 kΩ/sq measured for the reduced one, suggesting a considerable enhancement of conductivity. Consequently, the result confirms that the electrical features of graphene are almost completely recovered with the electrochemical treatment of GO.

4.3.2. MEASUREMENT OF ELECTROCHEMICALLY ACTIVE AREA

The electrochemically active areas were estimated by using two approaches in order to highlight the different phenomena that could affect the redox processes. The former method evaluates the double-layer capacitance of the system from CV, by measuring the currents recorded at a potential wherein no faradaic process takes place. In such a case the charging current, i_c, is equal to the product of the electrochemical capacitance of double layer (CDL) and the scan rate. The electrochemically active surface area (ECSA) is calculated by dividing CDL by the specific capacitance of the sample as reported by McCrory et al. [5]. In order to perform an accurate evaluation,

CDL was calculated as the slope of the line obtained by plotting i_c versus the scan rate ν.

Fig. 4.25a shows that the electrochemical reduction induces a remarkable ECSA increase for all five systems, as also confirmed by the SEM characterization (see below). Among reduced materials electro-reduced graphene oxide (ERGO) exhibits the highest value (8.7 cm^2), while the MWCNTs display the lowest one (0.4 cm^2). Comp, Bil-1 and Bil-2 show active area values that are close together and are placed at about halfway between ERGO and MWCNTs (about 3 cm^2). Since the same mass of the nanomaterials was deposited on the GCE, such results suggest that the presence of graphene is the parameter that rules ECSA when it is evaluated by the double-layer capacitance. Nevertheless, the capacitance measurements estimate all the area at electrode-solution interface without considering that some parts could not be approachable by the analyte. Therefore, ECSA was also estimated using a redox probe (ferricyanide) by means of Randles-Sevcik equation in order to better simulate the conditions for which an electron transfer process takes place (Fig. 4.35b). Fig. 4.25c shows the CVs recorded in acetate buffer (pH 4.0) containing 2 mM ferricyanide at the GCE modified with the different configurations of carbon nanomaterials. MWCNTs exhibit the lowest area (0.067 cm^2) which is practically identical to the geometric area of the underlying GC, and the highest value is observed for the composite (0.162 cm^2). Bil-1 also displays a high area (0.147 cm^2), while Bil-2 and ERGO have an active surface of 0.068 and 0.091 cm^2, respectively. Moreover, the CVs show that the response of ferricyanide is quasi-reversible for bare GCE, MWCNTs, Composite and ERGO, as checked from the separation between anodic and cathodic peaks, which is near enough to the theoretical value for a one-electron process.

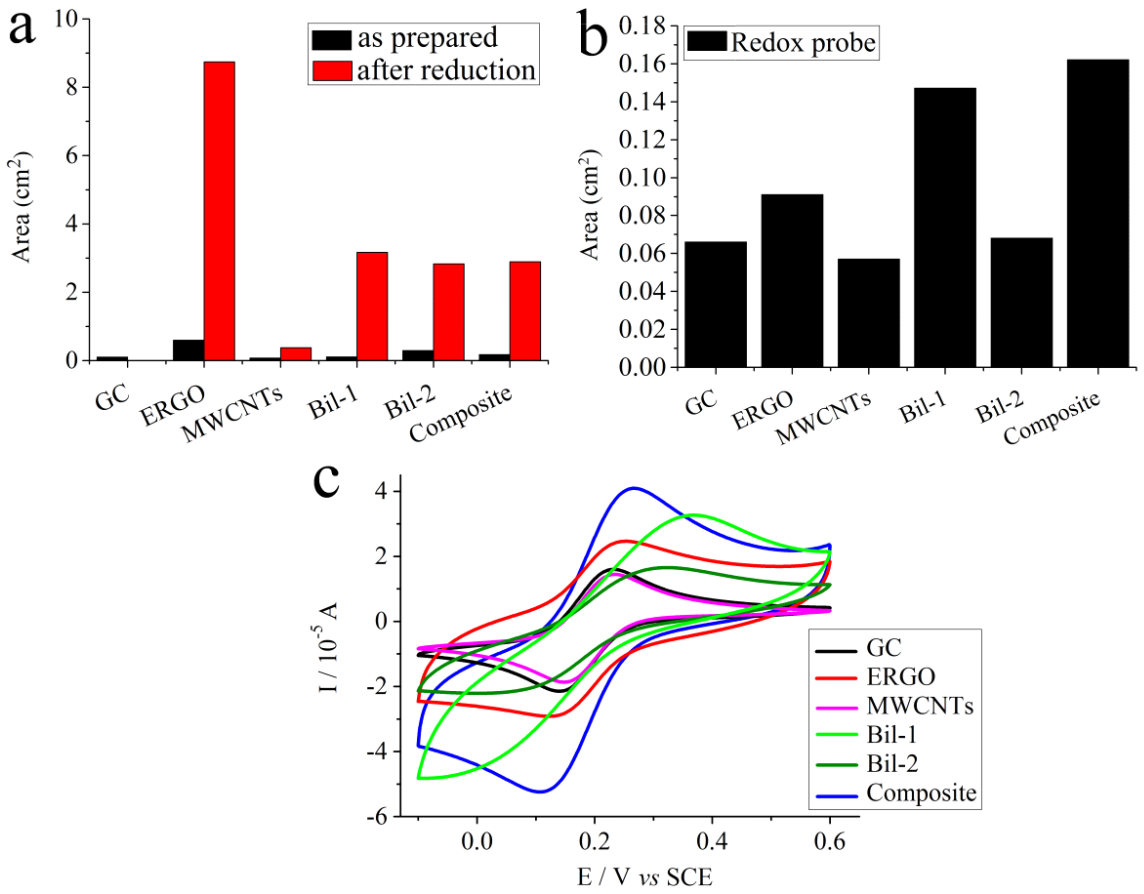

Figure 4.25 ECSA calculated for each type of modified electrodes from the double layer capacitance (a) and from the CVs recorded in the presence of the redox probe (b); CVs obtained in acetate buffer (pH 4.0) containing 2 mM ferricyanide at the different CMEs (c).

The different data obtained with the two methods are explained considering that ferricyanide does not cover the entire electrochemically active surface, as determined by the capacitive approach. Therefore, the porosity and the structure of the different nanomaterials play a key role in the evaluation of the area resulting from the use of the ferricyanide faradaic current. It has been demonstrated that graphene sheets have a tendency to restack as a graphite-like structure due to the occurrence of relatively strong inter sheet interactions [6]. Such interactions make the resulting films less porous and hinder the penetration of the electrolyte solution and, consequently, the diffusion of the redox probe is more difficult. On the other hand, in the presence of MWCNTs the restacking of graphene sheets is inhibited and the films are more porous [3]. The highest active area was observed for the composite because the co-deposition ensures an

optimum interaction between CNTs and GO, leading to the highest faradaic current. On the contrary, when the two nanomaterials were deposited in two steps, a deep contact could be established only when CNTs were beneath, whereas in the opposite configuration the synergetic effects were weaker and the faradaic response appeared less reversible and the active area was lower.

In conclusion, the active area increase is mainly ascribable to ERGO, but the efficient π- π stacking of this material generates a morphology that hinders the analyte diffusion. MWCNTs can prevent the interaction between graphene sheets and, consequently, when this phenomenon occurs, a greater electroactive area is available to the redox probe.

4.3.3. MORPHOLOGICAL CHARACTERIZATIONS

The morphologies of the composite before and after the electrochemical reduction, the two bilayers, GO and ERGO, coating graphene sheets were investigated by SEM. As shown in Fig. 4.26a, GO forms a smooth and uniform film which is attributed to the two-dimensional structure, however in many areas it is evident the presence of sheets agglomerates.

The film covers the entire electrode surface since the typical irregular graphite surface morphology is no more observable (inset of Fig. 4.26a). After the reduction treatment (Fig. 4.26b) the sample displays a quite different morphology ascribable to the presence of graphene unstacked sheets, thus the sample surface appears rougher than the one displayed by GO (a magnification is shown in the inset of Fig. 4.26b). The wrinkles present on the sample surface are due to the structural rearrangements which occur after the recovery of the conjugated system, and the removal of the hydroxyl and epoxide functionalities from the GO resulting from the electrochemical reduction [3].

This observation is consistent with the much higher ECSA value obtained for ERGO in comparison with the one calculated for the GO sample. Fig. 4.26c shows the morphology of the as-prepared composite. If compared to the smooth surface of GO

film, the composite exhibits a relatively rougher surface, due to a ripple texture which is attributed to GO in the composite, which is rather similar to the morphology displayed by ERGO. Even in this case, the image shows that the GO layers cover the whole area and the presence of CNTs is not visible, thus confirming the good dispersion of MWCNTs in GO aqueous solutions. In fact, CNTs are supposed to act as dispersing agents since they can prevent the GO sheets agglomeration and restacking [7,8]. The morphology of the reduced composite is shown in Fig. 4.26d. In this case, the presence of MWCNTs is well evident as the film displays a mixed morphology where MWCNTs seem to be interspersed randomly between the graphene nanosheets to form a homogenous three-dimensional network, uniformly deposited. This results in a more compact film, suggesting strong interfacial interactions between ERGO and MWCNTs. This particular morphology can explain the higher ECSA than the as prepared composite, in agreement with the calculated values.

The SEM image of Bil-1, shown in Fig. 4.26e, displays a morphology very similar to the one exhibited by the composite, where the main features are the surface corrugations due to GO sheets which seem to constitute a quite compact structure with lots of wrinkles whereas the underneath MWCNTs are not noticeable.

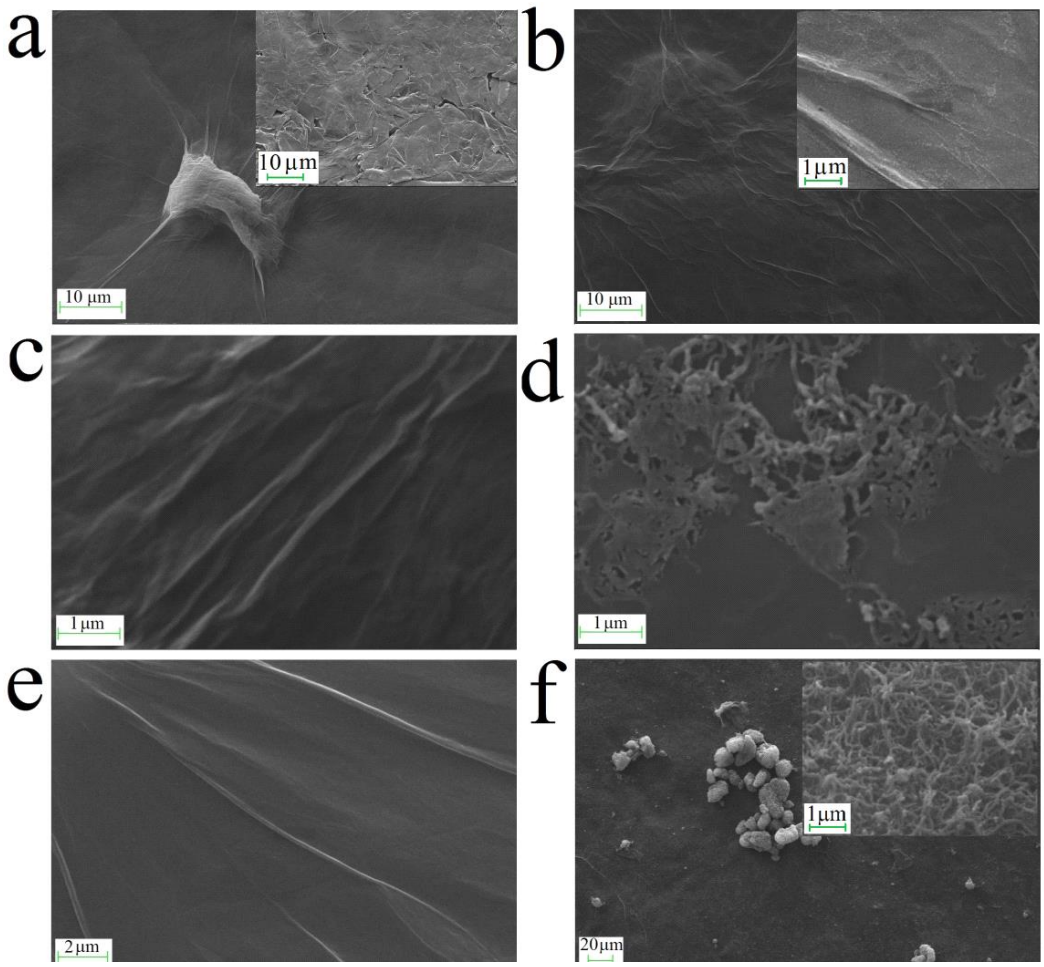

Figure 4.26 SEM images of graphene sheets coated with GO (a), ERGO (b), Composite before (c) and after (d) the electrochemical reduction, and Bil-1 (e), Bil-2 (f).

In the case of Bil-2 (Fig. 4.26f), GO covers the entire electrode surface forming a smooth coating as in the case of GO alone (Fig. 4.26a), since the irregular morphology of the graphite sheets beneath, is not evident even in this case. The sample reveals the presence of spherical structures, randomly distributed, ascribable to a large amount of MWCNTs agglomerated on GO. The inset in Fig. 4.26f shows a magnification of the MWCNTs agglomerates which display a diameter of several tens of nanometers and a length of ~1 µm.

In conclusion, the SEM studies further support that the composite after the electrochemical reduction displays a morphology which should lead to the highest surface area.

4.3.4. FT-IR AND UV/Vis CHARACTERIZATIONS

On the purpose of confirming the reduction of GO, FT-IR and UV/Vis techniques were employed to characterize the bilayers and the composite before and after the electrochemical CV treatment.

Fig. 4.27 shows the FT-IR spectrum of GO whose bands are in agreement with those previously reported [9,10]. The strong and broad absorption band in the 3600-3000 cm^{-1} region is related to the O-H stretching mode of intercalated water, C-OH, and phenols. Other strong bands are located at 1639 cm^{-1}, due to the C=C stretching originated from skeletal vibrations of unoxidized graphitic domains, at 1418, 1387, and 1059 cm^{-1} due to the C-O stretching (epoxy or alkoxy). Other weaker bands are located at 1830 and 1740 cm^{-1} due to the carbonyl and carboxyl C=O, respectively. After the 10 CV cycles all the absorption bands of the oxygen-containing functional groups significantly decreased or even disappeared in the FT-IR spectra of all the configurations of carbon nanomaterials containing GO, whereas the band at 1639 cm^{-1} was still present, indicating that the graphitic network of sp^2 bonds had been mostly restored and, therefore, confirming the effectiveness of GO reduction to give ERGO (black and red traces). In Fig. 4.27 the FT-IR spectrum of the MWCNTs is also reported for the sake of clarity.

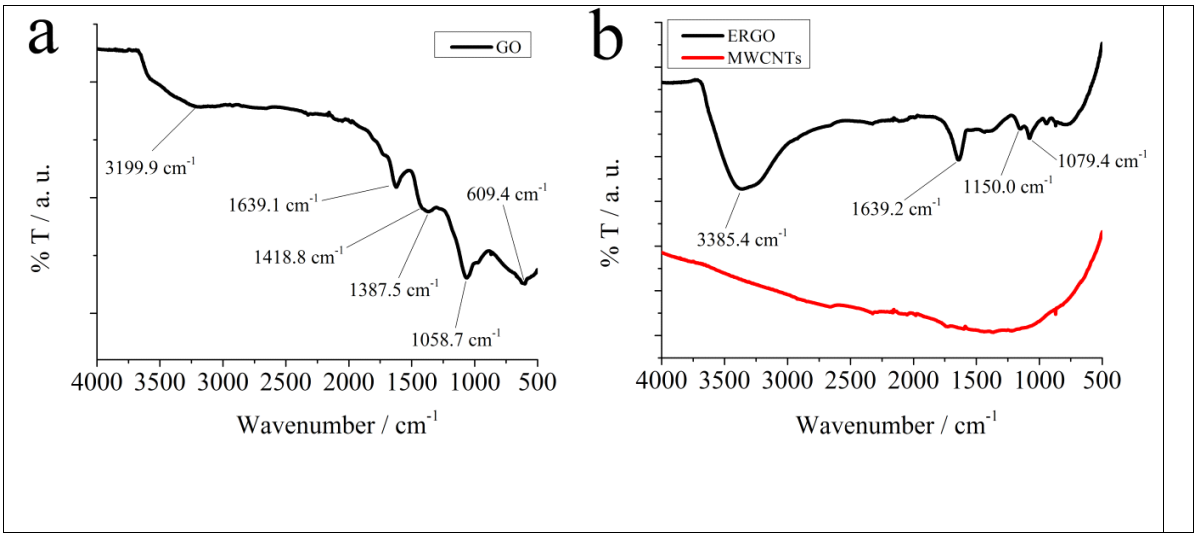

Figure 4.27 FT-IR spectra recorded for GO (a), ERGO and MWCNTs (b) casted on graphite sheets. The background signal, due to the support has been subtracted.

The UV-Vis absorption spectra of GO and ERGO were recorded to further confirm the reduction of oxygen functionalities after the electrochemical treatment. As shown in Fig. 4.28, GO spectrum shows a broad absorption at 247 nm which corresponds to $\pi \rightarrow \pi^*$ transition of the aromatic C=C bond. A shoulder around 325 nm is also observed, corresponding to $n \rightarrow \pi^*$ transition of C=O bond [11]. In the case of ERGO the plasmonic peak corresponding to the $\pi \rightarrow \pi^*$ transition is red-shifted to 250 nm and the absorbance is significantly increased at wavelengths above 230 nm. The overall increase in absorbance suggests that aromatic conjugated sp^2 clusters have been partially restored upon electrochemical reduction, as already reported in literature [12].

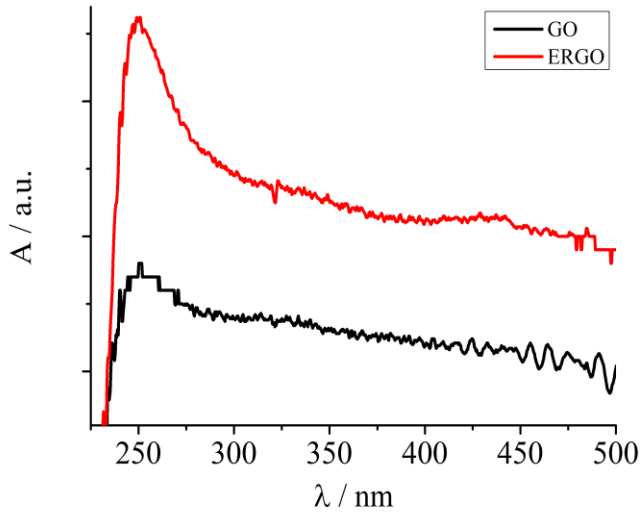

Figure 4.28 UV/Vis absorption spectra of GO and ERGO.

4.3.5. ELECTROCHEMICAL BEHAVIOR OF CATECHOL AND DOPAMINE

The electrochemical activity of catechol (CA) and dopamine (DA) was investigated by CV, at pH 2, 4, and 7, using the GC electrodes modified according to the five configurations above described. As an example, the CVs recorded at pH 4 are

shown in Fig. 4.29. It is immediately evident the capacitive contribution due to the presence of reduced graphene oxide, especially in the configurations Composite, Bil-1 and ERGO. In any case, both compounds exhibit reversible or quasi reversible redox waves, even if the reversibility is better for DA. Generally, only a redox system is present in the characterization CVs which involves two electrons and two protons as already reported by [13], but in the case of composite, CA displays two reversible systems which can be ascribed to two mono-electron processes (Fig. 4.29).

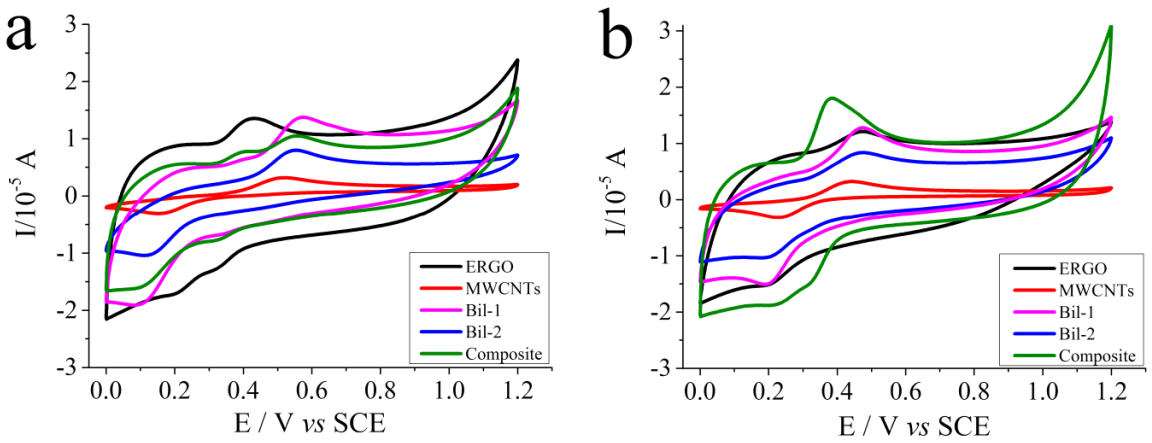

Figure 4.29 CVs obtained for the different configurations in acetate buffer (pH 4.0) containing catechol (a) and dopamine (b). Scan rate = 0.05 V s^{-1}.

Table 4.6 and Table 4.7 show the anodic peak currents recorded in 0.1 mM analyte solutions at pH 4 and 7.

When ERGO and MWCNTs are used as modifiers, the lowest currents are recorded. Only slightly increased currents are observed when the nanomaterials are in the Bil-2 configuration, for catechol at least. On the other hand, the highest responses are obtained for Bil-1 and Composite configurations. Such an evidence is in good agreement with the morphological characterization and with the electroactive area determination as estimated with the redox probe. In view of an amperometric determination of CA and DA it is evident that the best sensitivity is achieved at pH 4 due to the highest recorded currents.

At this pH, Bil-1 exhibits the best electroanalytical performance for catechol while Composite is the best electrode material for the dopamine oxidation. In particular, these two configurations display an enhancement of the current which is about 3-4 times greater than the value recorded when the nanomaterials are casted alone on GCE. This result means that MWCNTs and ERGO exhibit a stronger synergetic effect when they are present in Bil-1 or Composite configurations on the GCE.

Table 4.6 Increase in the peak oxidation current (in A) on addition of 0.1 mM of catechol to buffer solutions.

CME	pH 4 acetate buffer	pH 7 phosphate buffer
ERGO	1.91	1.12
MWCNTs	1.52	0.98
Bil-1	5.98	4.34
Bil-2	2.74	1.82
Composite	3.95	2.87

Table 4.7 Increase in the peak oxidation current (in A) on addition of 0.1 mM of dopamine to buffer solutions.

CME	pH 4 acetate buffer	pH 7 phosphate buffer
ERGO	1.62	1.01
MWCNTs	1.44	0.87
Bil-1	3.89	3.02
Bil-2	1.75	1.08
Composite	5.48	2.74

Since the modification of the electrode is easier and faster with Composite and the casting of the nanomaterials results more reproducible, this configuration was

further investigated to study the dependence of the response of both analytes on the solution pH. This choice was also supported from the consideration of a less extent of fouling effects at Composite, which always occur during phenols oxidation.

The investigation of the formal potential (E^{o}) dependence of CA and DA on pH was carried out performing CVs at a slow scan rate (ν = 0.01 V s^{-1}). In these conditions only one redox system was observed also for catechol. As the pH increased the E^{o} linearly decreases, with slopes of -0.062 and -0.065 V pH^{-1} for CA and DA, respectively (Fig. 4.30). These values suggest that the oxidation of two analytes involves the same number of electrons and protons, in agreement with the literature [13]. From the results shown in Fig. 4.30 it is clear that the best pH for CA and DA determination is 7, due to the low overpotential which is necessary to apply in order to oxidize the analytes. Being DA a neurotransmitter, its quantification is important in biological fluids whose pH is next to 7 and which contain a lot of possible interfering compounds as far as an amperometric measurement is concerned. CA is often employed as a model compound when polyphenols levels are to be determined by means of an amperometric method involving biosensors which are generally based on polyphenols oxidases. In such a case, the reduction current of the *o*-quinone produced by the enzyme is detected, working in a pH range from 4 to 6.5. Our results suggest that Composite is a good configuration for detection of *o*-quinones due to the reversibility of the electrochemical process of catechol which possesses a formal potential ranging between 0.35 and 0.17 V *vs.* SCE.

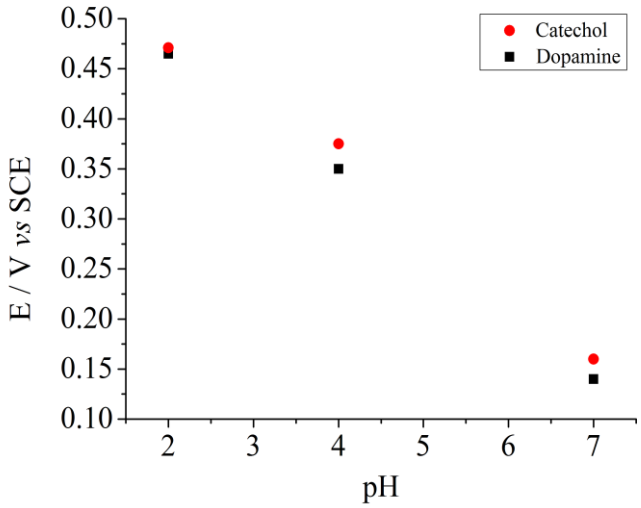

Figure 4.30 Dependence of catechol and dopamine formal potentials on the pH.

4.3.6. EVALUATION OF THE MODIFIED ELECTRODES FOULING

It is well-known that the electro-oxidation of phenols leads to the formation of high molecular weight polymers that precipitate on electrode surface so hindering the occurrence of redox processes. The extent of fouling was evaluated for the five configurations by CV at pH 4 and 7, using the ferrycianide/ferrocyanide couple as the redox probe. The detected signal was expressed as the ratio between the cathodic peak currents measured after and before performing the electro-oxidation of 0.2 mM catechol or dopamine solution.

When Bil-1 and Bil-2 were used the electrooxidation of two analytes led to a strong fouling of electrode surface, as suggested by the disappearance of the reduction ferrycianide peak in the CV. On the other hand, at the GCEs modified with ERGO, CNTs and Composite the redox probe signal displayed an intensity that was ranged 40-80 % of the starting one. The fouling effects were always greater when the analyte was CA when the pH was 7.

From our experiments, Composite can be considered the best system to modify the electrode with the examined carbon nanomaterials because it exhibits, at the same time, both high sensitivity and fouling resistance, which is not ensured by Bil-1 configuration.

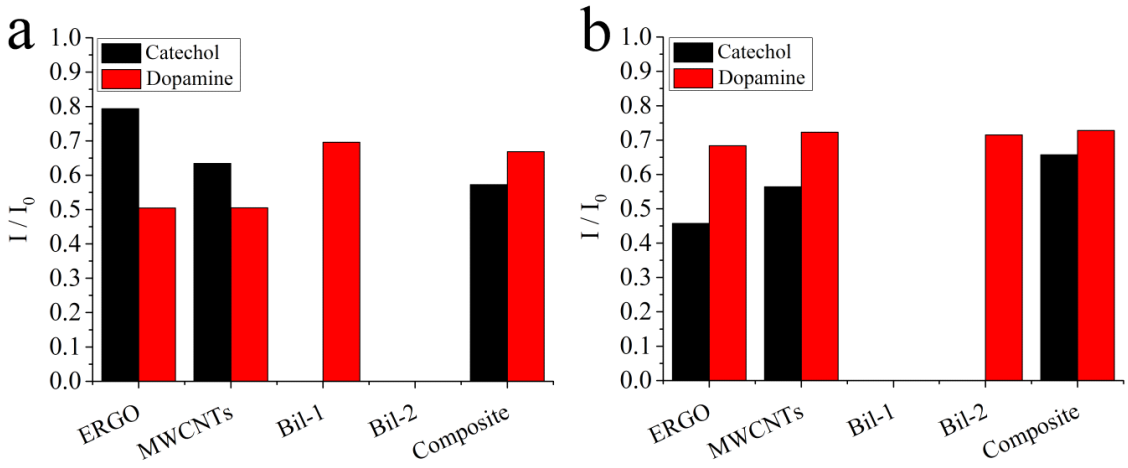

Figure 4.31 Electrode fouling experiments carried out using the different configurations at pH 4 (a) and 7 (b).

4.3.7. BIBLIOGRAPHY

[1] L. Qiu, X. Yang, X. Gou, W. Yang, Z. F. Ma, G. G. Wallace, D. Li, Chem. Eur. J. 16 (2010) 10653-10658.

[2] M. Zhou, Y. Zhai, S. Dong**,** Anal. Chem. 81 (2009) 5603-5613.

[3] A. Benchirouf, C. Müller, O. Kanoun, Nanoscale Res. Lett. 11 (2016) 4.

[4] F. Yang, D. He, B. Zheng, D. Xiao, L. Wub, Y. Guo, J. Electroanal. Chem. 767 (2016) 100-107.

[5] C.C.L. McCrory, S. Jung, I.M. Ferrer, S.M. Chatman, J.C. Peters, T.F. Jaramillo, J. Am. Chem. Soc. 137 (2015) 4347-4357.

[6] H. Chen, M.B. Müller, K.J. Gilmore, G.G. Wallace, D. Li, Adv. Mater. 20 (2008) 3557-3561.

[7] G.K. Ramesha, S. Sampath, J. Phys. Chem. C 113 (2009) 7985-7989.

[8] Y. Huang, J. Liang, Y. Chen, Small 8(12) (2012) 1805-1834.

[9] B. Haghighi, M.A. Tabrizi, RSC Adv. 3 (2013) 13365-13371.

[10] S.-J. Li, Y. Xing, D.-H. Deng, M.-M. Shi, P.-P. Guan, J. Solid State Electrochem. (2015) 19:861-870.

[11] K. Deng, C. Li, X. Qiu, J. Zhou, Z. Hou, J. Electroanal. Chem. 755 (2015) 197-202.

[12] J.I. Paredes, S. Villar-Rodil, P. Solís-Fernández, A. Martínez-Alonso, J.M.D. Tascón, Langmuir, 25(10) (2009) 5957-5968.
[13] M. Boulkroune, A. Chibani, F. Geneste, Electrochim. Acta 221 (2016) 80–85.

4.4. LDHs SYNTHESIS AND CHARACTERISATION

4.4.1 LDHs BASED ON Mg, Ni AND Al

LDHs based Mg, Ni and Al were synthesized on a FeCrAl foam using a potentiostatic technique. Varying concentration of Ni^{2+}, Mg^{2+} and Al^{3+} were prepared. The electrolytic solution used contained the salts of Al, Ni, and Mg in the form of nitrates. The concentrations of cations Al, Mg and Ni were, respectively: 0.06, 0.6 and 0.12 M. The potentiostatic technique used for the deposition of the LDHs, was investigated at various potentials so as obtain the maximum deposition of the LDHs on the metal foam.

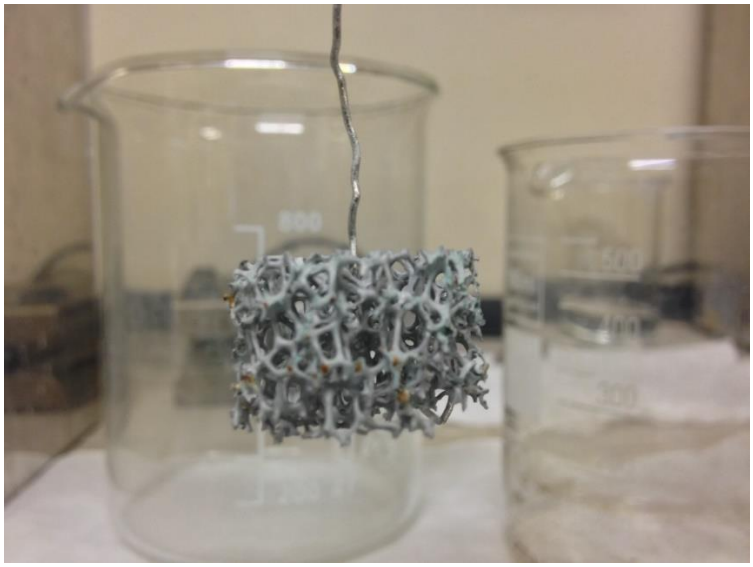

Figure 4.32 LDHs based on Ni, Mg and Al deposited on a FeCrAl foam

The best results were obtained by performing synthesis of a coarse foam using potentiostatic technique at a potential of -1.2 V vs. SCE. Multiple sample of the LDHs were prepared which showed varying thicknesses of the deposit from 1-2 microns to 6-7 microns, in dependence of the considered point of the foam. The duration of pulse applied for the deposition of LDHs was also varied, vis-a-vis a single potential pulse was applied for 1000 s or two sequential pulses of 1000 s each. Both deposits were characterized by electron microscopy coupled with EDX analysis.

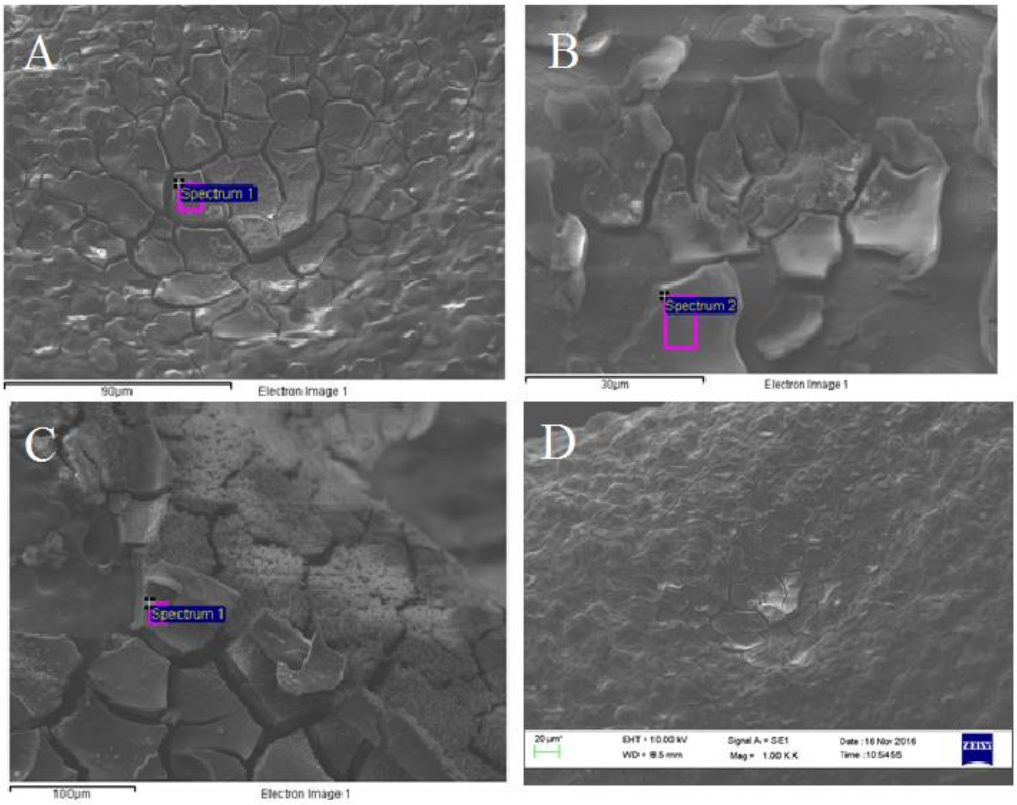

Figure 4.33 SEM images of LDHs based on Ni, Mg and Al deposited on a FeCrAl foam at various resolutions A) 90 µm B) 30 µm C) 100 µm and D) 20µm

Table 4.8 Elemental composition of the LDHs deposited on FeCrAl foam for the given concentration of the bivalent (0.72 M) and trivalent (0.06 M) cations in the electrolytic solution.

Element	Weight%	Weight% Sigma	Atomic%
N K	9.49	0.77	12.05
O K	66.13	1.60	73.51
Mg K	2.70	0.19	1.98
Al K	16.54	0.49	10.90
Ni K	5.13	2.10	1.55

Totals	100.00

It was found that on increasing the duration of the pulse a greater amount of LDHs was deposited on the metal foam. Further studies would be carried out to optimise the LDHs to be used as catalytic precursors in steam reforming reactions.

Chapter 5
CONCLUSIONS

The electroanalytical determination of thiols (CySH, GSH and BdSH) was performed by using a hybrid Cu-CoHCF modified glassy carbon electrode at which the electrocatalytic oxidation was found to occur at a reduced overpotential when compared to bare GCE. The mixed hexacyanoferrate was more stable than a single metal hexacyanoferrate with respect to both pH and cycling stress. A thermal treatment was also applied to the CMEs in order to increase their stability. This treatment was beneficial for the analytical determination of CySH and GSH. The chronoamperometric measurements yielded good results with excellent signal to noise ratio for the three thiol compounds even if the best sensitivities were observed for CySH and BdSH. Nevertheless, when detecting thiols some fouling was observed but this is not a big problem since the modification of GC is rapid and inexpensive. In fact, the CME can be prepared with off-the-shelf chemicals without the need for complicated fabrication techniques and the analysis is fast and simple to carry out.

A fast, sensitive and efficient electroanalytical method for the indirect electrochemical determination of Hg^{2+} was successfully developed. The approach is able to determine concentrations of Hg^{2+} as low as 250 nM, which is considered the LOQ, even though LOD is much lower (80 nM). Interference studies showed that Cu^{2+} was the major interferent with negligible interference from other cations and no interference from the most common anions. Amperometric studies demonstrated that the response of CySH towards Hg^{2+} was much faster compared to Cu^{2+} and this observation was exploited to overcome the interference from Cu^{2+} by a rapid measurement of the current after the addition of the analyte. The CME was used to successfully determine Hg^{2+} in spiked mineral water samples. It could also be employed to have a preliminary screening of the level of pollution in an environmental water sample.

MWCNTs and ERGO were employed alone and together to modify GCEs in order to check the best configuration in terms of sensitivity for the electro-oxidation of catechol and dopamine. Furthermore, the fouling effects of the electrode were also taken into account since they are a heavy drawback when those analytes need to be determined since they force to a continuous renewing of the electrode surface.

When using an aqueous stable dispersion of GO and MWCNTs (in a weight ratio 1:1) to modify the GC surface an uniformly deposited film of nanomaterials was obtained which displayed the highest electrochemically active area. This configuration allowed the most efficient electron transfer for the two analytes and minimized the fouling effects occurring if concentrated solutions are analysed. The reason of this result is to be ascribed to the strong interfacial interactions between ERGO and MWCNTs which lead to an effective synergism of the two nanomaterials in favouring the electrode kinetics.

With respect to LDHs, the preliminary studies carried out showed promising results. Further studies would be conducted to optimize the conditions for the deposition of LDHs, and then use it as a catalytic precursor for steam reforming and/ or catalytic partial oxidation reactions.

ACKNOWLEDGEMENT

I would like to first of all thank my supervisor Prof. Domenica Tonelli for giving me the opportunity to work in this exciting field of work. She had been very supportive and provided a lot of guidance in helping me carry out the PhD. I would like to extend my gratitude to my colleagues at the Analtitica Lab namely, Dr. Lorella Guadagnini, Dr. Isacco Gualandi, Dr. Marco Monti, Prof. Erika Scavetta and Prof. Marco Giogetti who were always ready to give advice regarding the direction of my work. I am also thankful to Alberto Mucchi from the Didactical Lab who helped me in obtaining a lot of the required chemicals for my work. Sincere gratitude also to the staff at the Department of Industrial Chemistry who rendered their support to me whenever needed. I would also like to thank the European Commission for the Erasmus Mundus scholarship.

Lastly, I am grateful to my family for giving me the freedom to pursue my ambitions and to all other people who have helped me in one way or another.